From Supramolecular Vanadate Receptors to Enzyme Models of Vanadium Haloperoxidase

INAUGURALDISSERTATION

zur

Erlangung der Würde eines Doktors der Philosophie

vorgelegt der

Philosophisch-Naturwissenschaftlichen Fakultät

der Universität Basel

von

Xiao-an Zhang

aus

Furong, Yueqing, Zhejiang, China

Basel, 2005

Genehmigt von der Philosophisch-Naturwissenschaftlichen Fakultät auf Antrag von

Prof. Dr. Wolf-D. Woggon

Prof. Dr. Andreas Pfaltz

Prof. Dr. Edwin Constable (Vorsitz)

Basel, den 8. Februar 2005

Prof. Dr. Hans-Jacob Wirz (Dekan)

For

Ganpan

Acknowledgements

Foremost, I would like to express my gratitude to my supervisor, Prof. Dr. Wolf-D. Woggon for his constant support, stimulation and guidance, regarding matters of a scientific and also a non-scientific nature, which has made this research a real pleasure and helped me to envisage my future career. Also special thanks to Prof. Dr. Antoinette Chougnet for her generous help during the past four years.

I sincerely thank Prof. Dr. Andreas Pfaltz for his function as my co-referee and his kind support for my future career.

I really appreciate Prof. Dr. Markus Meuwly for his collaboration regarding DFT calculation which provided in-depth evidence for our observation. I thank Prof. Hans-Jakob Wirz for stimulating discussions about the protonation equilibrium and the systematic knowledge of photochemistry from his lecture, and Dr. Urs Hengartner for his suggestions regarding synthetic chemistry.

Thanks to Dr. Gerd Scherer, Dr. Daniel Haeussinger, and Dr. Klaus Kulicke for teaching me how to handle NMR instruments, and in particular the ^{51}V-NMR measurement. I appreciate Dr. Markus Neuburger and Dr. Silvia Schaffner for determination of the X-ray structures, Dr. H. Nadig for EI and FAB-MS and Mr. H. Kirsch for elemental analysis.

I would also like to thank Alain Schlatter, Axel Buss, Roman Kovàsy, Pirmin Rösel and Stefan Graber for their contributions on the synthesis of thiourea cryptands during their *Praktikum* studies.

Thank Dr. Jefferson Revell for the proof reading of this thesis.

It has been my pleasure to work in the team with such a pleasant atmosphere, and my sincere thanks are given to all past and present members of the Woggon group whom I worked with during the past four years.

Thank Swiss National Science Foundation (SNF) for financial support.

Finally, my love and thanks go to my wife, Gan-pan, for her continual understanding, support, and love over the course of my study.

Contents

Theoretical Part

1. Introduction

1. 1. Haloperoxidases and Natural Organohalogen Compounds

Halogens are abundant constitutive elements of the biosphere particularly in marine environment. Ocean water is approximately 0.5 M in chloride, 1 mM in bromide and 1μM in iodide. Thus it is not surprising that halogens are incorporated into a number of natural organic compounds. More than 3,800 natural organohalogen compounds have been isolated and characterized to date,[1] which range in structural intricacy from the ubiquitous fungal and plant metabolite chloromethane to the complex life-saving antibiotic vancomycin.[1, 2] The biological functions of most natural organohalogens are important for many organisms, such as in chemical defense, in food gathering or as regulatory hormones. In many cases these compounds are also of pharmacological interest due to antifungal, antibacterial, antineoplastic, antiviral (e.g., anti-HIV), anti-inflammatory, and other action.[3, 4]

The main enzymes responsible for the incorporation of halogen atoms in organic compounds in nature are haloperoxidases (HPOs), which catalyze the formation of halogenated organic compounds at the expense of hydrogen peroxide according to **Eq. (1)**, where RH is organic substrate; X^- is chloride, bromide or iodide ion; and RX is the halogenated product.

$$RH + H_2O_2 + H^+ + X^- \rightarrow RX + 2H_2O \qquad (1)$$

Without suitable organic substrate, the two-electron oxidation of a halide may turn to produce singlet oxygen, see **Eq. (2)** and **(3)** .[5-7]

$$H_2O_2 + H^+ + X^- \rightarrow HOX + H_2O \qquad (2)$$

$$HOX + H_2O_2 \rightarrow {}^1O_2 + X^- + H^+ + H_2O \qquad (3)$$
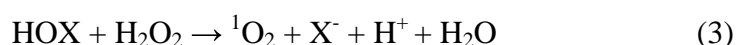
Since Hager's group purified the first chlorinating enzyme from *Caldariomyces fumago* in 1961,[8] more and more HPOs have been found in a broad range of

organisms, including mammals, molds, bacteria, algae, ferns, and higher plants.[5-7] The historical nomenclature convention of HPO is based on the most electronegative halide that the enzyme can oxidize (i.e., the chloroperoxidases (CPO) can oxidize both Cl$^-$ and Br$^-$ and bromoperoxidases (BPO) can oxidize Br$^-$). HPO does not have the driving force to oxidize the fluoride, however a fluorinating enzyme, fluorinase, has recently been isolated and is proposed to act by an S_N2 mechanism.[9, 10]

On the basis of their cofactor requirement HPOs are classified into the following three groups: heme-containing, vanadium-containing[11] and "metal-free" haloperoxidases.[12] Among them, vanadium Haloperoxidase (V-HPO) appears to be the most prevalent.[11, 13]

The catalytic ability of HPOs attracts broad interest of industry for biotransformations and as bleaching enzymes for laundering. The use of heme-containing enzymes in this application has the disadvantage of unsatisfactory stability due to rapid oxidation and cleavage of the prosthetic heme ligand and low substrate specificity.[14] Therefore, the remarkably high stability of V-HPO against high concentration of organic solvents and elevated temperature[15, 16] and their availability from large-scale process or expression systems afford greater potential for industrial application.[17]

1. 2. Vanadium Haloperoxidase

Evidence of the involvement of vanadium ions in the vanadium-dependent haloperoxidase enzymes was first discovered by Vilter in 1984.[17, 18] The bromoperoxidase isolated from *Ascophyllum nodosum* was inactivated by dialysis in pH 3.8 citrate-phosphate buffer containing EDTA and was slowly reactivated by vanadate in suitable buffers.[17, 18] V-HPO have now been isolated from a number of marine algae[11] and also from some lichens[19] and fungi.[20] The vanadium iodo- and bromoperoxidases (V-IPO and V-BPO) are predominantly found in marine organisms,[21] while vanadium chloroperoxidases (V-CPO) originate mainly from terrestrial fungi.[22]

All the vanadium haloperoxidases isolated to date share some common features[23]: they are composed of one or more subunits of around 67 kDa; they can be inactivated by dialysis against EDTA at low pH; their activity is only restored by addition of vanadium (as vanadate) and they seem to have similar coordination of vanadium in the active site.

V-HPOs have been studied in great detail using a variety of biophysical techniques including ^{51}V NMR,[24] extended X-ray absorption fine structure[25, 26] and electron spin echo modulation.[27, 28] Yet, only limited structural information had been obtained from these experiments until the first X-ray structure was resolved.

1. 2. 1. X-ray Structures of V-HPOs

1. 2. 1. 1. Structure of V-CPO from *Curvularia inaequalis*

Concerning the V-HPO family, the vanadium chloroperoxidase from the pathogenic fungus *Curvularia inaequalis* has been most thoroughly investigated. The X-ray structure of its azide-substituted form was the first of this family to be solved.[29] Thereafter, the native form, the peroxide forms[30], the apo-form (metal-free form) and the tungstate-substituted form[31] also became available. Moreover, the determination of the four active site mutants structures (H404A, H496A, D292A and R360A)[32] shed light on the characteristics of the active site and the mechanism of the enzyme.[29-33]

1. 2. 1. 1. 1. Overall Structure of V-CPO

The protein contains 609 amino acids with a calculated molecular mass of 67,488 Da, and the gene has been cloned and sequenced.[34] Determination of the crystal structure of this enzyme revealed a molecule with an overall cylindrical shape measuring about 80×50 Å. The secondary structure is mainly α-helical with two four-helix bundles as main structural motifs (**Fig. 1**). The active site of the enzyme is located on top of the second four-helix bundle.[29-33] It should be noted that the overall protein structure of

3

V-CPO is rather rigid and remains nearly unchanged in all of the different forms compared with the native V-CPO.[30-32]
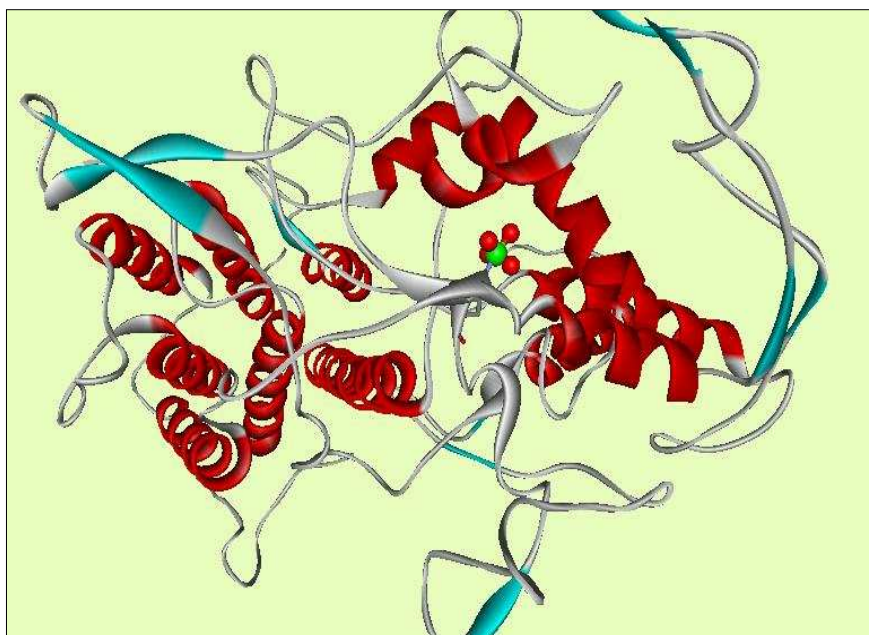
Figure 1. The 2.03Å crystal structure of V-CPO from *Curvularia inaequalis* (PDB ID: 1IDQ).[30] The figure was prepared with the program WebLab ViewerLite.

1. 2. 1. 1. 2. The Structure of Native Form of V-CPO

There are three positively charged groups at the active site: two guanidiniums from Arg 490, Arg 360 and one ammonium from Lys 353, all of which bind the cofactor hydrogen orthovanadate (HVO_4^{2-}) through electrostatic interaction (**Fig. 2**). Since charged groups of these residues are also good H-bond donors, they form, together with several amide–NH groups, a hydrogen bond network to the oxygen atoms of HVO_4^{2-}. The nitrogen (Nε2) of His 496 coordinates to vanadium and hence is the only direct bond from the protein to the metal center, generating a trigonal-bipyramidal geometry for the cofactor HVO_4^{2-}: a hydroxide and His 496 in the axial positions and three oxo moieties in the equatorial plane. The three equatorial V-O bonds are about 1.65 Å long, while the apical V-O bond length is 1.93 Å and the V-N bond is 1.96 Å (**Fig. 2**).[30, 31] Accordingly Coulomb interactions, H-bonds and coordination generate a highly organized receptor displaying a high affinity to HVO_4^{2-} with $K_d \sim 100$ nM.[35]

The active site forms a very rigid matrix designed for selective oxyanion binding, with relative affinities for $HVO_4^{2-} > HPO_4^{2-} > SO_4^{2-}$. The differences in the affinities for these oxyanions could results primarily from their capabilities to coordinate with the active site His 496, and further from the distribution of hydrogen bond donors in the protein in relation to the protonation state of the oxyanion.[32] From the ability to bind tungstate,[31] one may predict it to bond molybdate, as was shown for the V-BPO.[28]
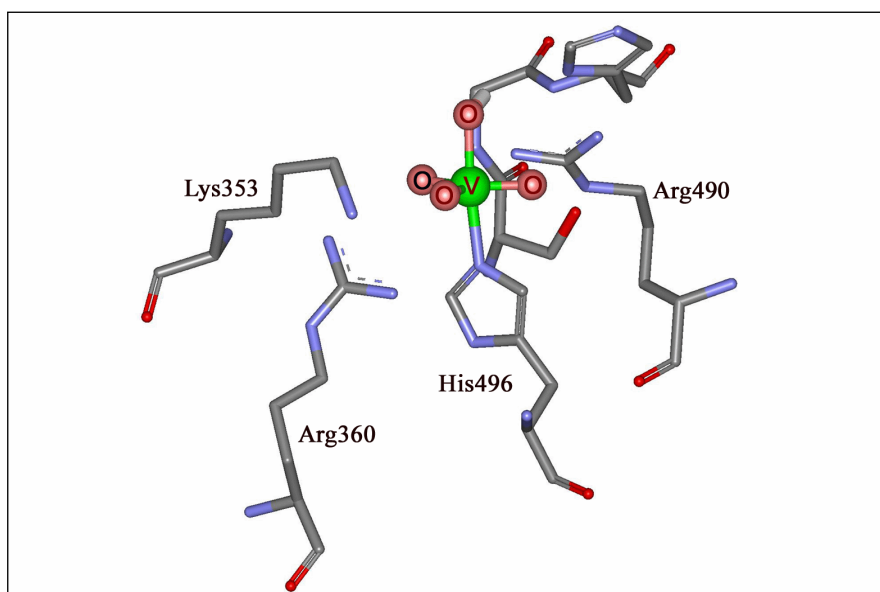
Figure 2. The active site of V-CPO from *Curvularia inaequalis* in the native form (PDB ID: 1IDQ).[30] The figure was prepared with the program WebLab ViewerLite.

1. 2. 1. 1. 3. The Structure of Peroxide Form of the V-CPO

The peroxide form was obtained by soaking the crystals in mother liquor containing 20nM H_2O_2. In the resulting 2.24 Å crystal structure (R = 17.7%), the peroxide is bound to the V in an η^2-fashion after the release of the apical oxygen ligand of the native state, thus vanadium is coordinated by four non-protein oxygen atoms and one nitrogen (Nε2) from His 496. The coordination geometry around the vanadium is a distorted tetragonal pyramid with the two peroxide oxygens O2 and O4 (bond lengths: V-O2 and V-O4 about 1.87 Å; O2-O4, 1.47 Å), one oxygen O3 (bondlength V-O3 1.93 Å) and the nitrogen (bond length V-N 2.19 Å) in the basal plane and one oxygen (V-O1, bond length 1.60 Å) in the apical position (**Fig. 3**).[30] It has been shown recently that the protein has a higher affinity to pervanadate than to vanadate.[36]
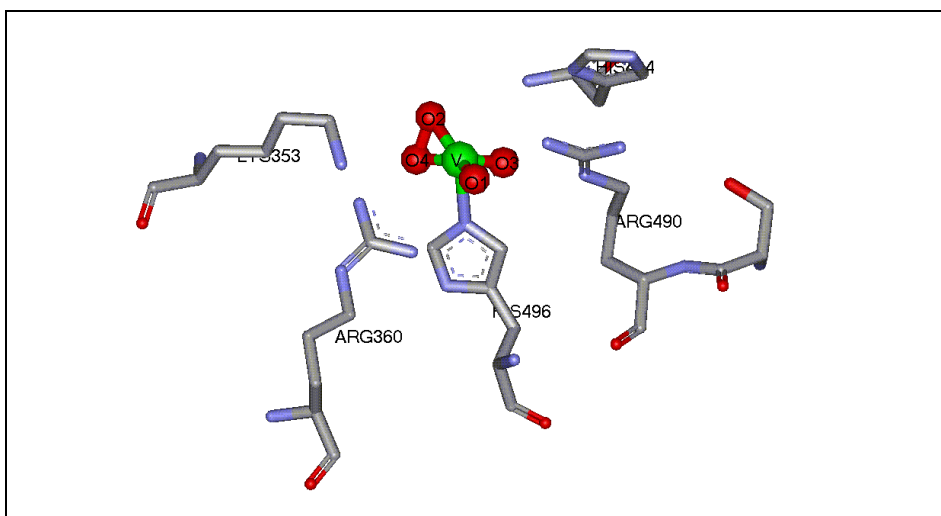
Figure 3. The active site of V-CPO from *Curvularia inaequalis* in the peroxide form (PDB ID: 1IDU) .[30] The figure was prepared with the program WebLab ViewerLite.

1. 2. 1. 2. Structural Comparison with other V-HPO enzymes

The X-ray structures of V-BPO from brown algae *Ascophyllum nodosum*(A-V-BPO)[14] in the native form and V-BPO from red algae *Corallina officinalis* (C-V-BPO) in the phosphate substituted form[37, 38] also became available recently. All the structures share a four–helix bundle motif known from V-CPO. Unlike V-CPO from *Curvularia inaequalis* crystallized as a monomer,[29] A-V-BPO shows a homo-dimeric structure[14] and C-V-BPO exists as a dodecameric form in solid state.[37] Although the sequence alignment among them show only very low similarity (21.5% sequence identity between V-CPO from *Curvularia inaequalis* and A-V-BPO,[14] 33% sequence identity between A-V-BPO and C-V-BPO[37]), the active sites are highly conserved in all three structures (**Fig. 4**), suggesting a common reaction mechanism.

(A)   **(B)**
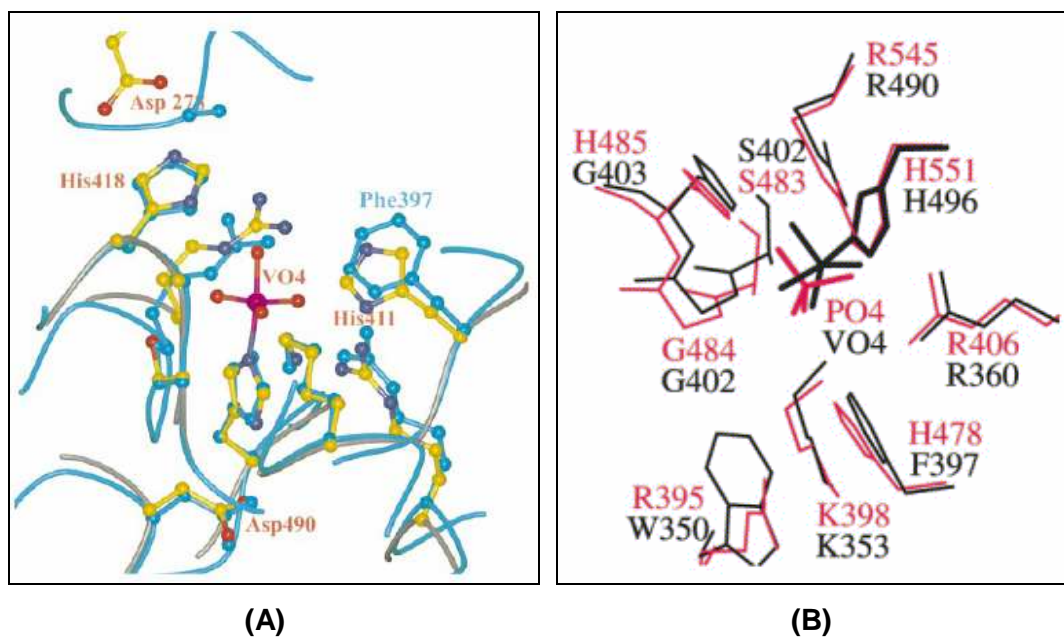
Figure 4. (A) The superposition of A-V-BPO and V-CPO structure near the active site. A-V-BPO residues in atom colors, V-CPO in cyan;[14] (B) The superposition of the active sites of the C-V-BPO enzyme (in red) and the V-CPO (in black).

1. 2. 2. The Proposed Mechanism of V-HPO

Since the vanadium (4+) or (3+) states have not been observed by EPR or K-edge X-ray studies in the presence of substrates or during turn over, and the reduced enzyme is inactive, apparently the redox state of the metal remains (5+) and does not change during the catalytic turnover. Hence it is believed that the vanadium ion plays the role of a strong Lewis acid with respect to the primary oxidant, H_2O_2.[28]

Mechanistic investigations have involved product analysis, kinetics, and have included studies of both the enzyme and the model systems. A general consensus currently exists for the mechanism for both the V-BPO and V-CPO catalyzed reactions and is described in **Scheme 1**.[39] The reaction proceeds initially by H_2O_2 addition, which is followed by protonation of the bound peroxide and addition of the halide, successively. Apart from direct evidence from the X-ray structure,[30] spectroscopic evidence for the enzymatic VO_2-O_2 intermediate was obtained using ^{17}O NMR spectroscopy.[40] There is no evidence however for an intermediate in which the halide binds to the vanadium atom.[41] The rate-determining step in the catalytic

cycle is the nucleophilic attack of the halide on the protonated protein-peroxide complex, generating a ("X^+") species, which immediately reacts with organic substrates and halogenates them. This step will generate singlet oxygen in the absence of RH, and has been investigated in detail with Cl^-, Br^-, and I^-.
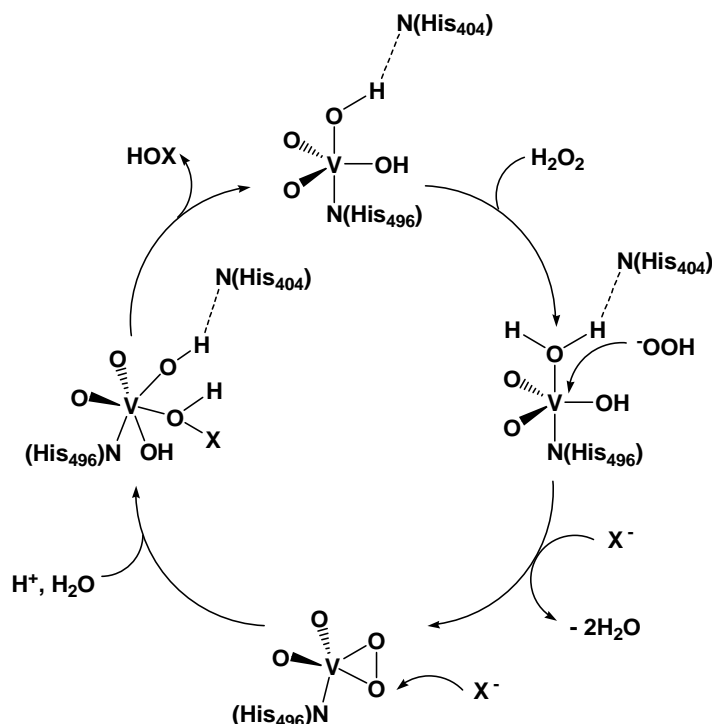
Scheme 1. Proposed mechanism of V-HPO catalysis.

Site-directed mutagenesis experiments (alanine scanning) have elucidated the relative importance of various active-site residues in catalytic activity.[42] His 496 is the primary chemical anchor for vanadium, and its replacement with Ala results in complete loss of activity. Substitution of the positively charged residues Lys 353, Arg 360, and Arg 490 revealed less severe effects, but of these mutants, the largest decrease in activity is observed for K353A. In fact, Lys 353 is the only residue which interacts with the peroxo-bound moiety directly. It has been suggested that it plays a role in polarizing the peroxo bond, making it more susceptible to nucleophilic attack.[30] The crystal structures indicate that Arg 490 is involved in two hydrogen bonds with oxygen atoms of the cofactor, both in the native and the peroxo forms, whereas Arg 360 donates only one hydrogen bond.[30] This difference agrees with a smaller catalytic efficiency of K353A and R490A as compared to the R360A mutant.

1. 2. 3. The Reactivity and Selectivity of the Reactions Catalyzed by V-HPO

Halogenation of monochlorodimedone (MCD) represents the standard assay for V-HPO, which was first developed to analysis the activity of heme-containing HPO.[43] The reaction is followed spectrophotometrically at 290 nm, monitoring the loss of MCD in the enol form ($\varepsilon = 20,000$ $M^{-1}cm^{-1}$).[11] In addition, phenol red is also used as a substrate to analyze the halogenation activity.[44]
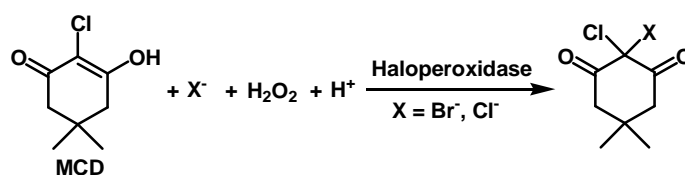
Scheme 2. Halogenation of MCD catalyzed by HPO.

However, the high reactivity of both substrates makes it impossible to distinguish whether the nature of the oxidized halogen intermediate is enzyme-trapped, enzyme-bound, or freely diffusible. Initial investigations into the reactivity of V-BPOs with various substrates, such as anisole or prochiral aromatic compounds failed to demonstrate any regio- or stereoselectivity upon bromination.[13, 45, 46] The apparent lack of selectivity at that time was interpreted to mean that V-BPO produces a diffusible oxidized bromine intermediate such as hypobromite, bromine or tribromide which would then carry out a molecular bromination reaction.[47] More recently, however, since more and more substrates have been tested, the chemo-, regio- and stereo-selectivity have been achieved to varying degrees and the selectivity seems to depend on the nature of the organic substrate.[13]

The competitive kinetic studies comparing the bromination of indole substrates by the V-BPO/H_2O_2/Br^- system to bromination by aqueous bromine (*i.e.*, the equilibrium mixture of HOBr $\rightleftharpoons$ Br_2 $\rightleftharpoons$ Br_3^-) under identical reaction conditions, showed that V-BPO-catalyzed reactions were not consistent with a freely diffusible brominating intermediate.[13, 48, 49] A competition experiment revealed that vanadium bromoperoxidase catalyzed preferentially the bromination and oxidation of indole derivatives over phenol red or MCD (equimolar mixtures). In contrast, the same reactions performed with aqueous bromine showed the simultaneous bromination of all substrates present in solution.[48-50]

The first regiospecific bromoperoxidative oxidation was reported by the group of Butler.[51] Both V-BPO enzymes from the marine algae *Ascophyllum nodosum* and *Corallina officinalis* catalyze the regiospecific oxidation of 1,3-di-tert-butylindole in a reaction requiring both H_2O_2 and Br^- as substrates, producing 1,3-di-tert-butyl-2-indolinone product nearly quantitatively. Although the product is unbrominated, a regioselective brominated intermediate is certainly involved (**Scheme 3**). By contrast, reactions with the controlled addition of aqueous bromine solution (HOBr = Br_2 = Br_3^-) produce three monobromo- and one dibromo-2-indolinone products, all of which differ from the V-BPO catalyzed product (**Scheme 3**).[48] Bromination and cyclization of terpenes is also reported by the same group.[52]
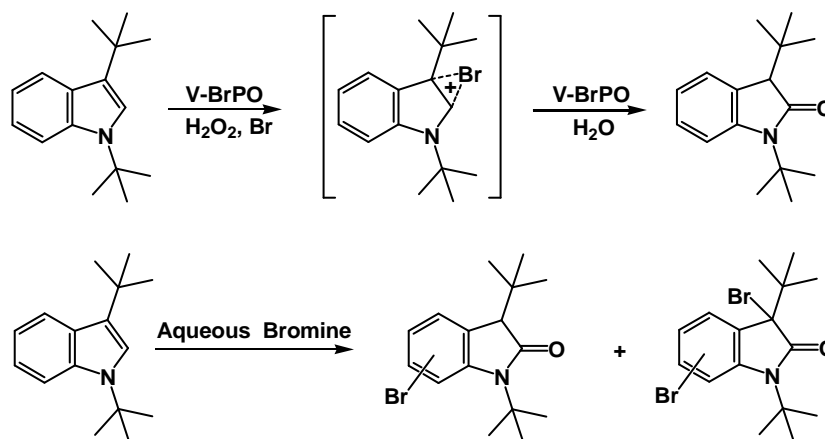
Scheme 3. V-BPO catalyzed regiospecific bromination of 1,3-di-*tert*-butylindole[51].

The only reported stereoselective reaction catalyzed by V-HPO is the oxidation of sulfides to sulfoxides in the absence of halides.[53-56] Depending on the substrate, up to 91% ee could be achieved, and different enzymes may produce different enantiomers from the same substrate (**Scheme 4**). However, the selectivity of sulfoxidation is exclusive to the marine algal V-BPOs, since V-CPO catalyzes the formation of a racemic mixture of the sulfoxide.[53-56] The reactivity of V-BPO (*A. nodosum* and *C. pilulifera*) to produce different enantiomers suggests that subtle differences in the substrate channel near the vanadium-binding site of these enzymes.[13]
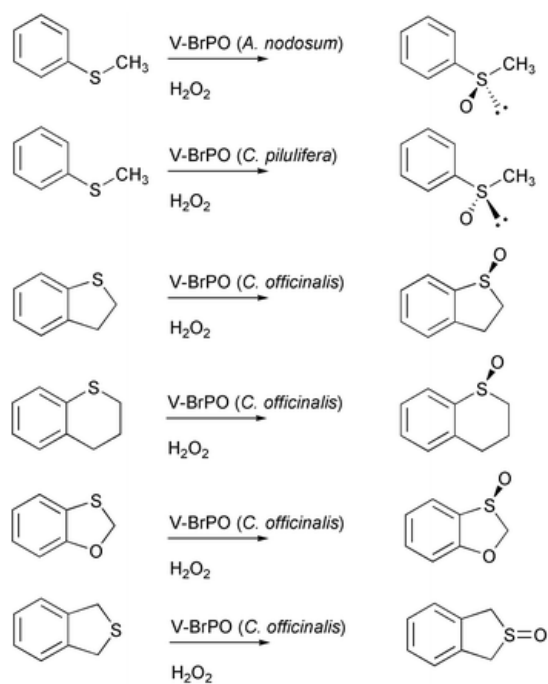
Scheme 4. V-BPO catalyzed enantioselective sulfoxidation.

1. 3. From V-HPOs to Acid Phosphatases

1. 3. 1. Structural Similarity

Interestingly, the amino acid sequence of the active site of vanadium haloperoxidase is conserved in a completely different group of enzymes, the acid phosphatases. Sequence motifs are shared between V-CPO and several lipid phosphatases, the mammalian glucose-6-phosphatase, bacterial nonspecific acid phosphatases and the *Drosophila* development protein Wunen.[57-59] The sequence alignment of several V-HPOs and acid phosphatases are shown in **Fig. 5 A**, from which a dendrogram can be drawn (**Fig. 5 B**).[57]
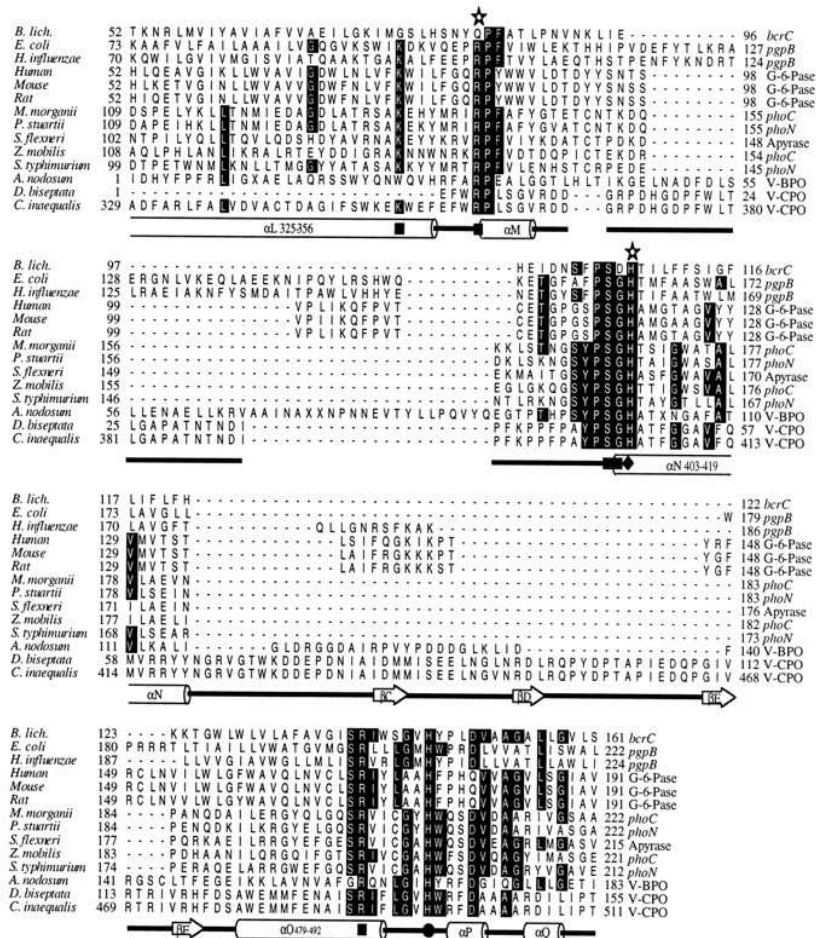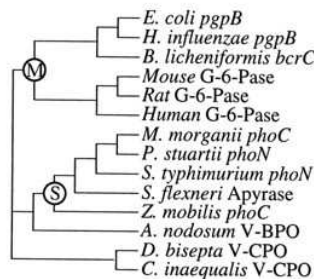
Figure 5. (A) Alignment of V-CPO of *C. inaequalis* with the enzymes proposed to contain a structurally similar active site. The residues contributing to the active site of V-CPO are given underneath the alignment together with the secondary structure elements in which they are present. ■, Residue hydrogen-bonded to vanadate in V-CPO; ♦, histidine proposed to be the acid-base group of -CPO. ●, histidine coordinated to vanadate in V-CPO; ☆, residue shown to be essential for glucose-6-phosphatase (G-6-Pase) activity; ▭,α-helix; ⇨, β-sheet; —, loop. (*B*) A dendrogram based on the alignment. The group of membrane-bound phosphatases is marked with an M, and the group of soluble phosphatases is marked with an S.[57]

The structural similarity of the active sites of V-HPOs and acid phosphatases is also reflected by the fact that phosphate inhibits or inactivates VHPOs and vanadate inhibits the phosphatases.[60-62] This similarity has been confirmed by structural determination of an acid phosphatase from *Escherichia blattae*[63] and its structural comparison with V-CPO (**Fig. 6**).[61] Striking similarities are also observed from the X-ray structure of the rat prostatic acid phosphatase which has been co-crystallized with a vanadate at its active site.[64, 65]
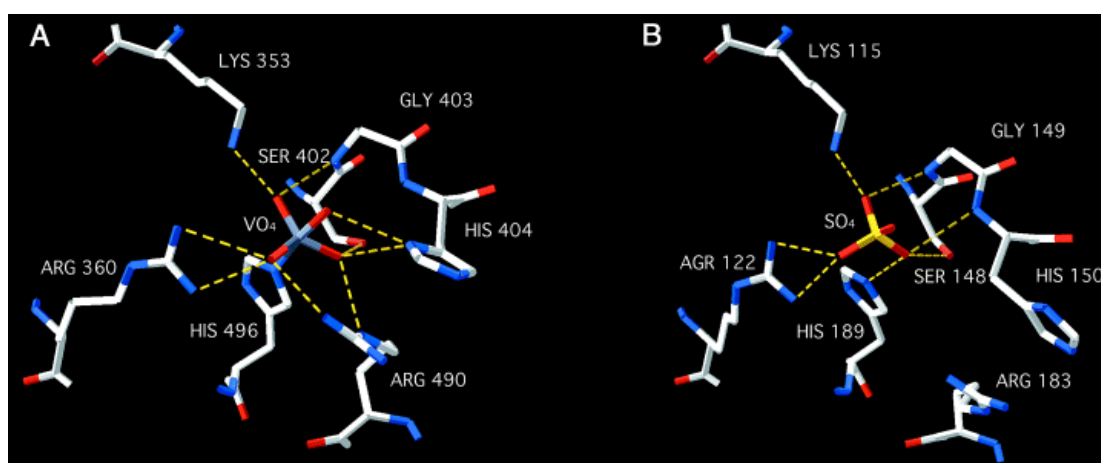
Figure 6. Structure of the active site of (A) vanadium chloroperoxidase from *C. inaequalis* (PDB ID: 1 IDQ) and (B) the acid phosphatase from *E. blattae* (PDB ID:1D2T). The phosphatase cocrystallized with sulfate.[66]

1. 3. 2. Dual Functions

V-HPOs and phosphatases have different biological functions. The former catalyze the oxidation of halide, whereas the later catalyze the hydrolysis of phosphoester and phosphor anhydride bond. As previously described, since these two different types of enzymes share the same supramolecular environment at their active sites, hence it is reasonable to assume that both of them may exhibit the dual activities. Indeed, as Wever *et al*. showed that phosphatase activity can be observed using the apo-protein of V-CPO isolated from *C. inaequalis*;[36, 57, 62, 67] kinetic data, however, indicates that the active site of this V-CPO is not optimized for phosphatase activity. The possibility that peroxidase activity could be observed for vanadate-incorporated phosphatases has been investigated for several systems. The first observation of chloroperoxidase

activity was reported with phytase, added vanadate and H_2O_2.[68] Since then reports have been made demonstrating that other phosphatases can be converted to peroxidases in the presence of vanadate and H_2O_2.[61, 68-72] Thus, at this time the analogy between these classes of enzymes includes both structural and catalytic aspects. However, the detailed structural requirement for these two reactions is still slightly different. As shown by mutation study of V-CPO, the mutant H404A can still oxidize bromide but phosphatase activity is completely lost.[36]

A major issue at the present time (and in the future) is whether the dual activity of these enzymes observed *in vitro* extends to the function and role of these enzymes *in vivo*.[73]

1. 4. Vanadate as Phosphate Analogy

Phosphate esters and anhydrides dominate the living world. DNA and RNA are phosphodiesters; most of the coenzymes are esters of phosphoric or pyrophosphoric acid; the principal reservoir of biochemical energy is adenosine triphosphate (ATP); phosphorylation and de-phosphorylation is most important means of signal transduction; many intermediary metabolites are phosphate esters, and phosphates or pyrophosphate are essential intermediates in biosynthesis and degradation.[74] Vanadate has long been recognized as a structural and electronic analogue of phosphate, encompassing the tetrahedral ground state and the penta-coordinated excited state, which is the chemical base of the wide range of vanadate biological activities.[73]

1. 4. 1. Comparison of Tetrahedral Form: the Ground State Analogy

Vanadate and phosphate analogy is most evident in the tetrahedral trianionic forms (VO_4^{3-} and PO_4^{3-}) as demonstrated by their similar protonation reactions (**Eq. 4-6**).[75, 76] However, the similarities of the pK_a values for vanadate (3.5, 7.8, and 12.5)[77] with those of phosphate (2.1, 7.2, and 12.7) document that the analogy also extends from structural to the electronic properties of these species.[62, 73, 75, 76]

$$H_3VO_4 + H_2O \rightleftharpoons H_2VO_4^- + H_3O^+ \quad \text{pKa } 3.5 \qquad (4)$$

$$H_2VO_4^- + H_2O \rightleftharpoons HVO_4^{2-} + H_3O^+ \quad \text{pKa } 7.8 \qquad (5)$$

$$HVO_4^{2-} + OH^- \rightleftharpoons VO_4^{3-} + H_2O \qquad \text{pKa } 12.7 \qquad (6)$$
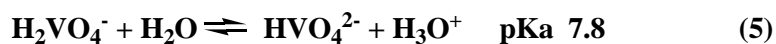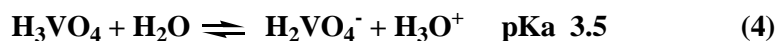
Given the central role of phosphate and phosphates in biology, a wide range of effects of two classes of V-compounds, vanadate anhydrides and vanadate esters, can be envisioned.

1. 4. 1. 1. Vanadate Anhydrides as Structural Analogues of Condensed Phosphates

In aqueous solution, vanadate undergoes a number of hydrolytic and self-condensation reactions. The equilibria within the various vanadate species (**Fig. 7**) are very sensitive to pH, concentration and ionic strength (**Fig. 8**). Around neutral pH, $H_2VO_4^-$ and HVO_4^{2-} oligomerize to form dimeric, tetrameric, and pentameric species.[78-80] These vanadate anhydrides are analogues of pyrophosphate, oligomeric, and polymeric phosphate anhydride. They readily undergo exchange in aqueous solution,[81, 82] whereas pyrophosphate and the corresponding oligomeric phosphate derivatives are stable and kinetically inert.
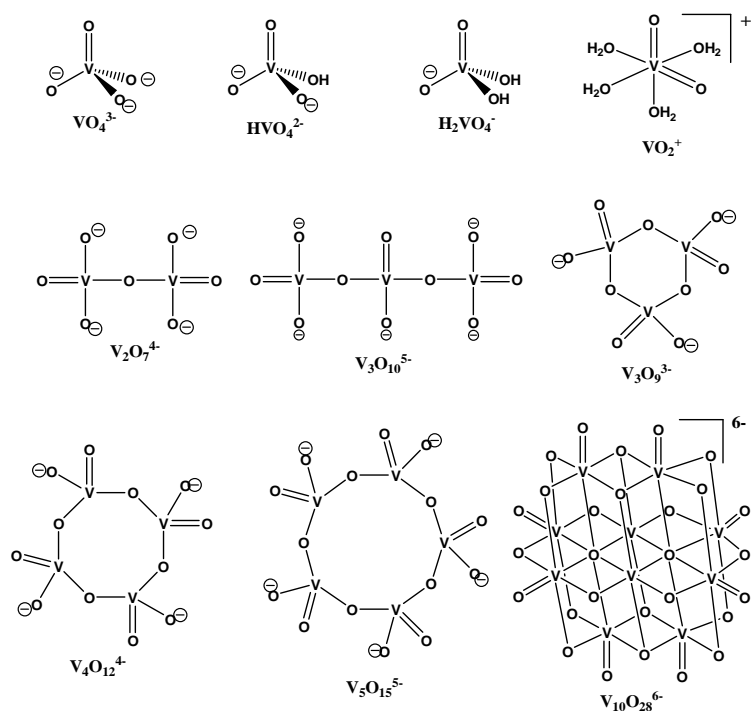
Figure 7. Aqueous structures for the major vanadate species.
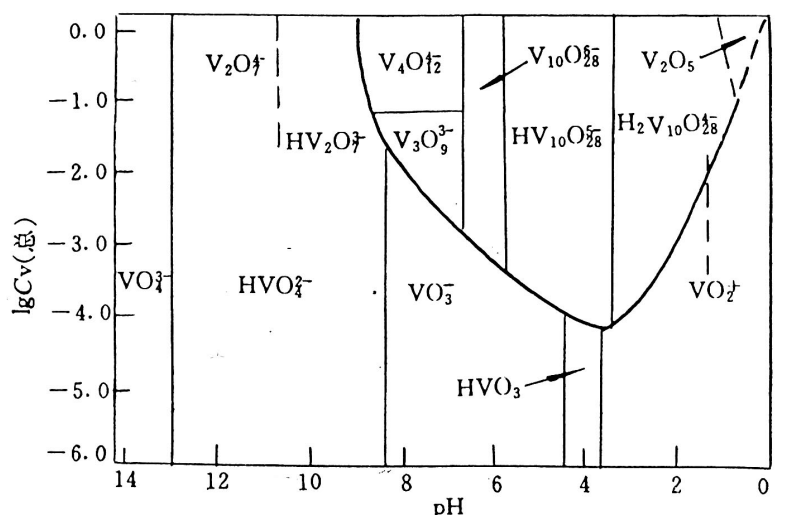
Figure 8. Phase diagram showing the distribution of vanadate species as a function of pH and total Vanadium concentration.

The tetrameric and pentameric vanadates are cyclic in solution and fail to show a structural analogy with the biologically interesting linear phosphates. The linear trivanadate $V_3O_{10}^{5-}$ has been observed in solution by ^{51}V NMR spectroscopy in the pH window of 8.8 to 9.2 at high ionic strength.[83] However, importantly a linear vanadate trimer was recently reported binding to phosphatase PhoE from *Bacillus stearothermophilus*.[84] Prior to this report, the structural analogy of these homovanadates were limited to the analogy between pyrophosphate and the vanadate dimer in purely inorganic systems.[85] No information is currently available on systems that support four-coordinate vanadium in a basic O_3POVO_3 unit.

The most important anhydrides analogues are those of ADP, ATP, and other nucleotides. Although a range of ADP and ATP analogues have been prepared in aqueous solution and spectroscopically observed, the most useful analogues are AMPV and ADPV. Applications of both these analogues as probes have been met with some success, particularly when the analogue is binding in allosteric sites.[86-88]

ADPV   **AMPV**
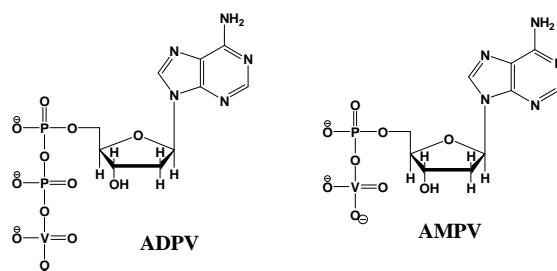
1. 4. 1. 2. Vanadate Esters: Functional Analogues of Phosphate Esters

Vanadate esters form readily in aqueous solution and are found to be enzyme substrates for a range of phosphate-involving enzymes including dehydrogenases, isomerases, and aldolases. One example of vanadate ester formation is the reaction between D-glucose and vanadate. D-Glucose contains one primary and several secondary hydroxyl groups that can form vanadate esters. Indeed, many species form in such solutions as indicated by ^{1}H and ^{13}C NMR spectroscopy (data not shown). However, as was shown first by Gresser, the small amount of glucose-6-vanadate that forms is recognized by glucose-6-phosphate dehydrogenase.[89, 90] In **Scheme 5**, the proposed conversions are shown, explaining the rapid oxidation of D-glucose to D-gluconate that does not take place at an appreciable rate in the absence of the vanadate unit.
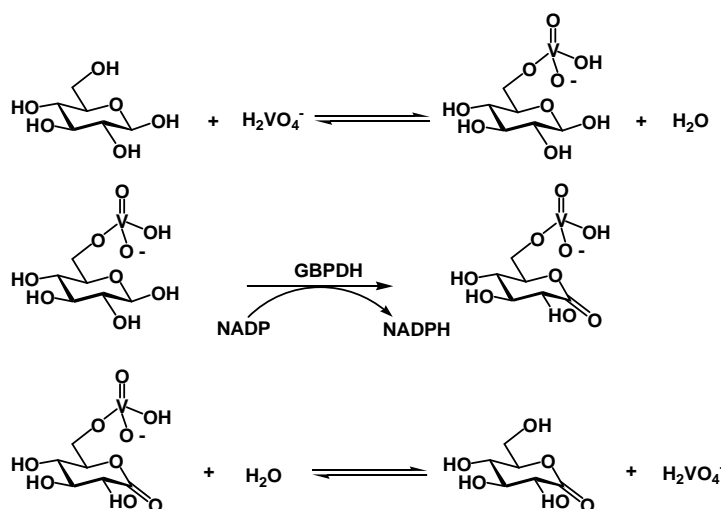
Scheme 5. Reaction of D-glucose with vanadate to form D-glucose-6-vanadate, a substrate for glucose-6-phosphate dehydrogenase. The oxidation of D-glucose catalyzed by glucose-6-phosphate dehydrogenase is shown next, followed by the hydrolysis of the vanadate ester.

1. 4. 1. 3. Differences

One difference between vanadate and phosphate is that near neutral pH the vanadate monomer exists primarily as a monoanion ($H_2VO_4^-$), while phosphate exists primarily as a dianion (HPO_4^{2-}). In contrast to the high stability of H_3PO_4, the existence of

H_3VO_4, although occasionally inferred, has not been documented,[78-80] presumably reflecting the conversion to VO_2^+, which is the major species of aqueous vanadate solutions at pH 1. Thermodynamic evidence has now been provided suggesting that the high stability of VO_2^+ is due to the increased coordination number of the hydrated form as compared to H_3VO_4.[91]

Another difference lies in the fact that, under physiological conditions, vanadates can undergo redox chemistry[92] while phosphates do not. The most important difference, however, is that penta-coordinated phosphate is thermodynamically unstable and are only inferred as high-energy intermediates, whereas vanadate can accommodate a higher stable coordination number, which accounts for the notion that penta-coordinated vanadates are analogues of penta-coordinated phosphate transition state.[93]

1. 4. 2. Penta-Coordinated Vanadate:Transation State Analogy of Phosphate

A large variety of phosphate-metabolizing enzymes including phosphatases, mutases, ATPases, kinases, lyases, synthases and some ribonucleases, catalyze phosphoryl transfer reactions, and share the same mechanism involving the formation of penta-coordinated phosphate as high-energy transition state. In general, these enzymes are potently inhibited by vanadate due to the chemical similarities between vanadate and phosphate combined with the ability of vanadate to readily undergo changes in coordination geometry (**Fig. 9**).[73, 94, 95]

high-energy transition state   stable state
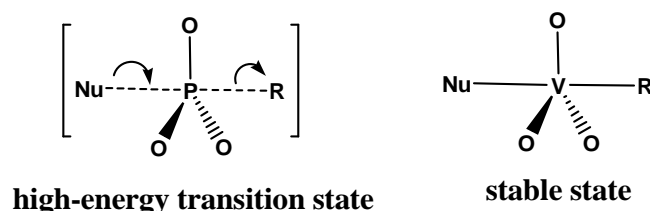
Figure 9. Schematic representation of penta-coordinated phosphate transition state and its vanadate analogy.

This unique feature of vanadate was first proposed more than 30 years ago,[96] and has been confirmed by structural determination of a broad variety of enzymes which have

been co-crystallized with a vanadate. 39 structures including protein-vanadate complexes are available from the Protein Data Bank till September 7, 2004. Twenty one of them have been classified as representing transition state. All of the vanadate complexes classified as transition state mimics exhibit trigonal bipyramidal or distorted trigonal bipyramidal geometry at vanadium, and at least one bond between the vanadium atom and atoms of the enzyme or substrate molecules.[94] The incoming "nucleophile" normally occupies one of the two apical positions of the trigonal bipyramidal vanadium complex. Based on the different electron donor in the active site, these enzymes therefore will show some variation in their interaction with the V-compounds (**Fig. 10**). For example, the alkaline phosphatase has a nucleophilic serine residue in the active site whereas some other protein phosphatases have a cysteine residue as nucleophile, and the acid phosphatases contain a histidine residue in the active site which bond vanadate similarly as VHPOs, which was described in **part 1.3**.
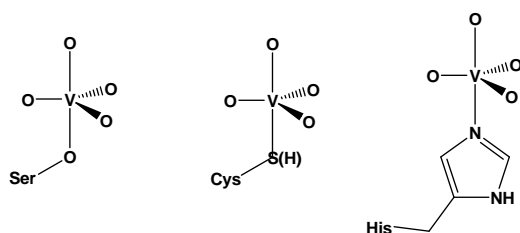
Figure 10. Schematic representation of different types of penta-coordinated vanadate as transition state analogue of different phosphate metabolizing enzymes.

1. 5. Coordinating Bond or Covalent Bond: Implication from X-ray Structures

The bond characteristic of the unique V-N linkage between the nitrogen (Nε2) of His-496 and vanadate at the active center of V-CPO was assigned as a covalent bond,[14, 29, 30, 32] although the original X-ray data may not exclude a more likely interpretation, that this is a coordinating bond. Actually, due to its special electronic property, histidine is often chosen by nature as a bio-ligand to bind metals at various enzyme active sites, via **coordinating bond**, such as that in the hemoglobin.[97, 98] The only confirmed covalent his-metal bond appeared in the biological system is the copper-zinc superoxide dismutase (CuZnSOD) enzyme, where a deprotonated histidine is

bound to a zinc and a copper ions simultaneously. However, two close metal ions is essentially required to form such a covalent bridge as shown in **Fig. 11**.[99-102]
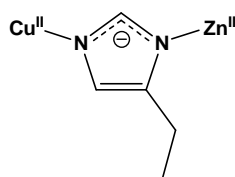
Figure 11. Schematic representation of "bridging imidazolate" of cupric form of CuZnSOD.

The comparison of the V-N bond of V-CPOs with other enzyme-trapped penta-coordinated vanadate should lead to a better understanding of the nature of this bond, since they are all formed from tetrahedral vanadium(5+) by accepting a fifth ligand without changing the oxidation state. If this newly formed bond is coordinating, the original V=O double bond should remain at one of the equatorial position, as shown in **Fig. 12** (Type 1); otherwise, all the five bonds are single bonds if the newly formed fifth bond is covalent bond (see **Fig 12**,Type 2). The bond order is visualized by the bond lengths as listed in **Table 1**. The length of the equatorial bonds of all available structures belonging to V-HPOs family (all type 1 in **Table 1**) is significantly shorter than that of type 2, reflecting there is one double bond exists for type 1, which may be averagely delocalized within the 3 equatorial bonds. Therefore, we suggest the V-N bond of V-CPO is a coordinating bond.
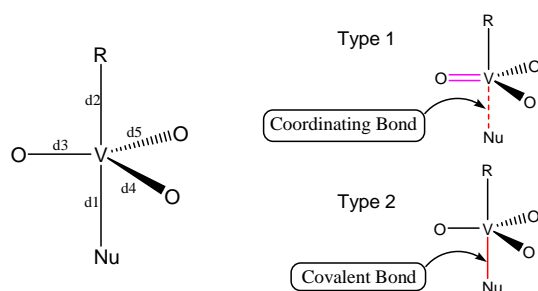
Figure 12. The schematic view of two different type penta-coordinated vanadate depending on the different nature of the fifth bond (marked in red).

Name/Type	PDB	Resol.	Nu	d1 (Å)	d2 (Å)	d3 (Å)	d4 (Å)	d5 (Å)	Ref.
VCPOs Native/1	1IDQ	2.03 Å	His	2,075	1,881	1,600	1,653	1,608	[30]
VCPOs Recombinant/1	1VNI	2.15 Å	His	1,940	2,147	1,600	1,600	1,608	[32]
VCPOs H404A/1	1VNG	2.20 Å	His	1,956	2,002	1,592	1,598	1,590	[32]
VCPOs R360A/1	1VNF	2.35 Å	His	2,006	1,774	1,585	1,609	1,622	[32]
VCPOs D292A/1	1VNE	2.15 Å	His	1,974	2,196	1,590	1,604	1,601	[32]
VBPO-Dimer-A/1	1QI9	2.05 Å	His	2,111	1,771	1,690	1,517	1,604	[14]
VBPO-Dimer-B/1	1QI10	2.05 Å	His	2,111	1,772	1,543	1,590	1,575	[14]
VCPO-N3/1	1VNC	2.10 Å	His	2,249	1,982	1,535	1,641	1,667	[29]
Alkaline-Phosphatase/2	1B8J	1.90 Å	Ser	1,721	1,921	1,771	1,719	1,721	[103]
Estrogen-Sul-transferase/2	1BO6	2.10 Å	5'-phosphate of PAP	2,079	1,990	1,662	1,691	1,676	[104]
Phospho-Glucomutase/2	1C4G	2.70 Å	Ser	1,880	2,007	1,731	1,738	1,714	[105]
Yersinia PTPase/2	(a)	2.2 Å	Cys	2.520	1.940	1.61	1.68	1.71	[106]
BovineLow MwPTPase/2	(b)	2.20 Å	Cys	2,160	1,720	1,600	1,620	1,620	[107]

Table 1. The statistic bond-length on the different 2 types penta-coordinated vanadate in enzyme.[a] Data from personal communication with Prof. Mark A. Saper at University of Michigan; [b] Data of bond length from the original publication; structural data of both [a] and [b] are not available at PDB.

1. 6. Synthetic Models of V-HPOs

Evidence of the involvement of vanadium ions in V-HPOs and its particular activity have stimulated interest in synthesizing biomimetic structural and functional models.[39, 73, 108-111] A *structural* model allows deduction of site characteristics by possessing sufficiently high adherence to the indicated features via spectroscopic comparison, which is especially valuable to reveal possible coordination characteristics at the active site before the high resolution crystal structure of the enzyme is available. A *functional* model sustains a stoichiometric, or better, a catalytic reaction which transforms substrate to product as does the enzyme, albeit at a different rate and not necessarily with the natural substrate specificity. A functional

model is not ineluctably a structural model, but, ideally, a high-fidelity structural **and** functional model will certainly leads to the ultimate goal of bioinorganic research: definition of function in terms of structure. [112, 113]

1. 6. 1. Structural Models of V-HPOs

Two general categories of complexes have been described as structural model complexes for haloperoxidase enzymes. The first class is defined as compounds containing V (5+) and even (4+) bound to ligands with O and N donors and almost all of them contain V-O-R covalent bonds as vanadate ester or mixed vanadate-carboxylic anhydrate; some examples are shown in **Fig. 13**. The largest group within this class of compounds is the Schiff base complexes. More than 200 crystal structures of V-containing Schiff bases can be found in a search of the crystallographic database and document the widespread interest in these types of compounds.[39, 114, 115]
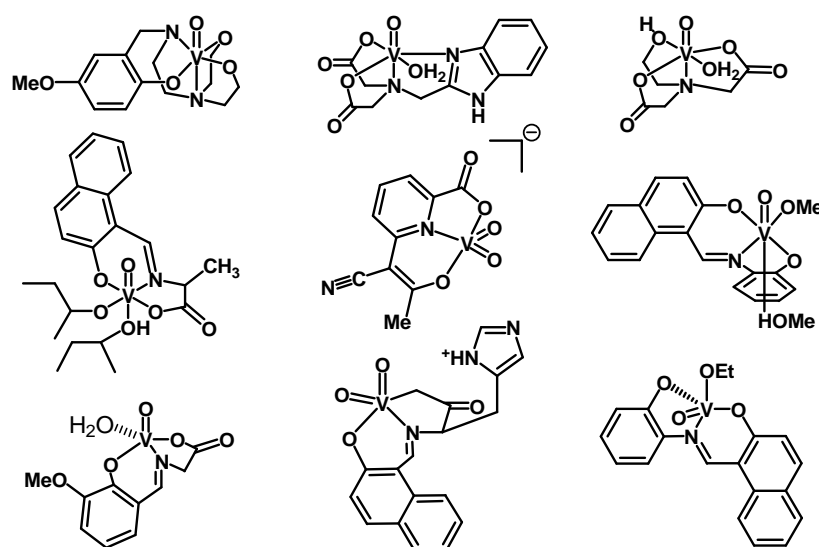
Figure 13. The selected vanadium complexes with O and N donors supposed to be structural models of V-HPOs.

The second class of model complexes includes peroxovanadium complexes. These complexes are of interest because vanadium peroxide is involved as an intermediate in the catalytic cycle of the VHPO reaction, and the peroxide form of V-CPO has been confirmed by crystal structure determination.[30] A wide range of peroxovanadium

complexes have been reported, and several reviews are dedicated to the discussion of the structure and chemistry of these systems. [73, 116, 117]

Combined methods using [51]V NMR spectroscopy, potentiometric data (glass electrode), electro spray ionization-mass spectrometry (ESI-MS), and ab initio calculations have been found to be excellent tools for obtaining direct information about the structure and chemistry of peroxovanadates in solution.[117-121] The number of peroxo groups and the auxiliary ligand that are coordinated to the vanadium atoms dictate the structures (and reactivity) of the peroxovanadium complexes. The peroxo group is bound side-on to the V(V) atom with V-O bond lengths on the order of 1.85 Å and O-O bond lengths of about 1.4 Å. Complexes are known with one, two, three, and four peroxo groups, although only the two former classes of complexes are found under the conditions required of functional mimics. Coordination numbers around the vanadium are generally 6 or 7, and the elaborate dimeric structures often fall apart upon dissolution of the compounds. However, detailed speciation has been characterized for a few simple systems, and this area has been recently reviewed.[122]

It is worth to note that there is one example in which the intramolecular hydrogen bond was taken into the consideration for the design of structural model.[123] However, the stability of the overall complex is still mainly contributed from the covalent bonds between vanadate oxygen and ligands, as shown in **Fig. 14**.
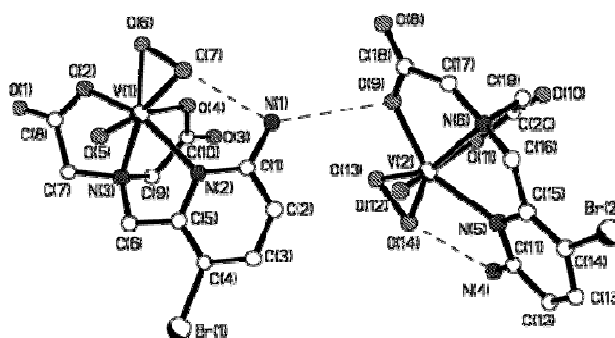
Figure 14. The ORTEP view of [VO(O$_2$)(^{BrNH2}pyg$_2$)]$^-$. Hydrogen bonds in dashed lines. All protons have been omitted for clarity. [123]

The structural information regarding the haloperoxidases active sites have now shown that these complexes are poor structural model systems.[39, 73]

1. 6. 2. Functional Models of V-HPOs

Initial studies on functional mimics of V-HPO were driven by the lack of spectroscopic techniques capable of observation of the vanadium site in the enzyme. Nevertheless, effective modeling of the V-BPO activity was obtained for *cis*-dioxovanadium (VO_2^+) in acidic aqueous solution by Butler and co-workers.[124, 125] Previously, oxidation of iodide under similar condition had been reported.[126] With this system, a detailed mechanism involving H_2O_2 binding to V, followed by bromide oxidation was proposed, similar to V-HPOs. Two important differences between this system and V-HPO are that a dinuclear species, $V_2O_2(O_2)_3$, was implicated as the active catalyst and strongly acidic conditions are required for activity (pH $\leq$ 2). The identification of dimeric active species was based on the fact that (1) the rate of halide oxidation showed clear second order dependence on [V], and (2) a maximum rate was observed under pH and H_2O_2 concentrations where $VO(O_2)^+$ and $VO(O_2)^-$ were equal, and thus, the concentration of the dimeric $V_2O_2(O_2)_3$ is maximized, **Eq. 7-9**. The proposed mechanism for this reaction is outlined in **Scheme 6.**

$$VO_2^+ + H_2O_2 \rightarrow VO(O_2)^+ + H_2O \qquad K_1 \qquad\qquad (7)$$

$$VO(O_2)^+ + H_2O_2 \rightarrow VO(O_2)^- + 2H^+ \quad K_2 \qquad\qquad (8)$$

$$VO(O_2)^+ + VO(O_2)^- \rightarrow V_2O_2(O_2)_3 \qquad K_3 \qquad\qquad (9)$$
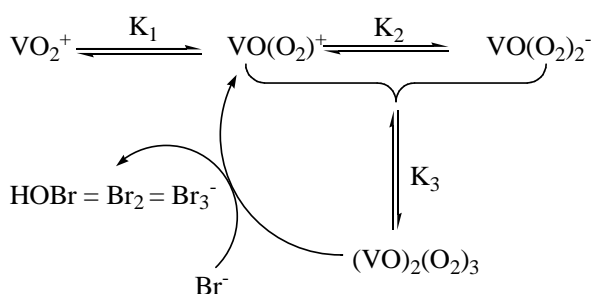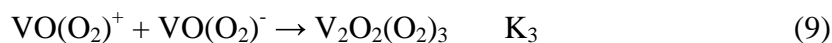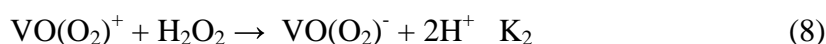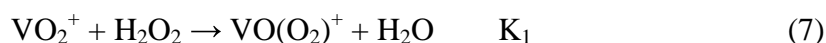
Scheme 6. Proposed mechanism of halide oxidation by $V_2O_2(O_2)_3$.[127]

While the structure of $V_2O_2(O_2)_3$ is not known, Pecoraro proposed the structure of the active $V_2O_2(O_2)_3$ to have an asymmetrically bridging peroxide of the form shown in **Fig. 15 (B)**,[128]based on the ^{51}V-NMR study in acetonitrile[129] and the crystal structure of tetraperoxo dimmer (**Fig. 15 (A)**)[130]. In **Fig. 15B**, the second vanadium could very well function as a "giant proton", activating the diperoxovanadate complex toward nucleophilic attack by the halide, comparable to the proton in the monomeric complexes, as suggested for V-HPOs.[128]
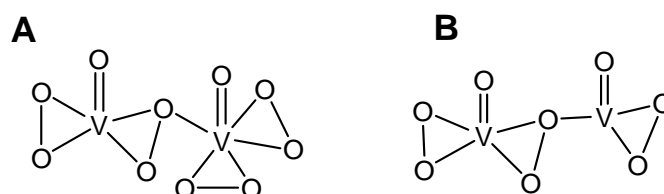
Figure 15. Drawing of (A) $V_2O_2(O_2)_4^{2-}$ and (B) proposed coordination of $V_2O_2(O_2)_3$.

Conte and co-workers designed a two-phase system (H_2O-$CHCl_3$ or H_2O-CH_2Cl_2); products analysis, ESI-MS and ab initio calculations were carried out to provide evidence for the hypobromite-like V-complex.[131-133]

These studies importantly demonstrated that not only do systems exist that mimic the enzyme reaction, but if the simple ion can catalyze this reaction, complexing ligands should be able to enhance and/or retard this reaction. Since then, a range of systems have been reported competent to carry out this reaction.[39, 73, 108, 114, 115, 117, 134] These complexes include the first monomeric complexes LVO(OEt)(EtOH) (L = N-(2-hydroxyphenyl)salicylideneamine or N-(2-carboxyphenyl)salicylideneamine) (**Fig. 16**) reported by Butler and co-workers, which showed that the bromination of the organic substrates proceeded exclusively via an electrophilic mechanism and involved no radical intermediates.[135]
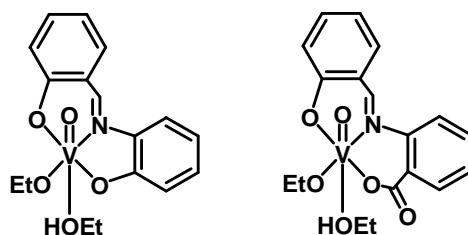
Figure 16. Drawing of LVO(OEt)(EtOH)[135]

Pecoraro and co-workers designed a model system with ligands which completed the coordination sphere of an oxoperoxovanadium unit.[128, 136-138] These most completely studied model compounds have been with tetradentate tertiary amine complexes containing different combinations of carboxylate, amine, alcohol, amide, or pyridyl donors (**Fig. 17**). The most efficient complex of this class, $[VO(O_2)Hheida]^-$, in the presence of excess acid and peroxide, up to 10 turnovers were accomplished within 3 min, and thus increased the rate of reaction by at least an order of magnitude greater than that observed for Butler's systems. The starting dioxovanadate complexes (VO_2L', L'= tetradentate ligand) and oxoperoxovanadate complex ($VO(O)_2L'$) (**Fig. 17**) have been isolated and structurally characterized. In addition, the kinetics of peroxide binding to the complex[136] and the kinetics of subsequent halide oxidation[137, 138] have been measured and a detailed mechanism proposed. These systems also catalyze O_2 formation in the absence of an organic substrate, similar to enzymes. Studies with $H_2^{18}O_2$ showed persuasively that the oxidation of bromide produced O_2, which was completely labeled with ^{18}O and thus indicated that peroxide is oxidized without oxygen-oxygen bond cleavage.[137] One key point with the kinetic studies of the VO_2L' complexes is that the reactions were run in acetonitrile. This less polar solvent was vital, since chloride, bromide and iodide oxidation were not observed under any aqueous conditions. Both bromide and iodide can be oxidized in acetonitrile, but chloride oxidation was not achieved in water or acetonitrile.

heida ligand **ada ligand** **nta ligand** **bpg ligand**
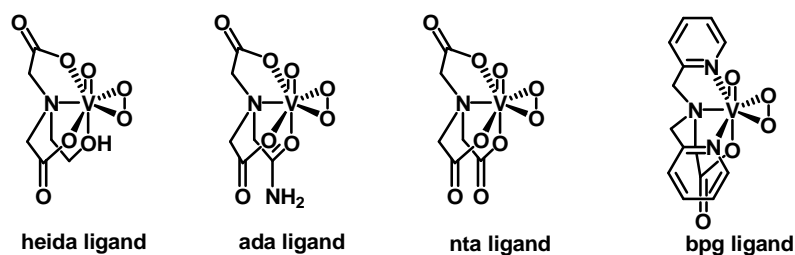
Figure 17. Oxoperoxovanadate complex ($VO(O)_2L'$) and the abbreviation (H_2heida = *N*-(2-hydroxyethyl)iminodiacetic acid; H_2ada = *N*-(2-amidomethyl)iminodiacetic acid; H_3nta = nitrilotriacetic acid; Hbpg = *N,N*-bis(2-pyridylmethyl)glycine.) of the ligand.

The kinetics of peroxide binding to the VO_2L' complexes to form the oxoperoxo complex, $VO(O_2)L'$, are first order in VO_2L'. In the absence of acid, Michaelis-Menton behavior was observed upon H_2O_2 addition, indicating the formation of a reversible $VO_2L' \cdot H_2O_2$ intermediate. Upon addition of acid, the Michaelis-Menton behavior is greatly diminished or disappears completely (depending on ligand and

acid concentration), and a first order dependence on H_2O_2 concentration is observed. The proposed mechanism for peroxide binding is summarized in **Scheme 7**.[136]
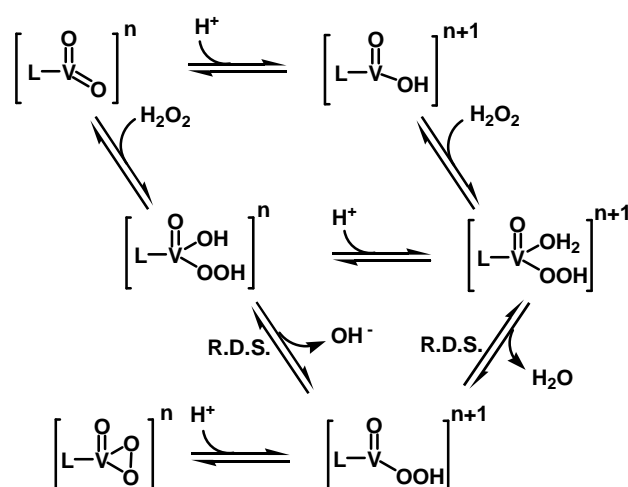
Scheme 7. Proposed mechanism for peroxovanadium complex formation.[136]

The kinetics of halide (Br^-, I^-) oxidation are first order in peroxovanadate complex and halide. Based on kinetic, UV-vis and NMR analysis, there is no evidence of halide binding to the complexes at any point during the reaction. One very important factor for achieving halide oxidation in acetonitrile is the need for one equivalent of acid. In the absence of acid, no reaction occurs. These results suggest that the complexes must be protonated (presumably at the peroxide) to become active. By studying the rate dependence on acid, estimated pK_a's for the protonated peroxovanadate complexes in acetonitrile have been obtained and range from 5.5-6.0, depending on the ligand. For comparison, the pK_a's of HI and HBr in acetonitrile are also in this range, while the pK_a of HCl is ca.9. Thus, Pecoraro provided an explanation for the lack of chloride oxidation in acetonitrile is that the chloride buffers the reaction, preventing the formation of the active protonated peroxovanadate complex.[137, 138]

Based on these studies, the mechanism in **Scheme 8**, has been proposed for the Pecoraro's model complexes. This mechanism is also consistent with enzymatic studies, where it was shown that the halide oxidation step proceeds faster at lower pH where protonation of the peroxide is favored[47]. In addition, His-404 and Lys-353 are both located near the vanadium binding site and may participate in activating the complex through hydrogen bonding interaction.[29, 30] With regard to the other model studies, no evidence for complex protonation was provided, but the reactions were all

run under acidic conditions because of the need for protons to drive the net reaction.[124]
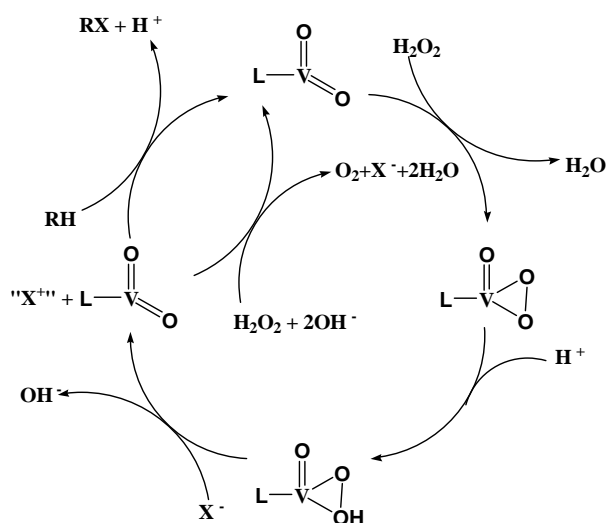
Scheme 8. Proposed mechanism of Pecoraro's model.

Although much progress has been made in recent years toward achieving bromide oxidation with model complexes, Cl⁻ oxidation has remained relatively elusive. It has been observed with $V_2O_2(O_2)_3$ in aqueous solution but no rates were reported, presumably because the rates were too slow to measure.[124] Chloride oxidation has been achieved by using mixed water/acetonitrile solvent. By adjusting water concentration in acetonitrile, vanadate has been shown to catalyze chloride oxidation, with a mximum rate occurring in 6% H_2O/94% CH_3CN.[128, 129] Presumably, this water concentration represents conditions where the concentration of the active protonated peroxovanadate species is at a maximum. Unfortunately, ^{51}V NMR shows that the equilibrium under these conditions is very complex, and the active peroxovanadate species has not yet been identified. Approximate first order dependence of the rate of halide oxidation on [V] strongly supports a monomeric complex as the active species. The rate dependence on Cl⁻ concentration has not been determined because Cl⁻ acts as both a substrate and an inhibitor.[128]

Although success was obtained to some extents with several functional model systems, the lack of the structural similarity, especially concerning the hydrogen bond net work and positively charged donor sites of V-HPO active pocket, the significance for mechanism comparison between models and enzyme, is limited.

2. Aim of this Work

Vanadium haloperoxidase (V-HPO) are one of the few natural occurring enzymes found that catalyze the halogenation of organic substrates. According to X-ray structure analysis of vanadium chloroperoxidase (V-CPO), the co-factor of the enzyme is a monovanadate HVO_4^{2-} bound to the protein in a unique supramolecular fashion, *i.e.* via H-bonding to the positively charged amino acids (Arg 360, Arg 490 and Lys 353) and via a single V-N bond to the nitrogen (Nε2) of His 496.

The enzyme works at slightly low pH and employs H_2O_2 and X^- (Br- and Cl-) which take part in the catalytic cycle. It is believed that the reaction mechanism passes through a peroxovanadate [Enzyme-$VO_2(O_2)^-$]. which is then protonated, and subsequently attacked by X^-. This X^- is then oxidized to X^+ for further electrophilic reactions.

Many details of the reaction pathway are uncertain and no enzyme model has been prepared which contain the unique cofactor-binding –mode of the native enzyme.

Therefore, the aim of this work has been the preparation of the receptors that (1) bind vanadate (and its structural analogue phosphate) in a enzyme like fashion and (2) catalyze the halogenation of organic substrates.

3. Results and Discussions

3. 1. Tris(2-guanidinium-ethyl)amine (TGEA), the First Supramolecular Receptor of Orthovanadate and a Spectroscopic Model of V-HPO

3. 1. 1. Design and Synthesis

Binding of anions through non-covalent interactions is a common structural motif of many enzymes[139] *inter alia* of proteins such as phosphatase and V-HPO. The development of supramolecular receptors for phosphate has been extensively studied,[140-145] while its structural analogues, such as vanadate, and other transitional metal anions, have been rarely investigated. From the conventional view of supramolecular chemistry or "host-guest" chemistry, the vanadate behaves like a dual property "guest": it accepts hydrogen bonds and Coulomb interactions via the oxygen atoms as a typical anionic "guest", while vanadium center maintains the capability to coordinate to ligands with lone pairs. In particular, this feature requires ligands to selectively bind vanadate that are different from those designed for phosphate.

To obtain a supramolecular receptor that binds vanadate in an enzyme-like fashion, we chose the tripodal ligand Tris(2-guanidinium-ethyl)amine (**1**, structure see **Scheme 9**), of which binding of phosphate has been already studied.[146] **1** contains three guanidinium subunits flexibly connected to a central nitrogen. It is important to note that this central nitrogen could bind to vanadium, i.e. mimicking the histidine N of the active site coordination in the enzyme. Further, the high pK_a value ($pKa=13.5$ for guanidinium in water)[147] of the three guanidiniums, which replace two arginines and one lysine in the active site of V-CPO, ensures protonation in a broad pH window providing positive charges and several hydrogen bond donor sites. The charge repulsive effect adjusts a low pK_{BH} value of the central nitrogen atom preventing protonation down to pH 2.48[146] and hence providing a lone pair to coordinate with vanadium at experimental conditions, *vide infra*.

It is worth to note that the guanidinium group is widely adopted for binding of anions either in biological systems[148] or in synthetic receptors because of its high pK_a value

and directional hydrogen bond donor ability.[149, 150] For other guanidinium receptors see references.[141, 142, 146, 150-169]
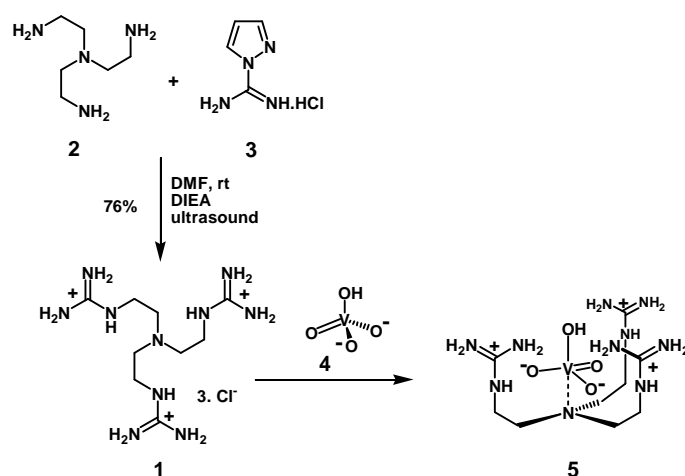
Scheme 9. Synthesis of TGEA (**1**) and proposed structure after binding of vanadate.

1 was conveniently synthesized in one step from **2** and **3** in the presence of 3 equivalents of diisopropyl-ethyle-amine (DIEA) under ultrasonic conditions (**Scheme 9**), and purified by crystallization from methanol/CH$_2$Cl$_2$ as the *tris*-HCl salt which co-crystallized with one molecule of methanol.
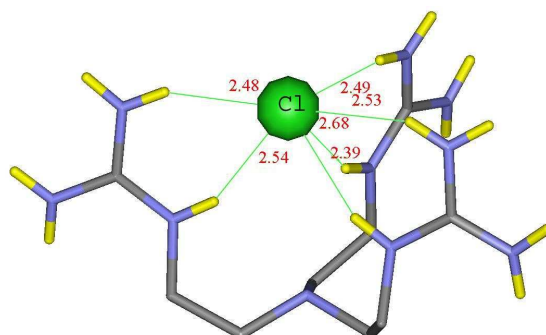
Figure 18. X-ray structure of **1**. The cocrystallized methanol molecule, another two chloride anions and the CH$_2$ hydrogen atoms are omitted for clarity. Hydrogen bonds are in dotted line with figures of the distances marked (Å). The figure was prepared with the program WebLab ViewerLite.

The crystal structure of **1** exhibits a basket shape (**Fig. 18**), binding one chloride anion inside the basket, by forming six hydrogen bonds with two NH hydrogen atoms of each of the three guanidinium groups, that are pointing towards the central axis of the

basket. The two nitrogen atoms of N-CH$_2$CH$_2$-N(G) adopt a *gauche* conformation and the central nitrogen atom has an *endo-* configuration, with its lonepair inside the basket. This special arrangement seems to be suitable to bind vanadate. Further, molecular modeling indicates that the three arms have a certain flexibility and hence the chloride shown in the crystal structure of **1** can be replaced by HVO$_4^{2-}$ to give a complex as **5** (**Scheme 9**).

3. 1. 2. Binding of HVO$_4^{2-}$ to TGEA, NMR Titration and ESI-MS

The formation of a complex between **1** and **4** causes the change of chemical shifts for both ^{1}H and ^{51}V nuclei, facilitating the binding study by NMR titration. ^{51}V NMR has been an indispensable technique in characterizing vanadium (5+) complexes[170]. Although nuclei with spin 7/2 usually give broad peaks in NMR spectroscopy, the unusually small absolute quadruple moment ($|0.037\times10^{-28}|$ m^2), the relatively large magnetogyric ratio ($\gamma = 7.0453\times107$ rad T^{-1}S^{-1}), and the high natural abundance make the ^{51}V one of the most favored nuclei for NMR with a relative sensitivity approximately 2000 times greater than ^{13}C[83, 86, 129, 170, 171].

To investigate the binding of vanadate **4** to ligand **1** the following important aspects have to be considered. Depending on concentration and pH, vanadate forms equilibrium mixtures of monomeric and oligomeric vanadates; thus, to facilitate NMR titration experiments conditions for the presence of only monovanadate (HVO$_4^{2-}$) should be used. The use of buffers can be abandoned since many of the possible ions bind to vanadate[172, 173] and/or to **1**. Further, according to earlier studies[122] the chemical shift of ^{51}V is extremely pH dependent. For these reasons a stock solution of HVO$_4^{2-}$ (Bu$_4$N$^+$ as counter cation) was prepared in water, pH 10.2, for which HVO$_4^{2-}$ is >90% the dominant species. This solution was titrated with **1** at constant pH 10.2. The titration was followed by ^{51}V NMR and ^{1}H NMR (**Fig. 19**). The ^{51}V resonance shifts from −536 ppm (**4**)[122] to −544 ppm (**5**) and protons at C adjacent to the central nitrogen shift from 2.77 ppm (**1**) to 2.65 ppm (**5**). Both NMR methods, using a nonlinear least-squares fitting reveal that the 1:1 complex **5** is formed and that **4** binds **1** with $K_a = 1.1 \times 10^3$ M^{-1}.
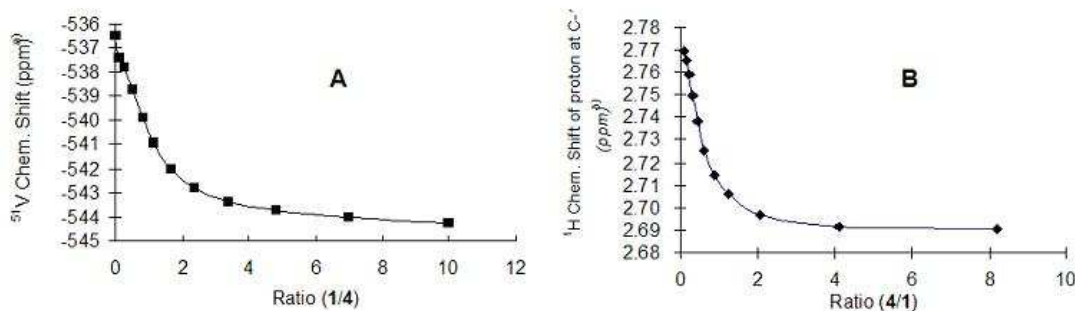
Figure 19. ^{1}H-NMR(**A**)- and [51]V-NMR(**B**)-titration curves of binding **4** to **1** in aqueous solution; pH was kept at 10.2 with (n-Bu$_4$N$^+$OH$^-$)/HCl, and total vanadate concentration is constant at 2 mmol/l to avoid concentration dependent [51]V chemical shift change. [51]V chemical shifts relative to VOCl$_3$ (0 ppm).

The binding of **1** and **4** is highly pH dependent. The titration performed at pH 12.01 showed a big difference on the tendency curve both of [1]H- (not shown) and [51]V-chemical shifts (**Fig 20**). Job plot[174, 175] displays a maximum at vanadate fraction ([**4**]$_{total}$/([**4**]$_{total}$+[**1**]$_{total}$) of 1/3, indicating the formation of 2:1 complex between **1** and **4**, which can be explained by changing of protonation states at higher pH: the positive charge number of **1** decrease and negative charge number of **4** increase due to deprotonation of both species.
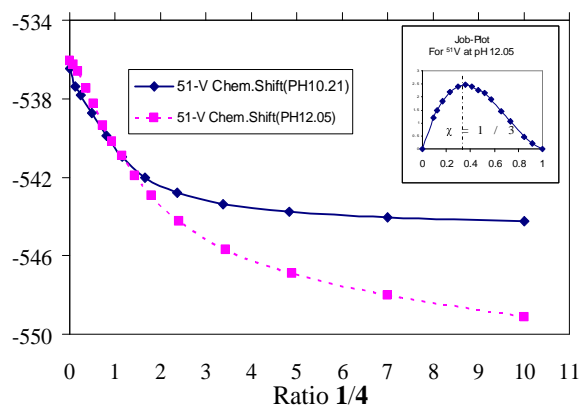
Figure 20. Comparison of [51]V-NMR titration curves of binding **4** to **1** at pH 10.2 and 12.01. Inlet is the Job plot at pH 12.01.

^{1}H-NMR titration was performed under identical condition to study the binding of **1** to phosphate, and the resulting highly similar titration curve reflects the structural analogy of HPO$_4^{2-}$ and **4** (**Fig. 21**). However, the ^{31}P chemical shift of phosphate is not sensitive enough to facilitate accurate titration.
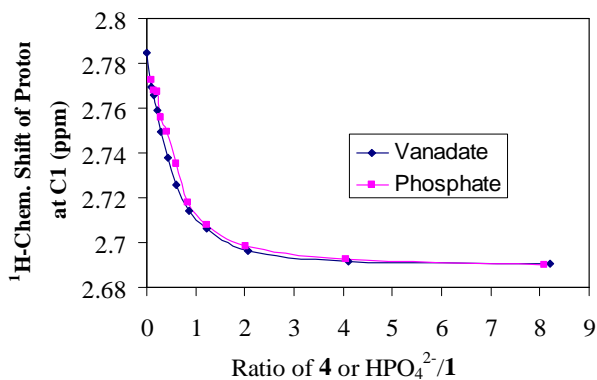
Figure 21. Comparison of ^{51}V-NMR titration curves of **1** binding vanadate and phosphate.

Further evidence for the formation of **5** was obtained by ESI-MS which showed a prominent peak at 391.2 (391.17, calculated).

3. 1. 3. V-N bond characterization: UV and TD-DFT study

The coordination of the nitrogen (Nε2) of His 496 of V-CPO of *Curvularia inaequalis* has been related to a particular UV absorbance at 312 nm.[67] It is interesting to note that the UV difference spectrum of **4** and **5** reveales the same characteristic displaying λ_{max}= 307nm (**Fig. 22**).
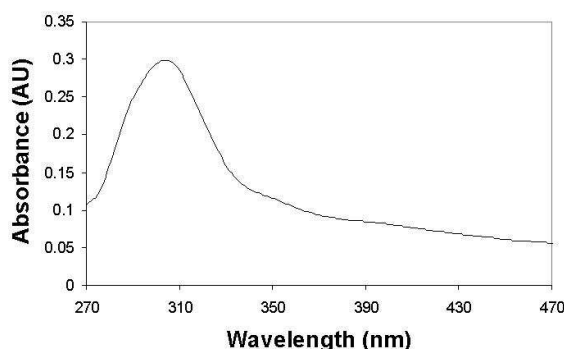
Figure 22. Difference spectrum of **5** and vanadate **4** in DMSO with total vanadate concentration of 0.2 mmol/l.

For in depth understanding of the relationship between the excitation and the structure, *ab initio* calculations were carried out with the GAUSSIAN98 suite of programs.[176] In all calculations the total wavefunction was converged to 10^{-7} at the 6-31G**/B3LYP (for closed shell) or 6-31G**/UB3LYP (for open shell) level. For the electronic spectra time-dependent density functional theory (DFT) was used. The starting structure for the partial optimizations was the X-ray structure of vanadium chloroperoxidase (V-CPOs, PDB code 1IDQ) with the Lys 353, Arg 360, His 404 side chains constrained to their respective positions in the crystal.[30] Subsequently, the structure of the His_{496}-HVO_4^{2-} system was optimized (**Fig. 23A**). With time-dependent DFT calculations the positions and intensities of the electronic absorption bands were determined on this optimized structure. The continuous spectrum was derived from converting the stick spectrum with a Gaussian lineshape with full width at half maximum of 7.5 nm centered around the calculated frequency and with peak intensity from the electronic structure calculation. For comparison, the electronic spectrum of isolated HVO_4^{2-} was also determined at its respective optimized structure (**Fig. 23B**).
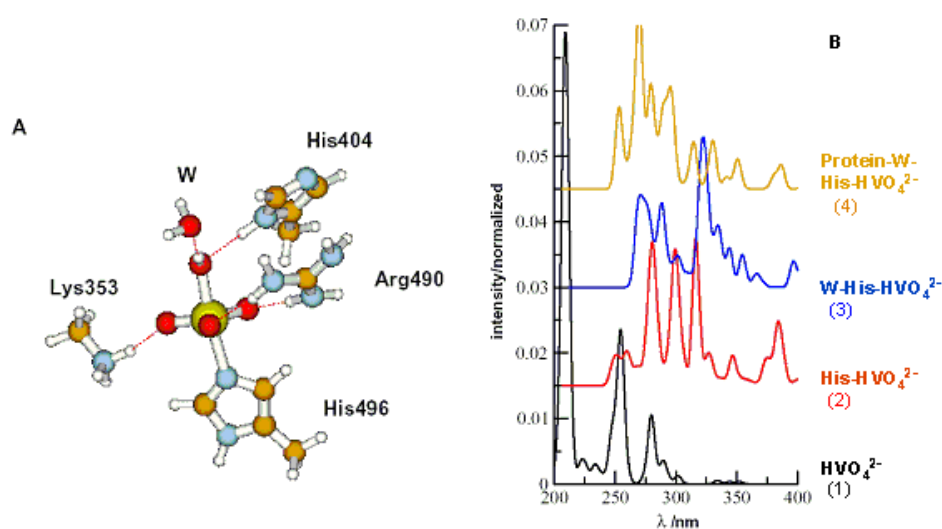
Figure 23. (A) Model system for the active site of 1IDQ. Position of H atoms were optimized while heavy atoms of the protein fragments were kept at their X-ray positions. (B) The calculated UV spectra of HVO_4^{2-} (trace 1 below) and after adding subunits of the enzyme-like micro-environment. Abbreviations: W: H_2O; protein: Lys 353, His 404, Arg 490.

The calculated UV spectra of HVO_4^{2-} and HVO_4^{2-}-His-protein, are shown in Figure 3. In good agreement with experiments the main absorptions of isolated HVO_4^{2-} are below 300nm (trace 1 in **Fig. 23B**). Approaching Nε2-histidine to vanadium of HVO_4^{2-} changes the geometry of V-coordination and leads to a V-N distance-dependent absorption above 300nm. When the V-N distance is set at 2.07 Angstrom, the distance found in enzyme (see also Figure 3A) the bands below 300 nm almost entirely disappear (**trace 2 in Fig. 23B**). Keeping the V-N distance constant the binding of water to the apical OH of HVO_4^{2-} (trace 3 in **Fig. 23B**), further H-bonding by His 404 to the same oxygen and Arg 490 and Lys 353 interactions to equatorial oxygen atoms of HVO_4^{2-} (trace 4 in **Fig. 23B**) qualitatively give the same picture: significant UV absorptions between 300 and 350 nm. The UV absorptions between 300 and 350 nm remain though their intensities are modulated depending upon the number of H-bonds. These results support the interpretation of the UV-difference spectrum of V-CPO from *Curvularia inaequalis* relating the observed absorbance to a V-N interaction.

Similar calculations were also performed for the model system **5** (**Scheme 9**). The proposed structure was partially minimized at the AM1 level. Then, the interatomic distances were further optimized by *ab initio* calculations using the methods and basis set described above. The flat potential energy surface along the coordination during optimization accounts for the flexibility of **5**. Electronic absorption spectra were then calculated at a series of V-N distances, namely 2.55, 2.35, 2.25 and 2.00 Å to study its influence on absorption. The resulting maxima of the absorption band above 300 nm and the maximum intensities are shown in **Fig. 20**. Both of them increase significantly as the V-N distance becomes shorter suggesting a strong relationship between V-N distance and excitation.
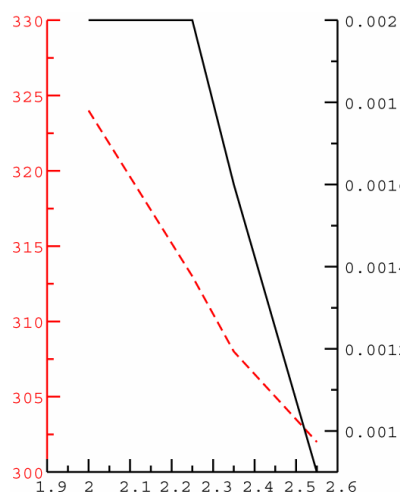
Figure 24. Change of intensity (solid line) and λ_{max} (dashed line) of the absorption band above 300 nm as a function of the V–N distance in **5**. For decreasing V–N bond length the maximum shifts further to the red and the intensity increases. The absorption is strongly dependent upon the V–N distance. Similar results were found for the model system for the active site of 1IDQ compound in **Fig. 23A**.

3. 1. 4. Binding of Peroxovanadate to TGEA 1

Whether peroxovanadate binds to **1** is of interest, because the **mono**-peroxide form is proposed as the key intermediate in the catalytical cycle of VHPO, which is confirmed by X-ray structure determination[30] (see chapter **1. 2. 1. 1. 3.**). Although the vanadate readily forms adducts with hydrogen peroxide in solution, it is almost impossible to prepare a stock solution in which the mono-peroxovanadate is a predominant species to facilitate the NMR binding study, because the interaction between vanadate and hydrogen peroxide gives rise to a variety of species and equilibrium.[177] For example, in the neutral aqueous solution of H_2O_2/V at a ratio of 1/1, mono-peroxovanadate is only a minor component, while di- and non-peroxovanadate are dominant species. Upon addition of one equivalent of **1** to this solution, the ^{51}V NMR peak of di-peroxovanadate shifted slightly to higher field (from -694ppm to -697ppm) and became a little broader indicating complexation of **1** and diperoxovanadate may occur. However, the presence of **1** did not change the vanadate equilibrium and no evidence could be obtained whether the system catalyzes the oxidation of Br^- to Br^+.

3. 1. 5. Tris(3-guanidinium-Propyl)amine (TGPA) and Solvent Effect

In order to study the influence of the length and flexibility of the linkers between the central nitrogen and the three guanidinium units, tris(3-guanidinium-Propyl)amine (TGPA, **6**) was synthesized in a same way as for **1**. However, the following NMR titration and UV study failed to demonstrate that the binding of vanadate to **6** occurred, presumably because **6** is too flexible and the charge repulsive effect of the guanidinium moieties favors a "dendrimeric" structure rather than a "basket", and hence disfavors binding.

6, 3 Cl⁻
8, 3 BPh₄⁻
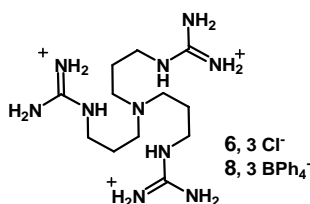
The polar inter-molecular forces such as hydrogen bonding and electrostatic interactions will be enhanced in less polar solvent. To improve the solubility of **1** and **6** in organic solvents, the Cl⁻ counter anion of both **1** and **6** were exchanged to tetraphenylborate (BPh_4^-), via precipitation in water with $NaBPh_4$. The resulting TGEA.3·BPh_4^- (**7**) and TGPA.3·BPh_4^- (**8**) are both highly soluble in acetonitrile. However, when **7** or **8** was titrated with vanadate in acetonitrile, a cloudy solid precipitated immediately and the solid could not be re dissolved in most of the organic solvents, not even in DMSO/H_2O mixture. The IR spectrum (KBr) of the precipitate is significantly different from that of **6**, the detailed assignment needs further investigation.

3. 1. 6. Summary of part 3.1.

In summary, NMR and UV spectroscopy of **5** revealed the structural similarity to the active site of V-HPO. DFT calculations identify V-N transitions as the origin of the observed UV spectra for both the enzyme V-CPO and its model **5**. Since it is obvious that the central nitrogen in **5** forms a coordinative bond to vanadium our results indicate that the vanadium-N$\varepsilon2_{His\ 496}$ interaction in V-CPO is of the same nature. Accordingly **5** is a spectroscopic enzyme model of V-CPO.

3. 2. Macrobicyclic Guanidinium-Cryptand: the Cage Shaped Receptor

3. 2. 1. Design and Retro-synthetic Analysis

Given the K_a of about 1×10^3 M$^-$ between **1** and vanadate, the 1:1 ratio of free and ligand bound vanadate (**5**) can be calculated for a solution containing 2M of each **1** and HVO_4^{2-}. The ratio of free vanadate will even increase if the total concentration decrease, hence to facilitate the study of catalytic activity, new receptors with higher affinity to vanadate are desired, such that most vanadate in solution is complexed and the activity from free vanadate can be eliminated to an acceptable extend. Inspired by the cryptand ligand, which was developed by Lehn over 30 years and achieved great success to tightly and selectively encapsulate cations[178-182] and anions,[180, 183] we designed the new macrobicyclic guanidinium receptors as shown below.
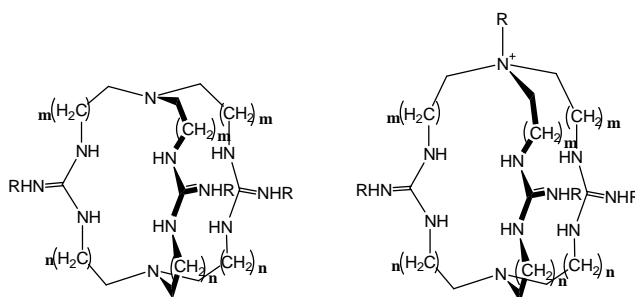
Figure 25. Schematic representation of the designed guanidinium cryptands.

These new receptors inherit the key structural features from the first generation receptor **1** which are needed to bind vanadate, namely, three guanidinium units linked to a central nitrogen by alkyl chains. However, unlike their open-armed precursor **1**, the other N-terminals of the three guanidiniums are tethered by another tripodal link, generating cage-shaped receptors. They should be conformationally more rigid than **1** and the cavity is expected to encapsulate vanadate with higher affinity. In principle, the size and geometry of the cavity can be tuned by varying the length of alkyl chain at one or both sides, and additional one more positive charge can be introduced at the top central nitrogen, which should further expand the size of cavity due to the exo-configuration of that nitrogen.

To the best of our knowledge, only one paper reported the synthesis of guanidine cryptand with a low overall yield,[184] and the binding study to any guest molecule is

not published. However, our synthetic strategy is expected to be applicable to a variety of different multicyclic cage-shaped guanidinium receptors to meet the need of our design. With this main aim in mind, the following retro-synthetic strategy is proposed (**Scheme 10**).
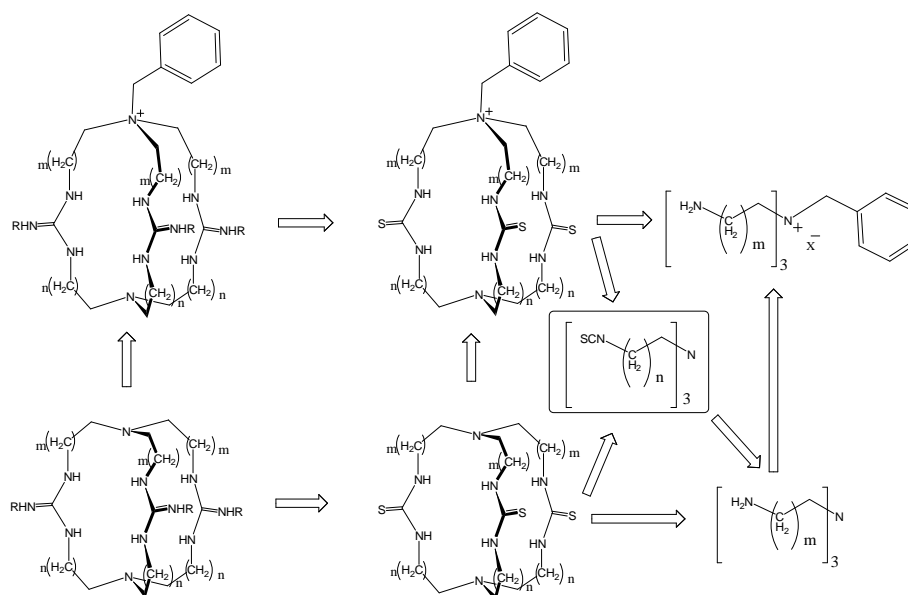
Scheme 10. The general retro-synthetic analysis of the guanidinium cryptands.

The thiourea analogue is chosen as a key intermediate because this functional group is a common synthetic precursor of guanidine compounds and various efficient methods have been developed, even for solid phase transformation[185]. Another important reason is that thiourea is also a relatively strong hydrogen bond donor and structurally similar to the guanidinium group except for the absence of charges. Both moieties adopt a "Y" type planar conformation due to the mesomeric π–character of the system, providing two hydrogen bond donor sites per unit. Indeed, thiourea has been extensively employed for the design of neutral anion receptors[186-204]. However, unlike guanidinium, thiourea is neutral, providing the chance to compare the influence of positive charges on the binding of vanadate. The thiourea intermediate can be obtained from the addition of the tris-amine (*i.e.* **2**) to tris-isothiocyanate compounds (**26, 27**). This is a very fast and efficient reaction facilitating the high dilution reaction which favors the cyclization over polymerization. Notably, the tris-isothiocyanate can be obtained from the tris-amine compound. The benzyl is introduced at the top central nitrogen from the very beginning of synthesis, and should be able to be removed by

reductive debenzylation at any step of the following reactions if needed. Therefore, this synthetic strategy is flexible and allows us adjusting the size and geometry of the binding cavity of the target guanidinium cryptand without changing the synthetic pathway.

3. 2. 2. Synthesis

Starting from commercial available N-4-bromobutyl-phthalimide **9** or N-5-bromopentyl-phthalimide **10**, the tris-NH_2 compounds with C4 (**17**) or C5 (**18**) alkyl chain were prepared according to the known procedures,[205, 206] respectively (steps *a* → *d*, **Scheme 11**), or through a slightly modified method: **9** and **10** were converted to their iodide derivatives (**19**, **20**) first, then reacted with benzyl amine to give quaternary ammonium iodide salts **21** or **22**, and the following stepwise cleavage of phthalimide and benzyl protecting group afforded the desired tris- NH_2 **17** and **18**. One advantage of the modification is the central-N-benzylated derivatives (**23, 24**) could be obtained via the same route without removal of the benzyl group. The tris-amine with shorter alkyl chains, see **2** and **25** are both commercial available. For practical purposes, only these two compounds were converted to their isothiocyanate derivatives **26** and **27** by reacting with CS_2 and DCC, although in principle the tris-NH_2 with longer arms can also be transform to isothiocyanates and then cyclize with the smaller tris-NH_2 counter partner, however is less convenient.
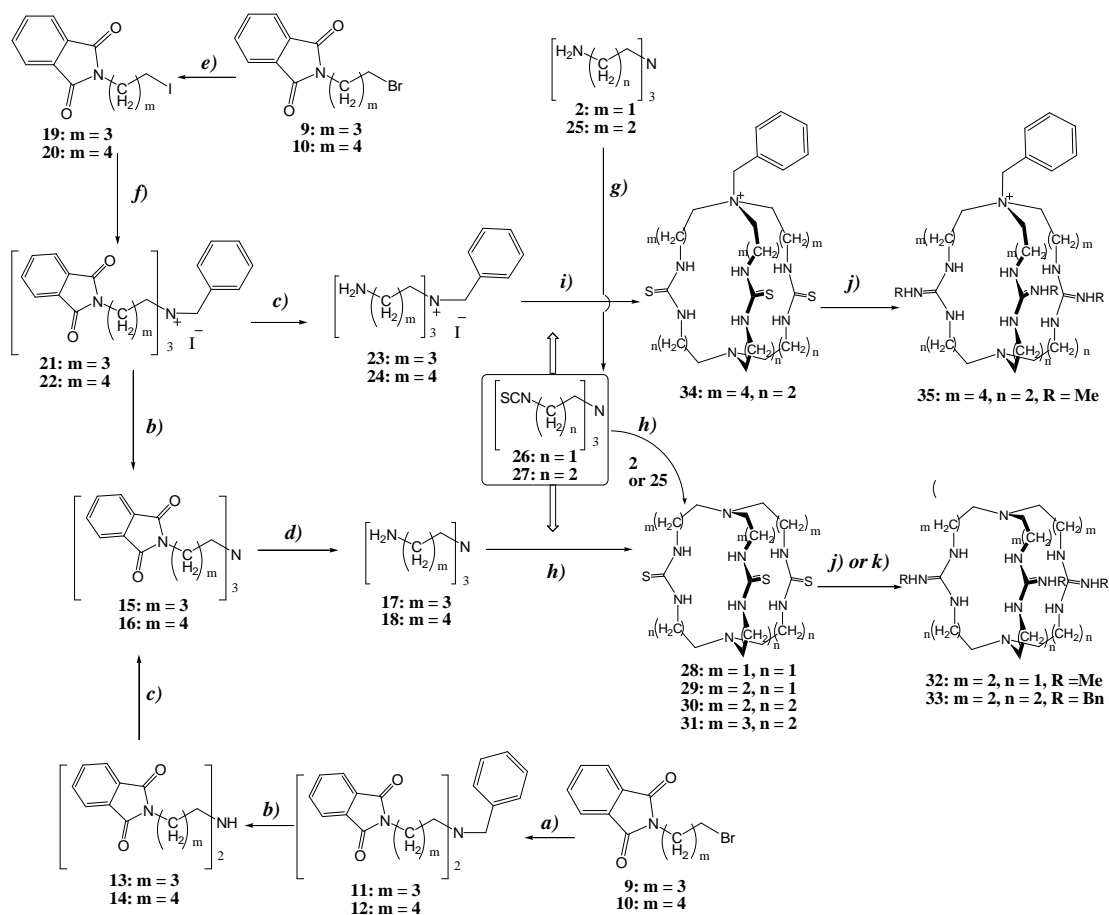
Scheme 11. The overall synthetic pathways for guanidinium cryptands. Reagents and conditions: (a) Benzyl amine, KF/Celite® 545, CH$_3$CN; (b) H$_2$/Pd-C, EtOH; (c) 9 or 10, KF/Celite® 545, CH$_3$CN; (d) hydrazine, EtOH, reflux; (e) KI, acetone; (f) Benzyl amine, KF/Celite® 545, CH$_3$CN, reflux; (g) CS$_2$, Et$_3$N, DCC, THF; (h) high dilution, tris-amine or tris-isothiocyanate, CHCl$_3$; (i) high dilution, tris-isothiocyanate, CHCl$_3$/DMF = 1 : 1; (j) MeI, then R-NH$_2$; (k) Muikaiyama reagent, R-NH$_2$.

Tris-NH$_2$ compounds are readily cyclized with tris-isothiocyanate under high diluted conditions to form the thiourea cryptands as key intermediates. Depending on the length of the arms, yields are different. In general, the smaller the size, the higher the yield. The smallest thiourea cryptand **28** with three identical –(CH$_2$)$_2$- links at both sides was prepared quantitatively, while for **34**, the largest one, only 24.4% yield could be obtained. DMF was chosen as solvent only when the solubility of the starting material is lower, such as for the ammonium salts tris-NH$_2$ (**23**, **24**), otherwise chloroform is more favorable. Compounds **28** and **29** have been crystallized and characterized by X-ray structure determination (**Fig. 26**). These two compounds exhibits certain conformational differences in the solid state, such as the thiourea

groups adopts **Z,Z**-conformation in **28**, but **Z,E**-conformation in **29**. Nevertheless, all the central nitrogen atoms are *endo*-oriented with the lone pair pointing into the cavity; accordingly both could coordinate to vanadium atom of the encapsulated vanadate. The broad NMR signals of all the thiourea cryptands suggest conformational equilibria existing in solution.
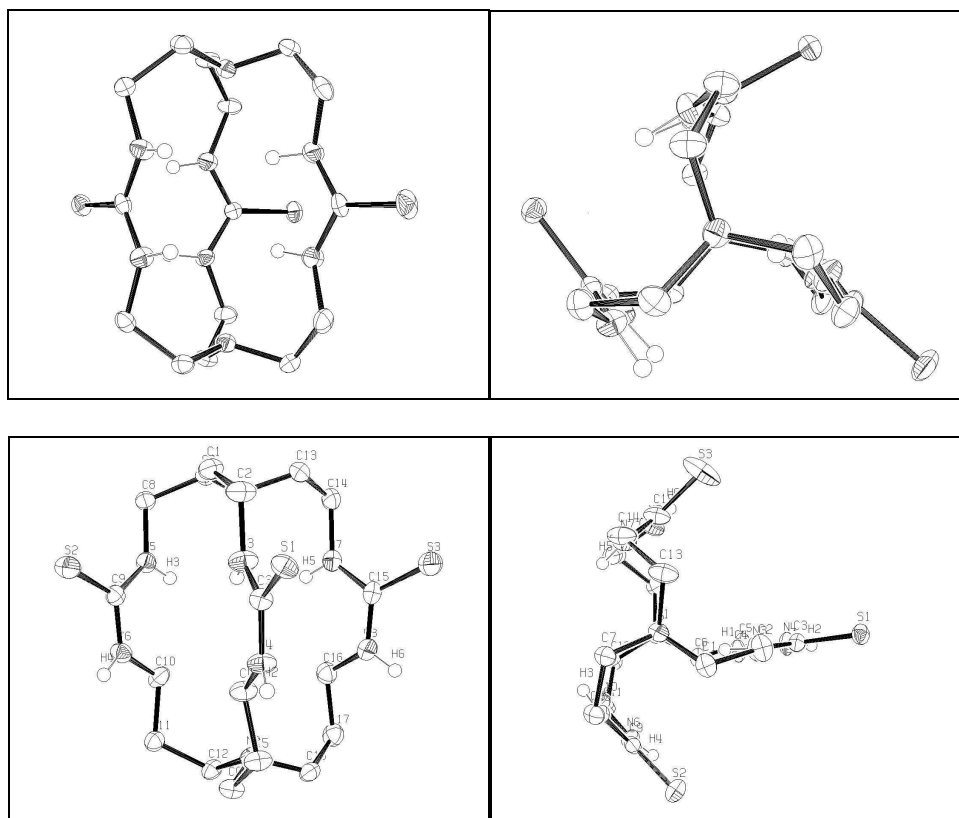
Figure 26. The ORTEP drawing of compound **28**, top-left: viewing from side, top-right: viewing from top; and compound **29**, bottom-left: viewing from side, bottom-right: viewing from top. All CH_2 hydrogen atoms are omitted for clarity.

Several methods had been tried to convert the different thiourea precursors to guanidinium cryptands. It has been found out that the feasibility of the method is depending on the structure. Mukaiyama reagent has been successfully used to synthesize the guanidinium **33** from the thiourea **30**, through a carbodiimide intermediate[207, 208] following by condensation with benzyl amine in one pot (Method A, **Scheme 12**). However, this method was failed for substrates with –$(CH_2)_2$- linkers, such as compounds **29** and **34**, though the formation of their carbodiimide intermediates had been determined by ESI-MS during the reaction. Finally an alternative method has been developed. These two compounds were converted to S-

methyl-isothiourea intermediates, without purification they reacted with primary amine by nucleophilic substitution finally to afford the guanidinium macrocycles **32** and **35** (Method B, **Scheme 12**).
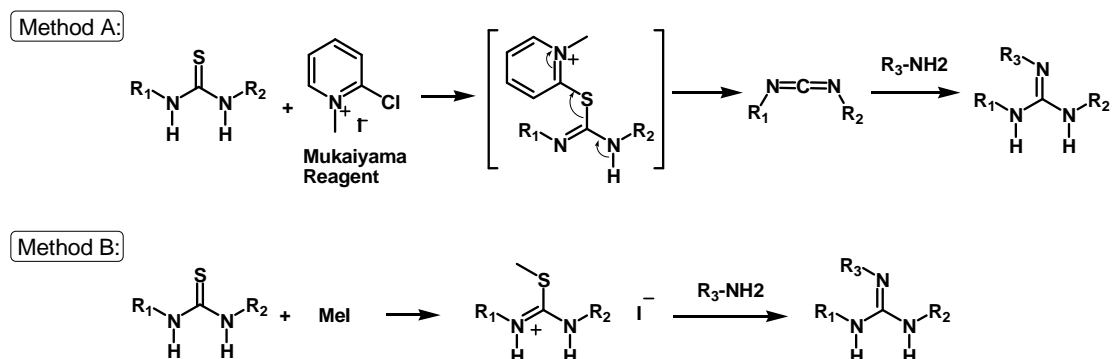
Scheme 12. The two methods applied to synthesize guanidinium cryptands.

3. 2. 3. pK_a of central nitrogen

An unprotonated central nitrogen atom is needed to form V-N coordination. Therefore, the pK_{BH} value of the nitrogen needs to be determined. Since the protonation of the central nitrogen is coupled with significant chemical shift change of related CH_2 signals, ^{1}H-NMR titration was used. For example, the protonation of the central nitrogen of compound **35** causes significant change of chemical shift not only for the adjacent H-atoms, but also to most others located far away (**Fig. 27**), including the benzyl and even phenyl protons which are at the other side of maclocycle. This remote effect is presumably due to charge repulsion, *i.e.* ring enlargement is accomplished by a change of the configuration of the central N from *endo* to *exo*.
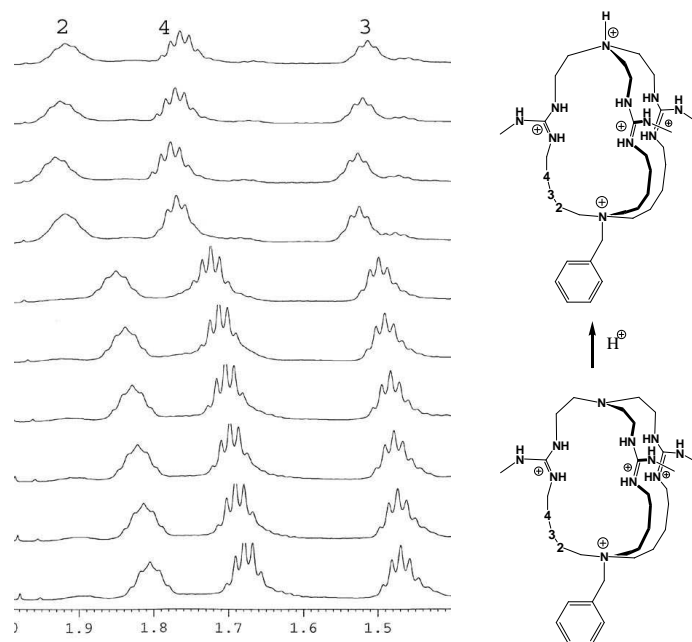
Figure 27. The partial ^{1}H-NMR spectra (left) of compound **35** indicating the chemical shift of the labled H-atoms (right) changes according the pH. The break point occurs at pH around to the pK$_a$ value of protonated **35**.

The determined pK$_a$ value of 3.2 for protonated **35** is in good agreement with that of compound **1**, as well as those of polyamine cryptands, of which the charge repulsive effect shifts the basicity of the bridgehead nitrogen to a very low value for tertiary amine.[209]

3. 2. 4. Binding of vanadate

No significant changes of chemical shifts were observed from either ^{51}V or ^{1}H NMR when compound **33** (with C3 links at both sides) was titrated by vanadate in water. Molecular modeling suggests the cavity of this guanidinium cryptand is too small to accommodate vanadate. For the biggest guanidinium cryptand ever synthesized, **35**, binding of vanadate leads to a 2 *ppm* ^{51}V shift to higher field, too small to be suitable to determine the stoichiometry of the adduct. Further, the tendency curve of ^{1}H chemical shift changes of the ligand (**Fig. 28**) suggests a stepwise formation of complexes of various compositions (similar phenomenon reported see reference[210]). These observations lead to the conclusion that **35** is a weaker receptor of vanadate than the open-armed **1**, and binding is likely to occur outside of the cavity.
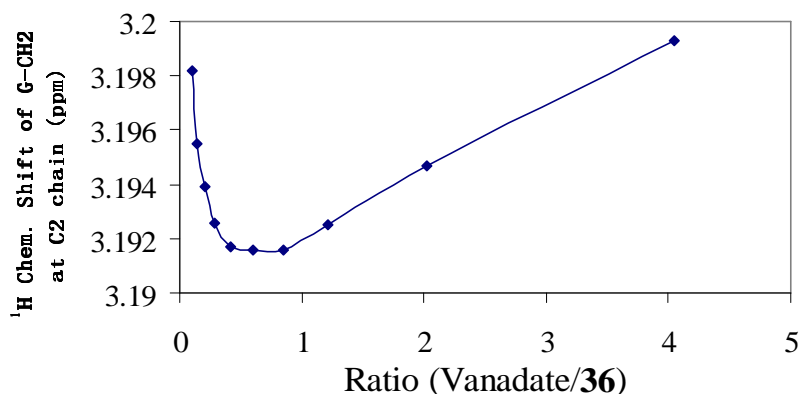
Figure 28. ^{1}H-NMR titration curves of binding HVO_4^{2-} to **35** in aqueous solution. The tendency curve of G–C$\underline{H}_2$-CH$_2$N chemical shift change indicates multi steps binding behavior.

3. 2. 5. Summary of part 3.2.

To improve vanadate binding a number of novel guanidinium cryptands containing rigid cavities of different size and geometry were designed and synthesized according to a general strategy via thiourea intermediates. The pK_{BH} value of the central bridgehead nitrogen was determined by NMR titration revealing a low basicity sufficient for V-N bond formation. It was, however, not possible to obtain evidence that vanadate binds inside these cages. NMR studies suggest that in general mixture of vanadate: cage adducts of undefined stoichiometry are found.

From these experiences, it can be concluded that this preferred conformations of cages such as **28** and **29**, see X-ray structures in **Fig 26**, do not bind HVO_4^{2-}, and further, the activation energy to change these cages into suitable receptors is too high. Nevertheless the lesson from these experiments is that more flexibility of potential receptors is required to allow the binding site of the host to self-adjust to a certain extent for the best fit to the shape of the guest molecule.

3. 3. Tris-(2- (N'-pyren-1yl-methyl-guanidinium)-ethyl)- amine (TPGEA): From vanadate sensor to functional model.

3. 3. 1. Design

Introducing three pyrene moieties at the N'-terminal of guanidinium of compound **1** leads to the modified receptor **36** (Tris-(2-(N'-pyren-1yl-methyl-guanidinium)-ethyl)-amine, **TPGEA)**, as shown below:

36
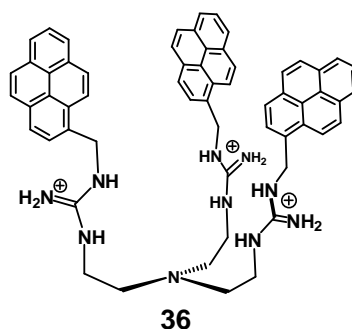
This modification seemed attractive for the the following reasons:

(1) the pyrenes "close" the basket by π- π stacking;

(2) this preorganization is comparatively weaker than that of cryptand receptors, and the binding of vanadate could be accomplished through a low activation barrier;

(3) the pyrenes are expected to increase solubility of the host in organic solvents in which naturally hydrogen bonding and Coulomb interactions are more fully expressed than in water;

(4) the photophysical feature of pyrenes in particular the excimer fluorescence exhibited by adjacent pyrenes are expected to be useful for investigating vanadate binding;

(5) the CH_2 link between the guanidinium and pyrene is the most common spacer facilitating the Photoinduced Electron Transfer (**PET**),[211] which has been the most extensively used and effective strategy for developing fluorescent sensors for cations and anions. As the direct binding site, the anticipated complexation with vanadate will change the redox potential of the guanidinium, which can be intramolecularly

transmitted to the fluorophore via PET. Therefore, visualizing the binding events by means of fluorescent signal changing becomes possible and reasonable.

3. 3. 2. Synthesis

The synthetic strategy is aimed not only for the preparation of **36**, but also to allow for the introduction of other functional groups at one arm, such as imidazole (see *i.e.*, compound **52, Scheme 13**), which can potentially mimic either His 496 or His 404 of the active site of V-CPO (see **chapter 1. 2. 1. 1. 2.**).
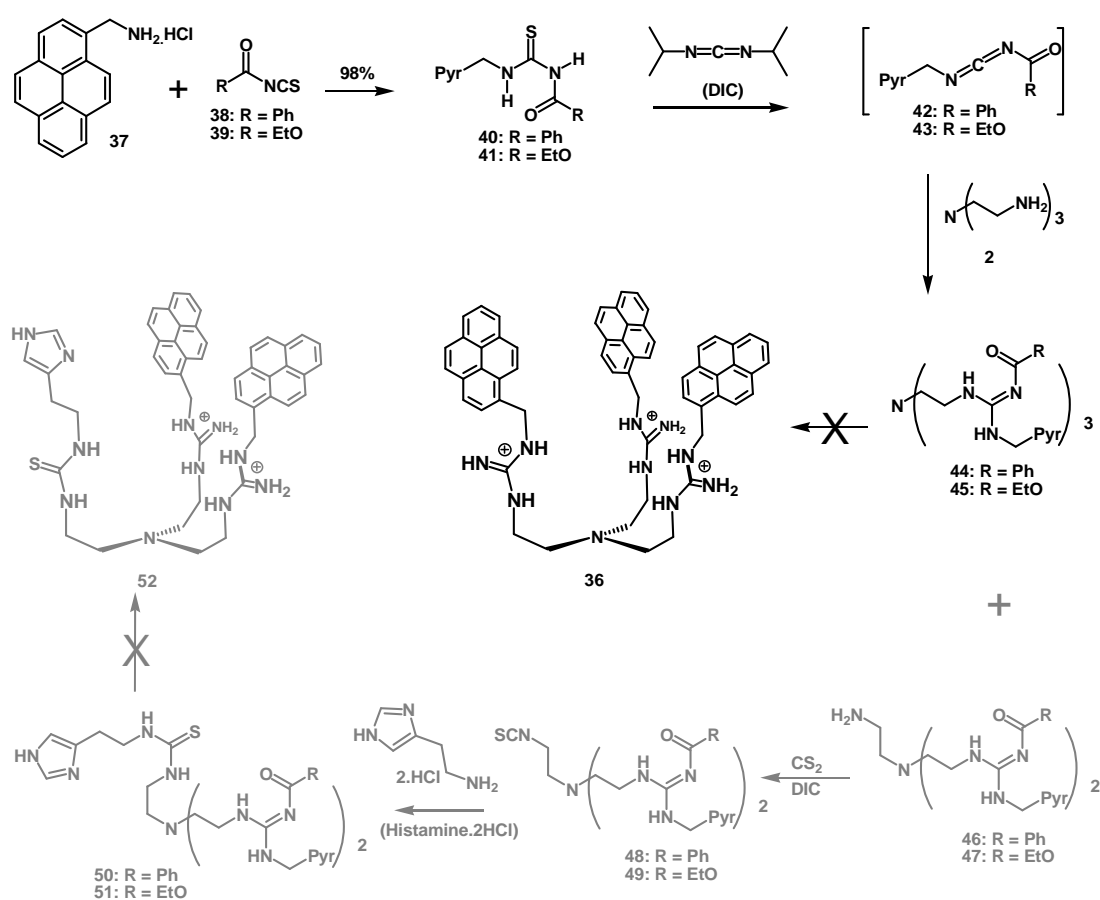
Scheme 13. Attempts to synthesize TPGEA (**36**) and the histamine modified derivative (**52**) (pathway in gray). Reagents and conditions: (a) CHCl$_3$, NEt$_3$, recrystallized from CHCl$_3$/Et$_2$O; (b) DIC, CH$_2$Cl$_2$, and TAEA, reflux 30 h; (c) in one-pot of previous step, CS$_2$ and second part DIC; (d) histamine, CH$_2$Cl$_2$.

According to previous experience, the number of positive charges and the high pK$_a$ value render the poly guanidinium compounds very polar and hence difficult to purify. Therefore, N-benzoyl or ethoxy-carbonyl protecting group were used, which greatly

decrease the basicity of the guanidine and ease the purification. The addition of 1-pyrene-methyl-amine (**37**) to benzoyl or ethyl-carbonyl isothiocyanate (**38** or **39**) quantitatively yields the protected thiourea (**40** or **41**). The resulting **40** or **41** were converted to carbodiimide **42** or **43** by DIC, which was reacted with TAEA in one pot to afford N-protected tris-guanidine (**44** or **45**). Varying the ratio between protected thiourea and TAEA from 3:1 to 2:1, a bis-guanylated **46** or **47** was obtained as the main product, of which the one remaining unreacted free amine could be transformed to the isothiocyanate within one pot since both step use DIC as reagent, followed by addition of histamine to yield **50** or **51**. Benzoyl has been extensively used as a protecting group for guanidine which can be removed by hydrolysis under acidic condition[212-223]. Unexpectedly, the desired product **52/36** were not obtained under routine or even harsher acidic deprotecting condition. Other debenzoylation methods such as basic hydrolysis, hydrazine or DIBAL[224] all failed to remove benzoyl protecting group from compound **44** or **50**. Presumably, the conjugation of guanidine C=N double bond with the carbonyl enhanced the strength of amide bond, which is very difficult to be cleave under normal condition, while the harder condition caused the decomposition of the starting materials. The same problem was encountered for the removal of ethyl-carbamate protected guanidines **45** and **51**. Even Me$_3$SiBr, the reagent which was reported to specifically cleave ethyl-carbamate from protected guanidines[225], also failed.

To avoid the problematic deprotecting step, a convenient strategy employing an alternative, flexible route was developed, see **Scheme 14**.
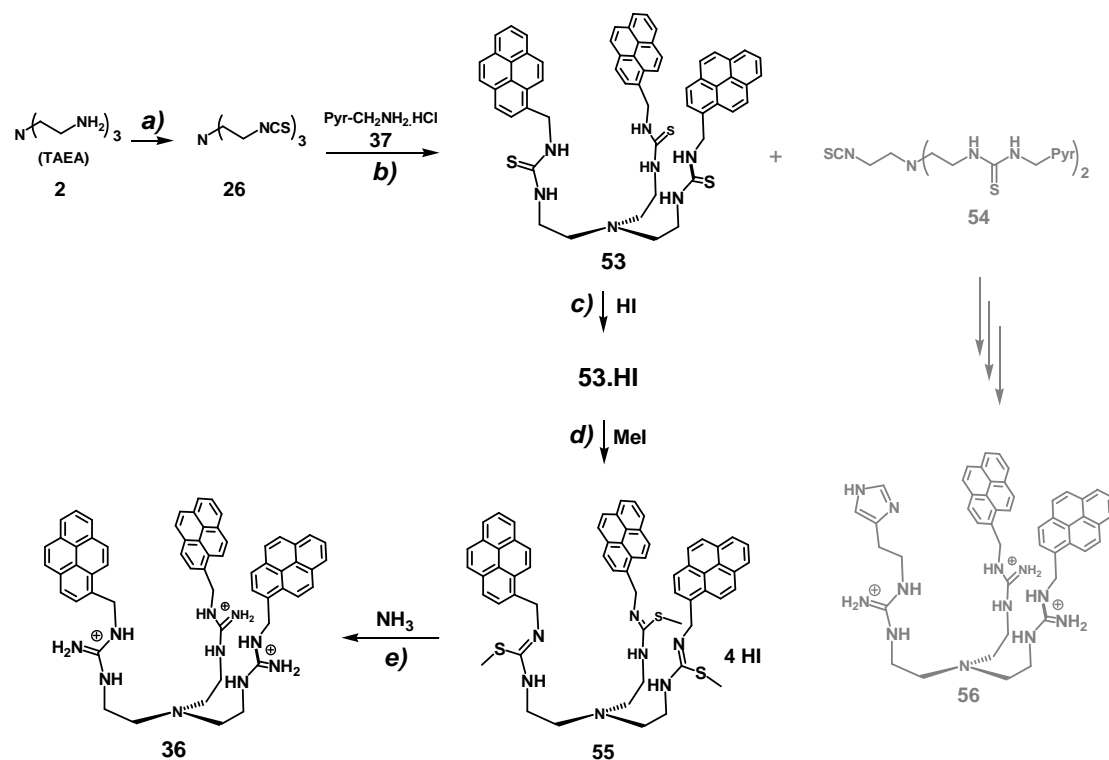
Scheme 14. Synthesis of TPGEA (**36**). Reagents and conditions: (a) CS$_2$, Et$_3$N, DCC, THF; (b) DIPEA, CHCl$_3$; (c) CH$_2$Cl$_2$/EtOH, *aq.* 55-58% HI; (d) MeI, 72 h, rt.; (e) in sealed tube with J. Young valve, 7 N ammonia in MeOH, 55 ˚C, 12 h.

The starting material TAEA **2** was converted to tris-isothiocyanate **26** as described in **Scheme 12**. After the addition of pyrene-1-methyl amine to **26**, compound **53** was obtained in 83.2% yield. As discussed in chapter **3. 2. 1.** , this tris-thiourea intermediate is a structure analogy of **36**. It has hydrogen bond donor sites with the similar geometry as **36**, but without positive charge, which provide a good opportunity to study the influence of positive charges on anion binding. To avoid the obvious electrophilic attack at central nitrogen, the smallest protecting group, protonation, was used by formation of HI salt. The following reaction with methyl iodide, therefore only happened at S-atoms, almost quantitatively yielding the tris-S-methyl-isothiourea derivative **55** as the *tetra*-HI salt. Without purification, it reacted directly with ammonia in methanol in a sealed tube. After separation and exchanging the counter anion to Cl$^-$ by ion-exchange resin, the final target compound **36** was obtained within only five steps totally.

Notably, the synthetic strategy is also flexible and compatible, allowing the structural modification at one arm or even two to facilitate the synthesis of other desired model

compounds. For instance, varying the ratio between tris-isothiocyanate **26** and pyrene-1-methy-amine **37** from 1:3 to 1:2, bis-thiourea compound **54** could be obtained as the main product, which contains an unreacted isothiocyanate group for introducing another desired functional moiety such as histamine. Following the same pathway for **36**, compound **56** was obtained as another potencial vanadate receptor.

3. 3. 3. Pre-organization of **36**: Fluorescent study

Receptor **36** is well soluble in acetonitrile/water (1:1) mixture and only slightly soluble in any of the solvent alone. However, to maximize the polar interaction with vanadate, the fluorescence and UV titrations were performed in acetonitrile. Upon excitation at 343 nm, the acetonitrile solution of **36** exhibits emission bands at 376 and 395 nm as typical fluorescence signals of pyrene monomer. However, the intensity of these monomer bands is rather low compared to another broad and structureless band at 478nm, which is assigned to the pyrene excimer (**Fig. 29**).[226]
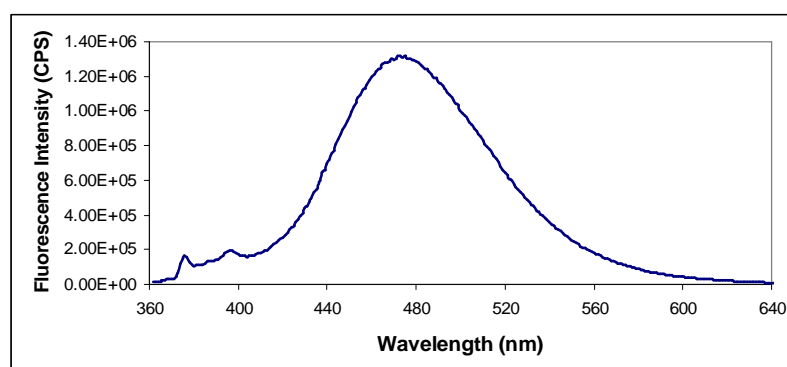
Figure 29. Emission spectrum of 36 (3.6 uM in acetonitrile, λ_{ex} = 343 nm).

Traditionally, an excimer can be defined as a complex formed by interaction of a fluorophore in the excited state with a fluorophore of the same structure in the ground state.[226] An important aspect is that the emission spectrum of the excimer is red-shifted with respect to that of the monomer, and in many cases, the dual emission of the monomer and the excimer is observed. In general, it is assumed that flat highly π-delocalized systems show greater tendency to form excimers, such as anthracene and pyrene. A crucial requirement for excimer formation is that two monomers are in

close proximity in order to give stacking interactions and the molecular excimer state. Further, a long-lived excited fluorophore is required, since it has to approach its ground state partner within its lifetime. Pyrene has long singlet lifetime and readily form excimer. Therefore it has been extensively applied as a fluorescence probe for many purposes by means of the excimer signal formation.[226-229]

The involvement of three pyrene moieties of **36** in excimer formation at low concentration suggests they are intramolecularly close to each other in space, which confirms the original design with respect to preorganization. According to earlier reported, two different types of excimer formation can be distinguished. The first type refer to two pyrenes that are sufficiently far apart from each other before excitation; only one is excited and then approaches its ground state partner by diffusion within its lifetime to form the excimer, which is termed as "dynamic excimer". By contrast, another type refers to the situation that (pre)association between two pyrenes already occurs in ground state, which absorbs the light as a ground-state dimer and the resulting excimer is termed as a "static excimer"[226]. Obviously, the later case should be favored in a preorganized system such as **36**. The existence of static excimer can be visualized by steady-state excitation spectrum. In contrast to monomer, the pre-associated ground state dimer should exhibit red shift and broadening of peaks. The widths of the band can be related to the parameters P_m (for monomer) and P_e (for excimer), which refer to the ratio of the fluorescent intensity of the most intense band (I_p, intensity of peak) to that of the adjacent minimum (I_v, intensity of valley) at shorter wavelength. As shown in **Fig. 30**, receptor **36** indeed exhibits the characteristic of static excimer to a certain extent: 1 nm red shift ($\Delta\lambda$) was observed for excitation spectrum monitored for excimer ($\lambda_{em} = 476$ nm) relative to that for monomer ($\lambda_{em} = 376$ nm). Futher, the broadness parameters ($P_m > P_e$) qualitatively indicates that the excitation spectrum of the excimer is than that of monomer. Potential surfaces of both pyrene ground-state dimer and excimer had been calculated by Warshel and Huler in order to study the influence of distance between two pyrenes, revealing a minimum at the 3.44 Å distance between two ground state pyrenes and 3.26 Å for that of excimer.[230] For receptor **36**, the close proximity of pyrenes observed by fluorescent study is in good agreement with the solid state structure of its structural precursor **1** (**Fig. 18**).
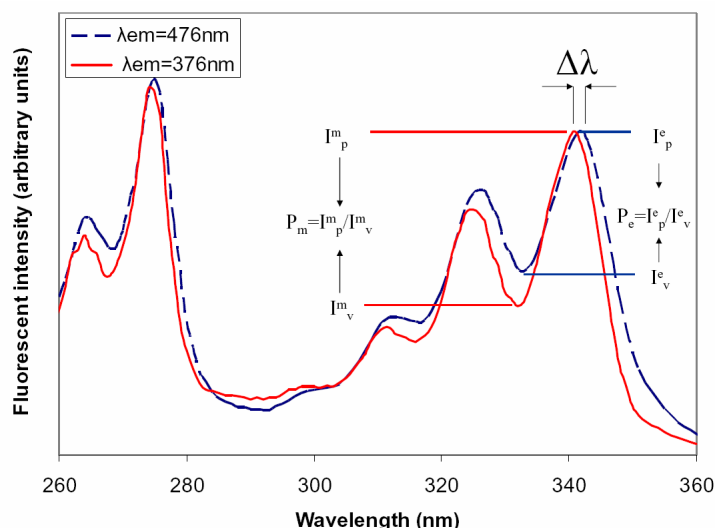
Figure 30. Normalized excitation spectra of **36** (3 μM in acetonitrile), monitored at 376 nm (monomer, red solid line) and at 476 nm (excimer, blue dashed line).

It is interesting to note that the thiourea analogy **53** also shows very similar fluorescence spectra, which strongly indicates the conformational similarity to **36**.

3. 3. 4. UV-vis and Fluorescent Titration: Sensor of Vanadate

Using Bu_4N^+ as a counter cation makes the vanadate soluble in organic solvents. The 5.4 mM stock solution in acetonitrile was prepared by dissolving 135 μl of 0.2 M vanadate aqueous solution in 5 ml acetonitrile. As already described in **chapter 3.1.2.**, the 0.2 M aqueous solution can be prepared by reaction of vanadium oxide (V_2O_5) with four equivalent $Bu_4N^+OH^-$ in water.

Significant change were observed when 3 μM of receptor **36** in acetonitrile was titrated with the vanadate solution (**Fig. 31**), indicating that complexation of vanadate by **36** occurred. Upon stepwise addition of vanadate, almost all characteristic bands of pyrene shift to red, *i.e.* the transition at 343 nm shows 6 nm red shift to 349 nm. Meanwhile, bands become much broader, which is qualitatively represented by the parameter P_a. Similar as P_m shown in **Fig. 30**, P_a is defined as the ratio of absorption intensity of a peak (AU_p) to that of the adjacent valley (AU_v) at shorter wavelength (**Fig. 31**). It is important to note that there is almost no change for the over all integral of the spectrum before and after adding vanadate. These observations strongly

indicate that the pyrene moieties are getting more packed upon the interaction with vanadate. Hence it is reasonable to assume that vanadate is bound within the three arms of **36** and pulls all three pyrenes closer to each other by electrostatic and hydrogen bonds with the guanidinium units.

Notably, before two equivalents of vanadate (calculated for monomer, V1) are added, the changing of intensity at a specific wavelength of UV spectrums of **36** is almost proportional to the amount of vanadate used, while only very little change can be observed > 2 equivalents, which indicates the formation of 1:2 complex (**36**:V). Additionally, the clear isosbestic points suggest only one complex is generated between **36** and vanadate. However, the background absorption from vanadate itself interferes the accurate determination of association constants from UV titration, especially at high total vanadate concentration and at wavelength < 300 nm.
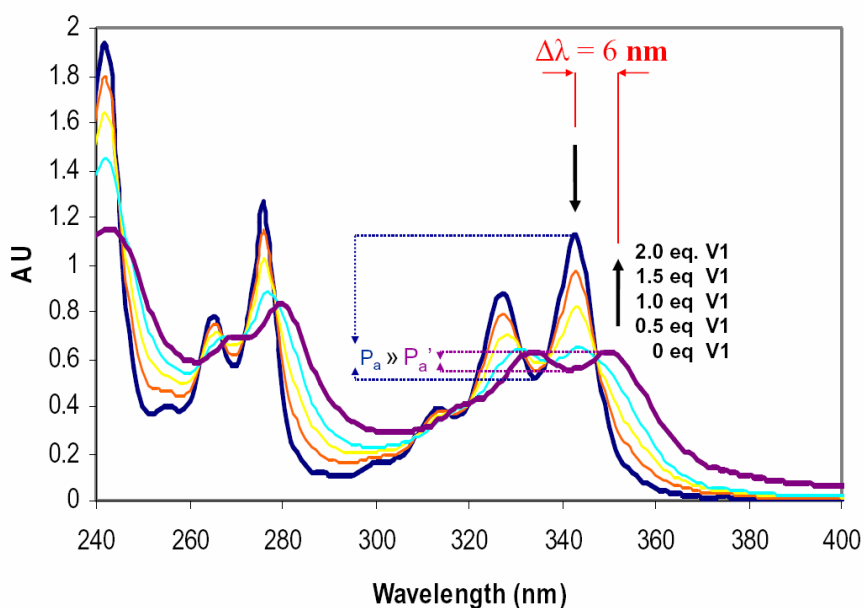
Figure 31. UV titration of **36** (12 μM in acetonitrile) by vanadate. Bands became red shifted (represented by $\Delta\lambda$) and broader (qualitatively indicated by peak to valley ratio of intensity, $P_a = AU_p/AU_e$) upon the increasing ratio of vanadate.

Fluorescence titration was also performed at the lower concentration than that for UV. The excitation wavelength of 345 nm was chosen from the isosbestic point of UV-vis spectra. Quenching of fluorescence was observed for both monomer and excimer emissions (**Fig. 32**) upon the portionwise addition of vanadate. The titration curve following the intensity at 474 nm against the ratio of vanadate/**36** reveals almost

linear quenching < 2 equivalents of vanadate (counted as V1), and the excimer emission is almost completely quenched at 2 equivalents of V1 (**Fig 33 A**). The sharp break point at V1/**36** = 2 and the nearly linear tendency before and after this break point suggest that **36** very tightly forms a complex with vanadate dimer (V2), not monomer, which is compatible to the result from UV titration. Additionally, the Job plot gives the maximum at the molar fraction (χ = [**36**]/([**36**]+[V])) of 1/3 if vanadate monomer is counted for vanadate concentration. In contrast, maximum at 1/2 can be obtained if using [V2] instead of [V1] (**Fig. 33 B**).
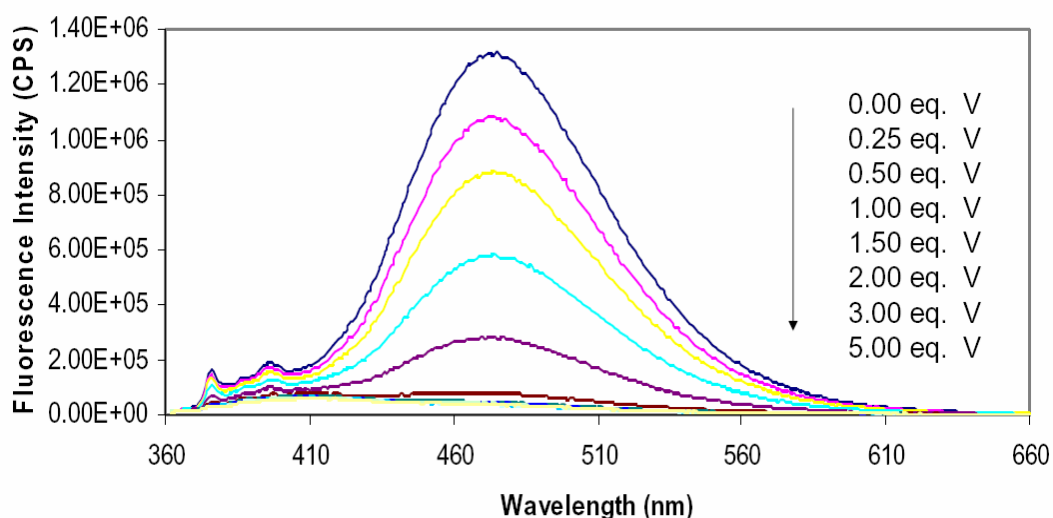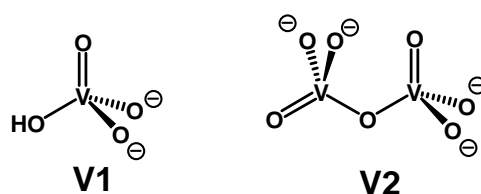
Figure 32. Fluorescent spectra of **36** (3 μM in acetonitrile) at diffirent ratio vanadate (λ_{ex} = 345 nm). Both monomer and excimer bands were quenched upon the increasing ratio of vanadate.
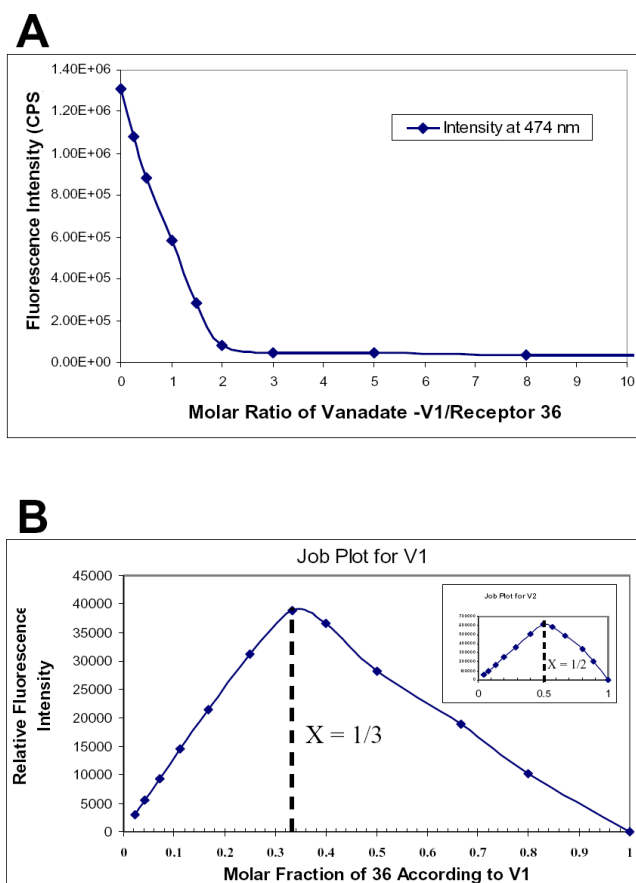
Figure 33. (A) The titration curve monitoring the fluorescent intensity at 474 nm against the ratio of V1/**36**. (B) Job plot according to vanadate monomer and dimmer (inlet).

However, an accurate binding constant can not be deduced from the data of fluorescent titration because of two reasons. Firstly, all the vanadate species are involved in elusive equilibrium in acetonitrile, so it is not possible to determine the concentration of the species of interest since the concentration is too low to get meaningful ^{51}V-NMR spectrum. Secondly, it is known that only when the concentration of the analyte is in the range of $(1/(10K_a)) <$ [analyte] $< (10/K_a)$, the systematic error for calculation of binding constants K_a is acceptable.[174] In this case, the affinity of **36** to V2 is too high to be fitted, as one can see from the sharp break point. Nevertheless, it is obvious to judge that the $K_a \gg 10/$[analyte]. Namely, the binding constant is much higher than 3×10^7 mol^{-1}.

The quenching observed with vanadate can be rationalized in terms of the change in redox properties of guanidinium (**Fig. 34**). Due to occupancy of the lone pair by protonation, the vanadate-free guanidinium has a relative lower HOMO level below

that of an excited pyrene (pyr.[*]); therefore its influence to fluorescent intensity is negligible. However, the formation of complex with vanadate by hydrogen bond weakens the N-H bonds of guanidinium; hence the HOMO level increases to be above that of pyr.[*] such that the electron transfer from the former to the half filled later one occurs, interrupting the fluorescence process of pyr.[*]. Consequently, the quenching of fluorescence is observed (**Fig. 34**).[227]
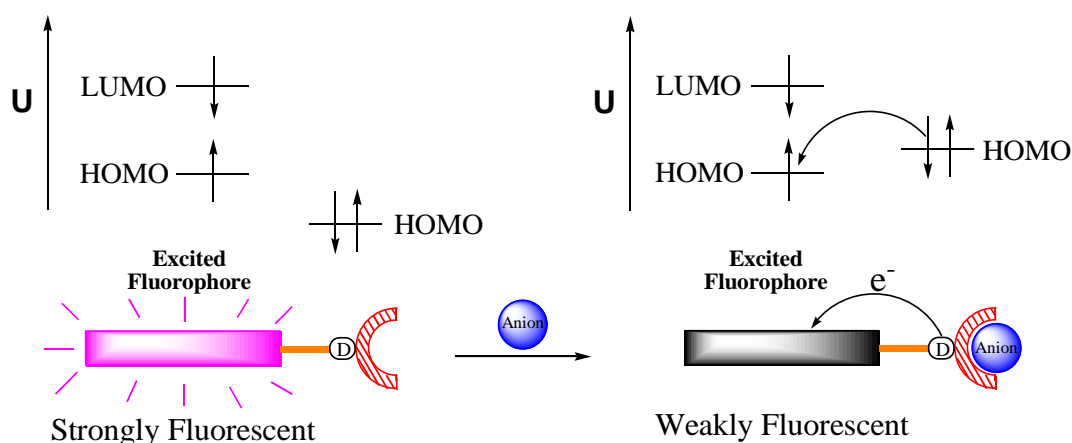
Figure 34. Principle of fluorescence quenching induced by anion recognition of fluorescent PET sensors.

3. 3. 5. [51]V-NMR Titration

Due to the low solubility of the complex formed between **36** and vanadate, a mixture of D_2O/DMSO-d_6 (1:3) was finally chosen as solvent for the ^{51}V-NMR titration. The 0.5 mM vanadate stock solution alone shows three peaks at -546, -574 and -585 ppm, which can be assigned to V1, V2 and V4 respectively (structures see **Fig. 35**).[129] Upon the proportional addition of **36**, the ratios of V1 and V4 peaks decreased while that of V2 (suggested from the stoichiometry of UV and fluorescence titration) increased and the peak significantly became broader (**Fig. 35**). The broadening of the V2 peak evidently suggests that complexation occurs. When the ratio of **36**/vanadate$_{total}$ reached 2:1, most of the V4 signal disappeared, and the V2 became predominant species (**Fig. 35**). The remaining small portion of V1 is tentatively assigned as VO_4^{3-}, which can not be dimerized due to not being protonated, since the dimerization requires protons to eliminate one equivalent H_2O, as shown in **Eq. (10)**.

$$2 \times \mathrm{HVO_4^{2-}} \rightarrow \mathrm{V_2O_7^{4-}} + \mathrm{H_2O} \qquad (10)$$
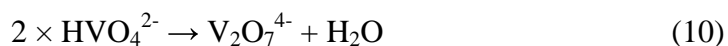
The result of ^{51}V-NMR titration provides consistent evidence that **36** preferentially binds V2, which drive the equilibriums towards the formation of V2 over V1 and V4.
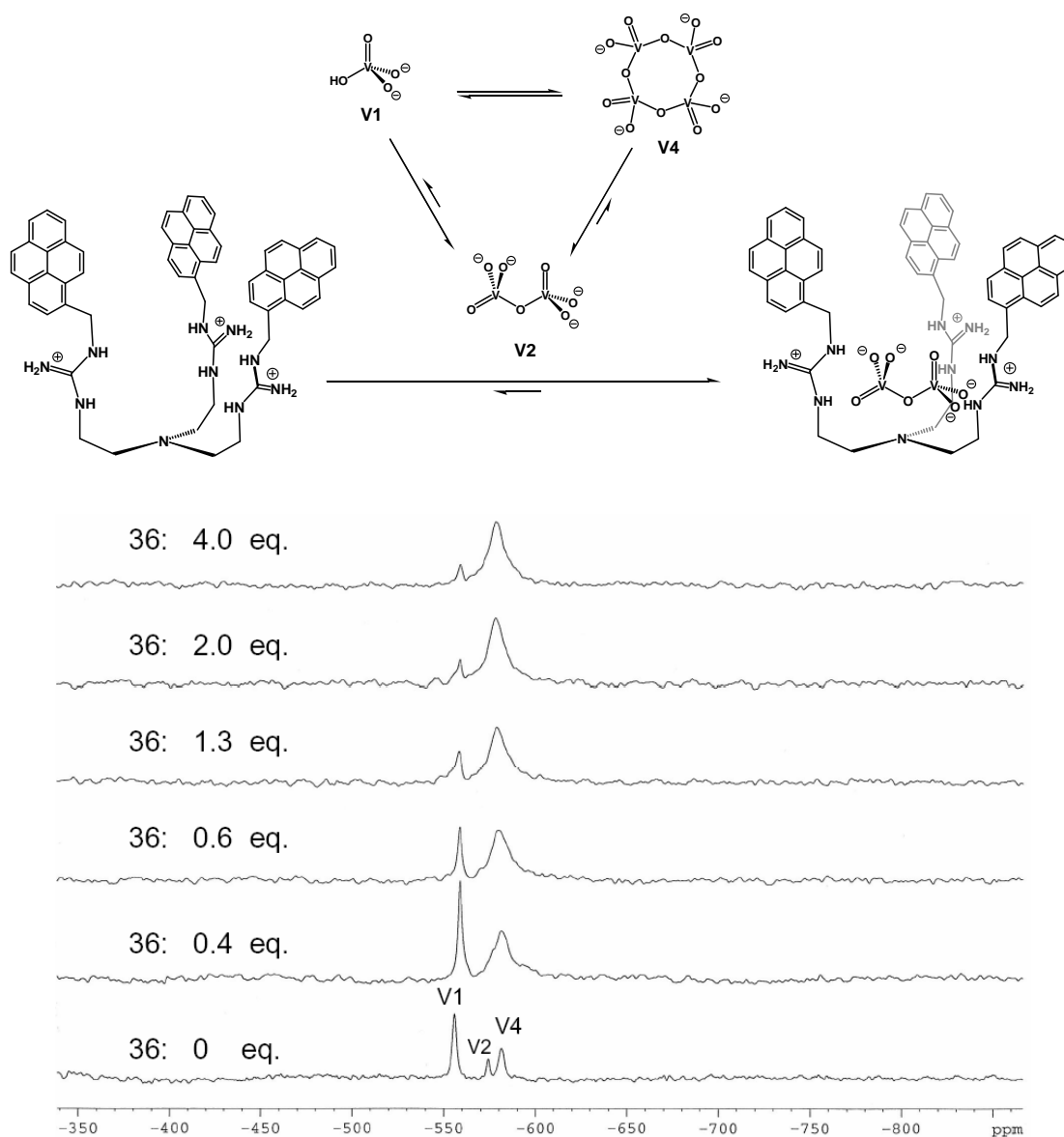
Figure 35. 36 preferentially binding V2 over V1 as indicated by ^{51}V-NMR spectra of 0.5 mM vanadate in DMSO-d_6/D$_2$O (3:1) with different ratio of **36**. The total concentration of vanadate is counted according to V1.

^{1}H-NMR spectra were also measured to follow the change of signals from **36** upon the binding with V2. All the ^{1}H peaks became much broader with the increasing ratio of vanadate. The broadening of signals observed both from ^{1}H and ^{51}V NMR spectra suggest a slow exchanging process between free and complexed state due to tight

binding. In principle, measurement in lower temperature can further slow the exchanging rate down to NMR time scale to get information of different individual state. However, the high melting point of DMSO excludes the possibility to be cooled down to a meaningfully low level.

3. 3. 6. Binding Inorganic Pyrophosphate (PPi) and Phosphate—Structural Analogues of Vanadates $V_2O_7^{4-}$ and HVO_4^{2-}

It is reasonable to assume that **36** should bind pyrophosphate (PPi), the structural analogue of vanadate dimer in a similar fashion. In addition, unlike V2, which is involved in fast equilibrium with other vanadate species in solution, PPi is kinetically inert. Therefore it should be easier to characterize the stoichiometry and binding affinity between **36** and pyrophosphate than those between **36** and V2.

Strikingly similar changes on UV spectra were observed when **36** was titrated with the solution of $(nBu_4N)_3HP_2O_7^{3-}$ in acetonitrile (**Fig. 36**) as that from the titration with vanadate (see **Fig. 32**). Most of the bands are red shifted and became broader upon the stepwise addition of PPi till one equivalent PPi was added. Job plot shows a maximum at 0.5, revealing 1:1 binding mode. This UV change clearly indicates a similar binding mode of PPi and V2, respectively to **36**.
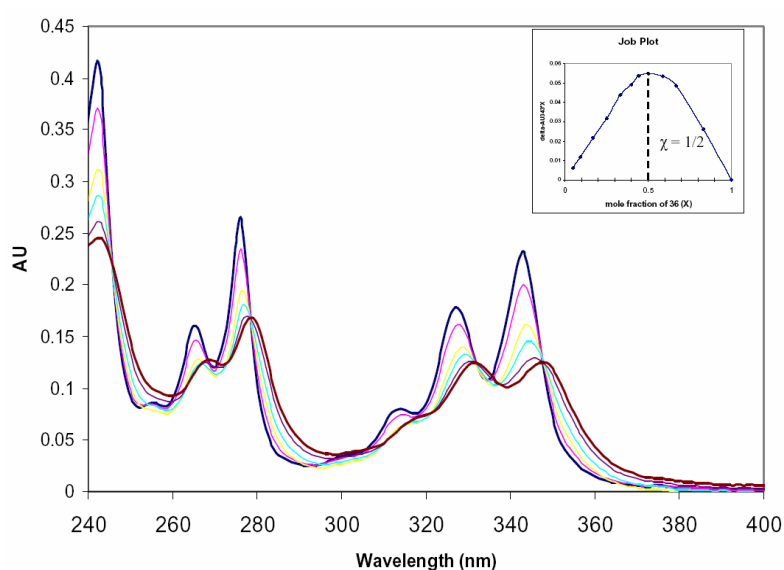
Figure 36. UV titration of **36** (3 µM in acetonitrile) by pyrophosphate and the related Job plot (inlet).

Similar fluorescence quenching was also observed (**Fig. 37**) both for excimer and monomer emission when **36** was titrated with PPi. However, the quenching efficiency of PPi is less than that of V2, consistent with 14% of the remaining intensity of excimer emission even after adding of 10 equivalents of PPi, while for V2, quenching is almost completed at 1 equivalent. In addition, the titration curve of PPi is less sharp than that of vanadate, indicates **36** binds V2 more tightly than PPi.
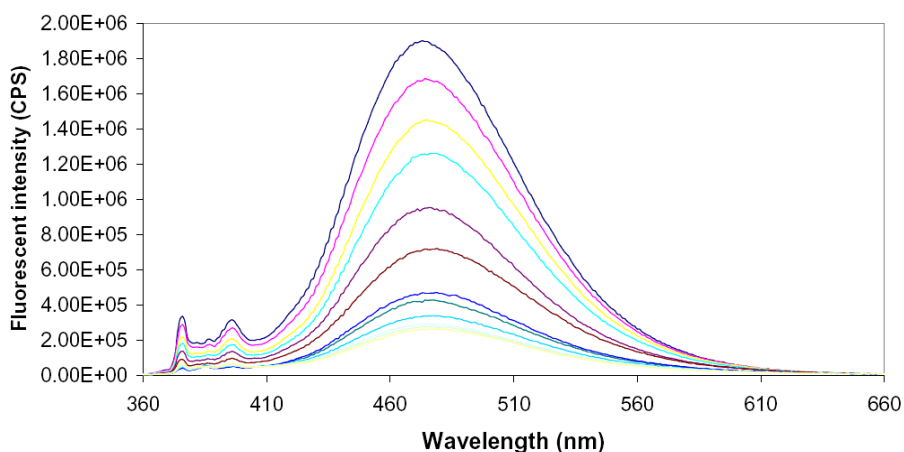
Figure 37. Fluorescent titration of **36** (3 μM in acetonitrile) by tetra-n-butyl-ammonium pyrophosphate.

The binding constant is determined by non-linear curve fitting. The following general equation (**Eq. 11**)[174] is applied for both fluorescence and UV titration:

$$I_{obs} = I_{H_o} + \frac{(I_{HG} - I_{H_o})}{2[H_o]} \left([H_o] + [G_o] + \sqrt{([H_o] + [G_o] + \frac{1}{K})^2 - 4[H_o][G_o]} \right) \quad (11)$$

In **Eq. 11**, I refers to the intensity of UV absorption or fluorescence emission; H is the host molecule (**36**) and G is the guest molecule (*i.e.* PPi or V2); HG is the 1:1 complex of host and guest; K refers to binding constant which need to be fitted. This equation describes the relationship of the observed spectroscopic data (I_{obs}) from the host entity with total amount of guest molecule being added (G_0). In principle, **Eq. 11** can be applied to any supramolecular system for the formation of 1:1 complex coupled with continuously observable spectroscopic change. Applying Eq.11 on experimental data obtained from the UV titration (see **Fig. 36**) gave a very good fit (**Fig 38**), from which the binding constant of 1.5×10^7 mol^{-1} was calculated.
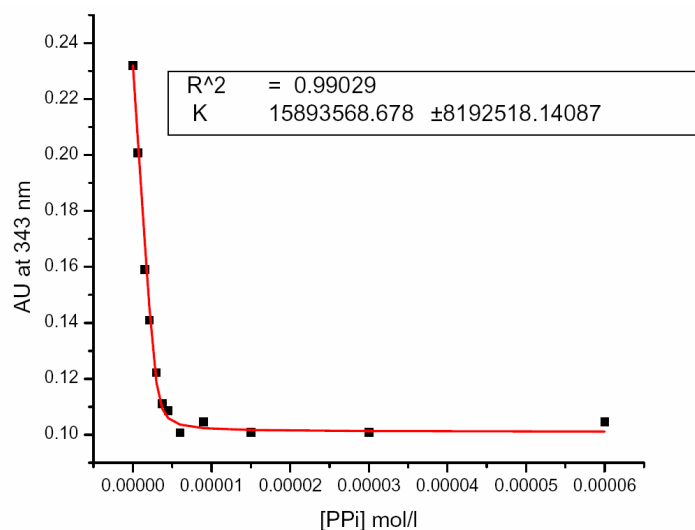
Figure 38. UV titration data of **36** (3 μM in acetonitrile) by pyrophosphate monitoring at 343 nm, and the calculated binding curve (in red) with $K_a = 1.5 \times 10^7$ mol^{-1}.

The complex of **36** and PPi also shows low solubility in most of the organic solvents and water. Therefore, the NMR titration was performed in DMSO-d_6. Since the ^{31}P NMR chemical shift PPi is not sensitive in terms of formation of hydrogen bonds, only ^{1}H-NMR spectra of **36** were measured to follow the changes upon the binding with PPi. As expected, broadening of ^{1}H resonances was observed (**Fig. 39**), similar as for the titration with vanadate.
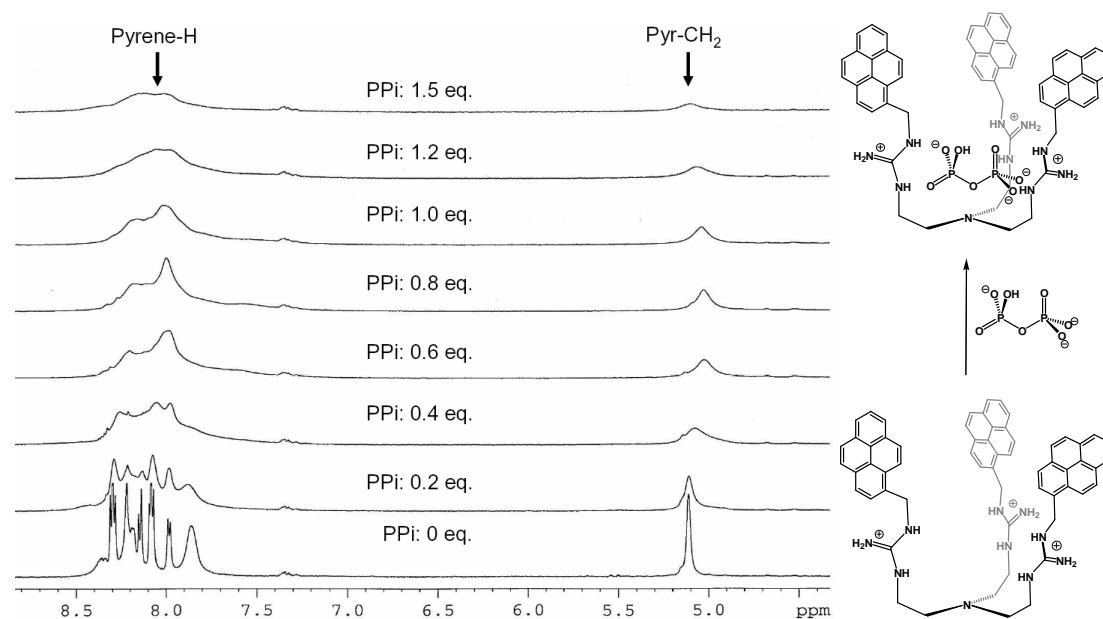
Figure 39. Part of the ^{1}H-NMR spectra of 0.5 mM **36** in DMSO-d_6 with different ratio of PPi.

Using parameters from the X-ray structure of **1**, the molecular structure of complex formed by **36** and PPi was calculated with program Titan® at the AM1 level. It is important to note that although the size of PPi is much larger than chloride, the binding pocket of **36** can still accommodate PPi by self-adjusting the geometry of the binding site inside the basket.
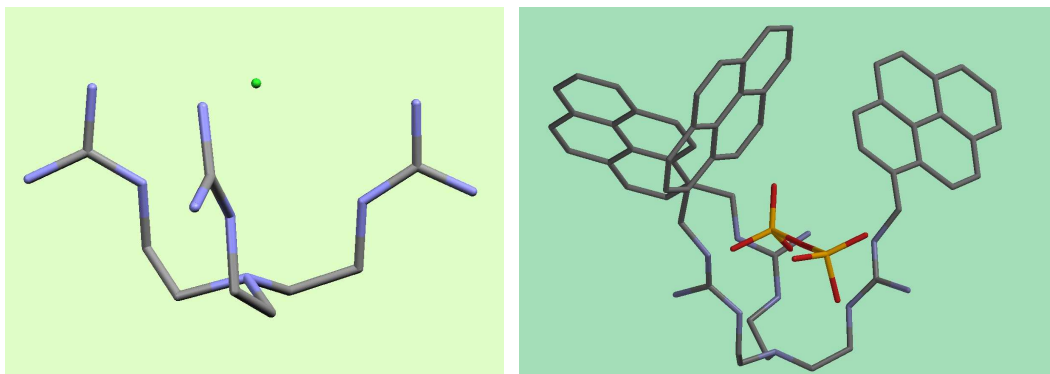
Figure 40. The proposed structure of complex of **36** and PPi (right) based on the X-ray structure of 1 (left). The molecular modeling is calculated at AM1 level with program Titan®.

For comparison, the binding of phosphate to **36** was investigated by UV, fluorescence and NMR titration. Changes, similar to PPi-binding were observed, such as red shifting and broadening of UV bands, quenching of fluorescent emissions and broadening of ^{1}H-NMR signals, however, the changes observed with all these methods were less significant, indicating the lower affinity of phosphate to **36**. Further, no clear stoichiometry can be deduced from the titration data, suggesting the formation of different complexes between host and guest molecules. For example, the ^{1}H-NMR titration curve following the chemical shift change of the benzyl protons of **36** at different ratios of phosphate shows a very complicated tendency (**Fig. 41**), revealing equilibria between several multi-components complexes. Apparently, **36** is not an optimal receptor for phosphate.
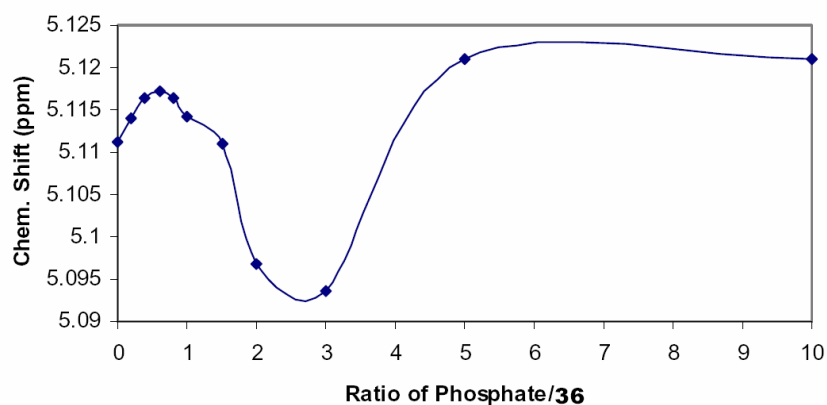
Figure 41. ^{1}H-NMR titration curve of **36** in DMSO-d_6 by phosphate, monitoring the chemical shift of proton at benzyl position of **36**.

3. 3. 7. Comparison of 36 and the Thiourea-Analogue 53 as Anion Receptor

The thiourea precursor **53** is a close structural analogue of guanidinium receptor **36**, but carries no positive charge for coulomb interaction with a guest molecule, the capacity to bind any kind of vanadate or phosphate hence can only originate from the formation of hydrogen bonds. For direct comparison, the same solvent and vanadate stock solution were used for the UV and fluorescent titration. Almost no influence to the UV spectrum was observed when vanadate was added portionwise to the acetonitrile solution of **53**, except for the background absorption caused by vanadate itself. However, quenching of fluorescent emission was obtained. It is interesting to note that the quenching is mainly observed for the excimer emission, while the monomer fluorescence intensity decreased only to a small extent compared to the excimer (**Fig. 42**). Clear stoichiometry has not been possible to be determined since the Job plot from fluorescent profile gave two maxima (**Fig. 42**), indicating that more than one complex was generated between **53** and vanadate. If the main change of fluorescence intensity is associated with the formation of 1:1 complex with V1, the binding constant about 1.4×10^5 mol^{-1} can be estamated. This assumption is based on the non-linear fitting results with $\gamma^2 = 0.984$. Therefore, it is reasonable to conclude that the binding constant of **53** to vanadate is at least two orders magnitude lower than that for **36**, due to the lack of positive charge for electrostatic interaction.
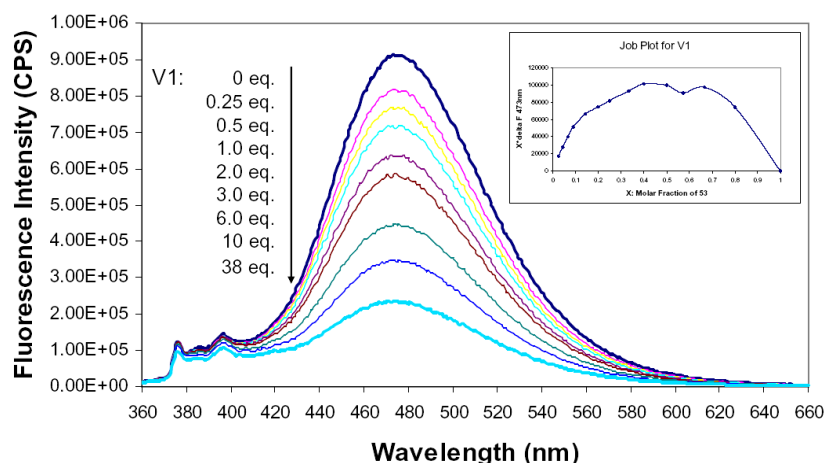
Figure 42. Fluorescent titration of **53** (3 μM in acetonitrile) by vanadate (the total equivalent was counted as V1), and the related Job plot.

All the titration studies with phosphate and pyrophosphate showed that both anions influenced the UV-, fluorescence- and ^{1}H-NMR spectra of **53**, however, none of the experiment gave any clear stoichiometry between host and guest molecules. Apparently, **53** is not an optimal receptor for these anions.

It is worth to note that during the ^{1}H-NMR titration, significant change of chemical shift to higher field was observed for the signals from the counter cation, nBu_4N^+, which is normally believed to be innocent for binding due to its non-coordinative nature. The N-CH$_2$ is the most shifted signal, with the maximum downfield shift of about 1 ppm at the ratio of **53** : $nBu_4^+NH_2PO_4^- = 1:1$ (**Fig. 43**).

This observation can be associated with the ion-pair formation. When the neutral receptor **53** binds the anion by hydrogen bonds, the resulting complex **57** is negatively charged. Therefore, the counter cation is attracted closer to form ion-pairs such as **58** (**Scheme 15**). Due to the shielding effect from the large conjugated π electron system of pyrenes, proton signals of nBu_4N^+ shift to higher field. Understandably the positively charged **36** displayed almost no change of chemical shift of nBu_4N^+ part and has much higher affinity to anions. The possibility that **53** alone may bind nBu_4N^+ by π-cation interaction can be excluded, because no influence on the chemical shift was observed when **53** was titrated with $nBu_4N^+BPh_4^-$, of which the anion BPh_4^- is non-coordinative, and hence, does not form a complex with **53** by hydrogen bonding.
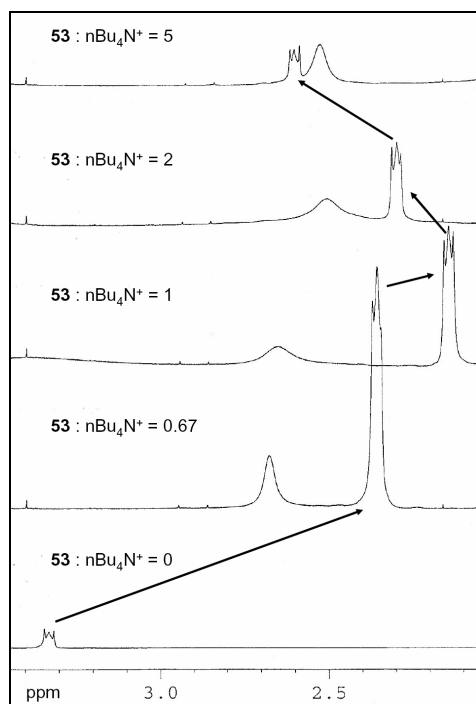
Figure 43. Partial ^{1}H-NMR spectra of n-Bu$_4$N$^+$H$_2$PO$_4^-$ with different ratio of **53**. Signals marked belong to N-CH$_2$ of n-Bu$_4$N$^+$.

It is possible that the formation of the ion-pairs also has an influence on the UV and fluorescence spectra, especially if nBu$_4$N$^+$ is embedded within the three pyrenes, which will enlarge the distance between pyrenes and reduce the ratio of excimer formation. This may explain why the UV and fluorescence titration data did not fit the simple 1:1 complex mode. More experiments are needed in order to verify the modified mode shown in **Scheme 15**, which taken the ion pair formation into the account of the overall equilibriums. Nevertheless, the neutral receptor **53** opens the possibility to probe the process of ion-pair formation, which is potentially helpful to interpret many phenomena in supramolecular chemistry especially in low dielectric constant solvents, but only attracts little attention nowadays.[231, 232]
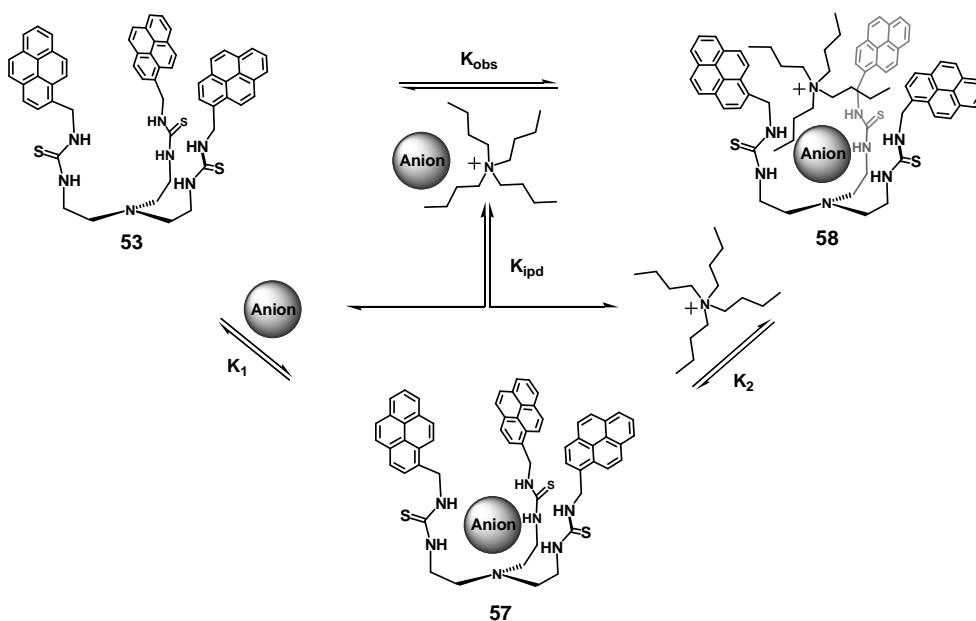
Scheme 15. The equilibriums of anion binding of **53** coupled with ion-pair formation.

3. 3. 8. Summary of Part 3. 3.

Introducing pyrene-CH$_2$- to the N-terminal of the all three guanidinium arms of **1** leads to a new class of vanadate and phosphate receptors distinct from **1**. **36** can be synthesized from its thiourea analogy **53**. The pyrene chromophores of both **36** and **53** couple the UV and fluorescence responds to anion binding, *i.e.* excimer formation and the PET type fluorescence quenching can be observed. The pyrenes of **36** hold the three arms together by π-π interaction, preorganizing itself to bind vanadate. In addition, compared to **1**, **36** is more soluble in organic solvent. Therefore, deduced from the UV, fluorescence and ^{51}V-NMR titration, **36** exhibits an association constant $\gg 3 \times 10^7$ mol^{-1} with pyrovanadate (V$_2$O$_7^{4-}$) in acetonitrile, which is at least 4 orders of magnitude higher than that of **1** to HVO$_4^{2-}$. The preference of **36** binding V2 over V1 was also confirmed by comparison with titration studies of pyrophosphate and phosphate, the structural analogues of pyrovanadate and vanadate. The neutral thiourea receptor **53** shows much smaller binding constant and almost no preference to any vanadate or phosphate species mentioned above, revealing the importance of positive charges on the affinity and selectivity for anion binding.

3. 4. Catalytic Activity: Functional Model of V-HPO

3. 4. 1. Activity of Vanadate alone in Acetonitrile: Solvent Effect

As already mentioned in **chapter 1.6.2.**, Butler first reported that simple vanadate can mimic the function of V-HPO in acidic aqueous solution; namely, it can catalyze the oxidation of Br^- in the presence of H_2O_2 to Br^+ and the subsequent bromination organic substrates.[124, 125] The active species of the system was proposed as $V_2O_2(O_2)_3$.[125, 129] The catalyst was later applied in a two-phase system (H_2O-$CHCl_3$ or H_2O-CH_2Cl_2) by other group.[131, 132] However, it has never been tried in homogenous pure organic solvent in which the inorganic vanadate is not soluble. As described previously, using nBu_4N^+ as counter cation, it has been able to prepare vanadate stock solution in organic solvent. Therefore we first investigated the catalytic activity of vanadate alone in acetonitrile to compare the solvent influence on bromide oxidation and bromination of organic substrate.

Since "Br^+" exists as the equilibrium mixture (*i.e.* HOBr $\rightleftharpoons$ Br_2 $\rightleftharpoons$ Br_3^- in water), the oxidation of Br^- to "Br^+" can be followed by UV-vis, monitoring the increasing of absorption at 268 nm, which is a characteristic band of Br_3^- (**Fig. 44**). It is worth to note this absorption maximum in acetonitrile is slightly red shifted compared to that in water (λ_{max} = 267 nm). The catalytic reaction is dramatically accelerated by changing solvent from water to acetonitrile. However, the exact turn over rate is difficult to be obtained for this reaction, because the equilibrium constants of "Br^+" $\rightleftharpoons$ Br_2 $\rightleftharpoons$ Br_3^- have not been established in this solvent.
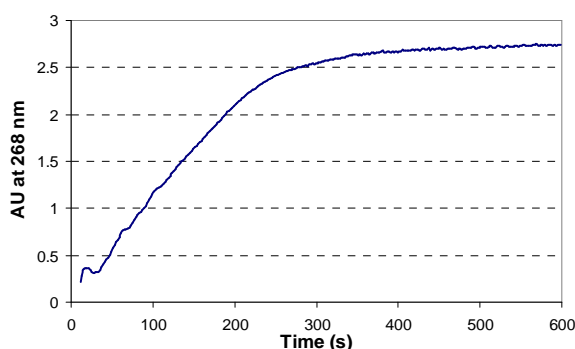
Figure 44. Vanadate catalyzed oxidation of Br^- to "Br^+" as followed by UV-vis spectroscopy at 268 nm. Reaction conditions are 6 μM vanadate (counted as V1), 0.48 mM H_2O_2, 1.2 mM *n*-Bu$_4$NBr and 0.24 mM HClO$_4$. The reaction is initiated by addition of HClO$_4$.

Monochlorodimedone (MCD) and phenol red have been used as standard substrates for the catalytic bromination of organic compounds since these reactions can be followed by UV-vis spectroscopy.[110, 127] Phenol red (**59**) is tetra-brominated to give bromophenol blue (**60**). The significant difference of the absorption maxima between **59** (λ_{max} = 429 nm; ε = 21.4 mM^{-1} cm^{-1}) and **60** (λ_{max} = 598 nm; ε = 70.4 mM^{-1} cm^{-1}) in water buffer solution renders phenol red one of the most favorite bromination substrates for catalytic analysis. As one can judge from the compounds' names, the distinct colors of educts and product make it possible to visualize the reaction process even by the naked eyes (**Scheme 16**). However, since phenol red can be tetra-brominated, and every single step of bromination is coupled with different extend of color change, accurate quantification of the kinetic data from UV measurement is very difficult. Surprisingly, this source of errors has been ignored by most authors.[137, 233-236] In addition, unlike the situation in water buffer solution, **59** and **60** show only small difference of UV in acetonitrile, because they mainly exist in the form of yellow γ-sultones (**61** and **62**) in organic solvents (**Scheme 16**)[234, 237]. Pecararo studied the kinetics of catalytic bromination of phenol red in acetonitrile spectrophotometrically, however, the reaction aliquot had to be diluted in water buffer solution for UV measurement from time to time. In our system, the reaction is too fast; hence a quantitative analysis is not possible if following this way.
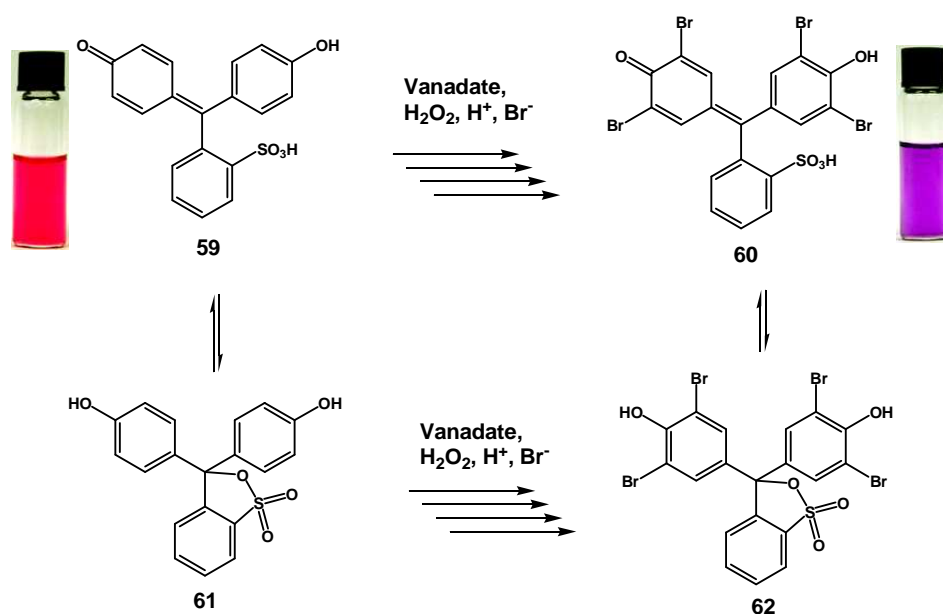
Scheme 16. The catalytic bromination of phenol red to bromophenol blue and their tautomerization equilibriums in acetonitrile.

MCD has maximum absorption at 258 nm in acetonitrile with the extinction coefficient of 11.8 mM^{-1} cm^{-1}, which is different from that in water (λ_{max} = 290 nm, ε = 20 mM^{-1}cm^{-1})[11]. The bromination of MCD can be quantitatively followed at loss of UV intensity at 258 nm (**Scheme 17**). The overall reaction needs one equivalent of both H^{+} and Br^{-}, which can derive from HClO$_4$ and n-Bu$_4$NBr separately or HBr directly. No significant influence on reaction rate was observed when different H^{+} and Br^{-} sources were used. The latter is preferred for convenience and more economic especially in preparative scale.
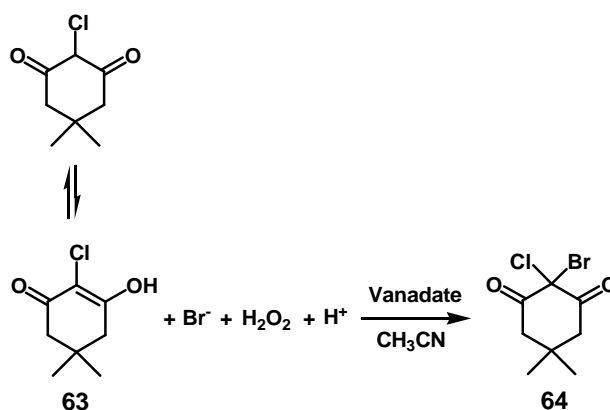
Scheme 17. The catalytic bromination of MCD in acetonitrile.

The bromination of MCD catalyzed by vanadate is rapid and stoichiometric on each H$_2$O$_2$, H^{+} and Br^{-} consumption. About 10 turnovers were achieved within 7 minutes, which is half-life of the reaction. As shown in **Fig. 44**, the increase of absorption at 258 nm at the beginning of reaction time is due to the formation of Br$_3^{-}$ (λ_{max} = 268 nm), which disturbs the measurement of initial rate. Therefore, the rate could only be determined after ca. 120 seconds. Compared with the reported reaction rate in water[124], similar value of (d[MCD]/dt) can be obtained at much lower concentration of both catalyst and reactants in acetonitrile, *i.e.*, [vanadate] was 30 times lower than that in water, while [H$_2$O$_2$], [H^{+}] and [Br^{-}] were 20, 400 and 1000 times lower respectively, indicating the over all rate constant in acetonitrile is several orders of magnitude higher than that in water.
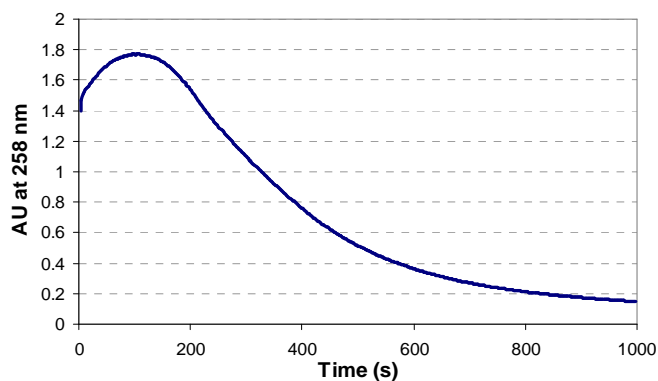
Figure 44. Vanadate catalyzed bromination of MCD as followed by UV-vis spectroscopy at 258 nm. Reaction conditions are 6 μM vanadate (counted as V1), 0.12 mM MCD, 0.3 mM H$_2$O$_2$, 0.12 mM HBr. The reaction is initiated by addition of HBr.

The rate of bromination depends on the reactivity of organic substrates. Due to the electrophilic nature of the Br$^+$, electron rich substrates are brominated much faster, for example, 100 turnovers were achieved within less than 10 minutes for the bromination of 1,3,5-tri-methoxy-benzene (TMB, **65**), which is about 50 times higher than that reported in water.[124] The dramatic rate enhancement by simply changing solvent can be reasoned to the mimicry of hydrophobic environment at the active site of enzyme. It is becoming especially clear in the field of bioinorganic chemistry that the metallic enzyme normally has a less polar active site interiorly which is provided by protein folding. More specifically, as Pecoraro proposed for his functional models,[128, 129] using acetonitrile as solvent might facilitate the protonation of peroxovanadate by increasing the pK$_a$ value of its conjugated acid, since the protonation is key step of the catalytic cycle.

If stoichiometric HBr or H$_2$O$_2$ was used, bromination of TMB quantitatively yields mono-brominated product **66**. If both reactants were added in excess, further brominated product could be obtained. This bromination reaction can be readily scaled up for preparative use. Several aromatic substrates were brominated in gram scale (**Scheme 18**). Notably, the first bromination step of activated aromatic compounds is exclusively *para* selective (see **68** and **70**), indicating the active-brominating species may be vanadate-bounded, rather than freely diffusible "Br$^+$", since the bromination by Br$_2$ alone leads to the mixture of regio-isomers[238]. With excess of HBr or H$_2$O$_2$, the second bromination happened in *ortho* position (*i.e.,* **71**).

Chlorination of TMB was also achieved in a preparative scale, and a second chlorination is possible if an excess of reactants was used. Although oxidation of chloride catalyzed by simple vanadate was observed in water, no detail was reported presumably because the reaction is too slow in aqueous solution[124]. However, the chlorination highly depends on substrate reactivity, *i.e.*, even in acetonitrile, chlorination of MCD can not be observed. The reason of apparent rate determination by the reactivity of organic substrate is not obvious, which need further in depth kinetic investigation.
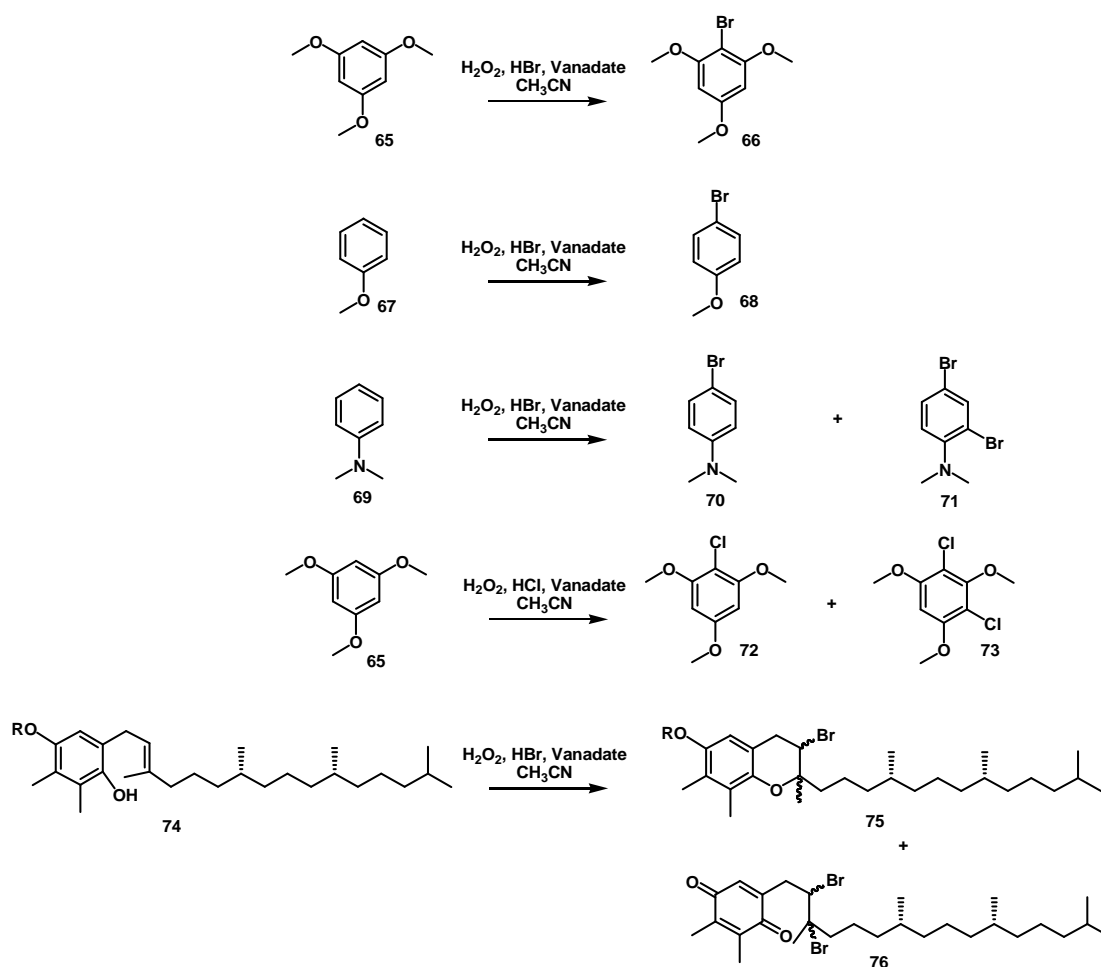
Scheme 18. The halogenations of organic substrates catalyzed by vanadate in acetonitrile.

It is interesting to note that a bromination coupled cyclization has been achieved for a mono-protected phytyl-hydroquinone **74**, yielding a brominated γ-tocopherol derivative **75**. The γ-tocopherol belongs to vitamin E family which is of industrial interest as important food and cosmetic additive, as well as therapeutic drug. The acid-promoted cyclization of phytyl-hydroquinone is the key step in the biosynthesis

of γ-tocopherol. It has been discovered by Woggon's group that this enzyme-catalyzed ring closure proceeds by *Si* protonation of the double bond and concomittant *Re* attack of the phenolic oxygen atom via a carbon-cation transition state[239, 240]. Therefore, the cyclization of **74** suggests a cationic nature of the active brominating species. However, although the cyclized product is exclusively the 6-membered chromane, a side product **76** from the oxidative cleavage of the protecting group by H_2O_2 diminishes the yield of **75** to only 41%.

3. 4. 2. Catalytic Activity of Vanadate-**36** Complex

To investigate the vanadate catalyzed bromination by the vanadate-bound supramolecular receptor which mimics the protein part of V-HPO is the final goal of this study. As already mentioned in the introduction, coordination of hydrogen peroxide to vanadate to form peroxovanadate is the common first step of catalytical cycle for both the V-HPO and some of the reported functional models. Therefore, the affinity of the supramolecular receptor **36** to peroxovanadate was first studied in order to confirm that vanadate keeps being bounded during the whole process. It is known that peroxoxvanadates apparently do not oligomerize beyond the formation of dimers, but their solution chemistry is easily as complex as simple vanadate because of their ability to bind between 1-4 peroxides[116]. The equilibria of peroxoxvanadates in acetonitrile and acetonitrile/water mixture have been studied by ^{51}V-NMR at mM concentration by Pecoraro. $H_xV_2O_3(O_2)_4^{x-4}$, which is a dimer of diperoxovanadate $VO(O_2)_2^-$, becomes the predominate species at low water concentrated acetonitrile solution at the presence of excess of H_2O_2[129].

The binding of peroxoxvanadates to **36** was studied by UV and fluorescence titration as the way described previously. Peroxovanadate was prepared by addition of 10 equivalent excess of H_2O_2 to the 5.4 mM vanadate solution in acetonitrile. Addition of this peroxovanadate to the acetonitrile solution of **36** caused the broadening of UV bands, indicating that complexation occurred. The change became saturated after the addition of 2.5 equivalents of peroxovanadate (counted as V1). It is important to note

that the final state of the UV spectrum of the **36**-peroxovanadate complex is different to that of the **36**-vanadate mixture (**Fig. 45**), reflecting their structural difference. The same final UV spectrum can also be obtained by forming **36**-vanadate complex first, then adding excess of H_2O_2 later.
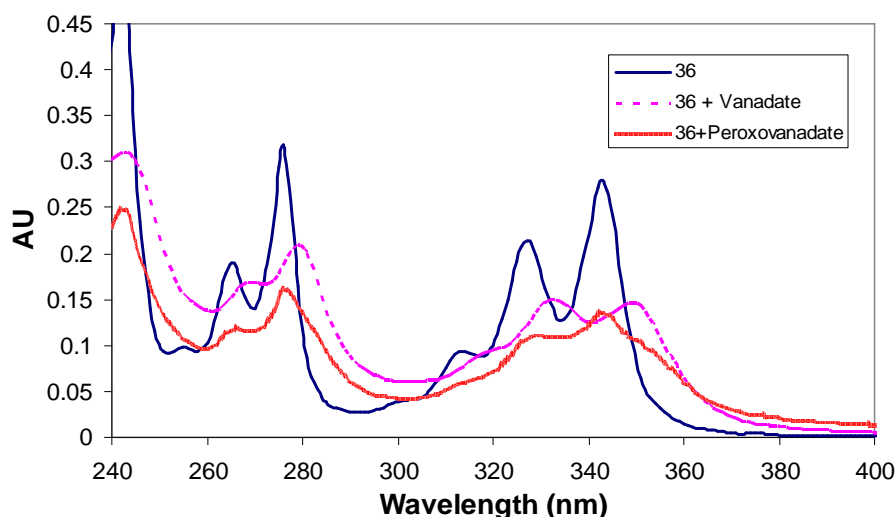
Figure 45. Comparison of UV spectra of **36** alone (blue solid line) and at the presence of vanadate (violet dash line) or peroxovanadate (red dotted line).

Similar as that observed with vanadate or pyrophosphate binding to **36**, the peroxovanadate induced UV change was also accompanied by fluorescence quenching. After addition of 1.5 equivalents of peroxovanadate (counted as V1) to **36**, the quenching of both the excimer and monomer emissions were almost complete. (**Fig. 46**). The elusive break points of UV and fluorescent titration are not consistent to each other, which suggest that more than one peroxovanadate species may be involved in complexation with **36** simultaneously. As reported by Pecoraro, two minor species of unknown structures are detectable in the [51]V-NMR spectrum of peroxovanadate in acetonitrile solution together with the main species, $H_xV_2O_3(O_2)_4^{x-}$. [129] It is possible that these unknown species may be involved in the complexation with **36.** Details are not clear yet because no suitable solvent is available which can well dissolve both **36** and vanadate while is innocent to peroxide. Nevertheless, the sharp binding curve clearly indicates that the major peroxovanadate species is tightly bound to **36**.
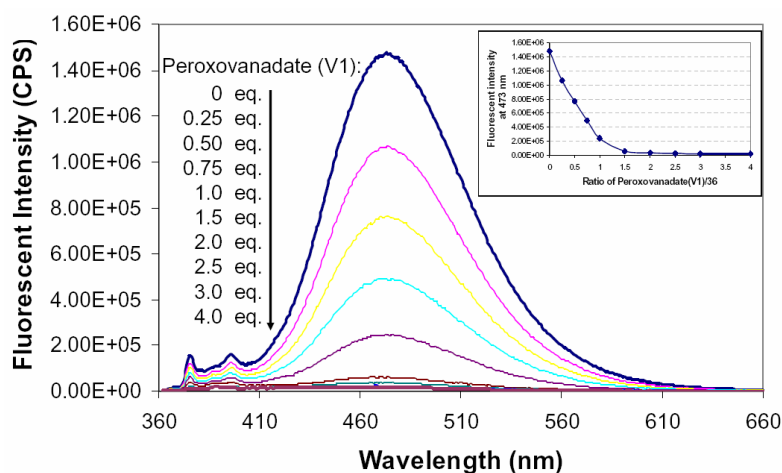
Figure 46. Fluorescent spectra of **36** (3 μM in acetonitrile) at the presence of the different equivalents of peroxovanadate (counted as V1) and the related titration curve (inlet).

Since the peroxovanadate complex with receptor **36** could be prepared, the catalytic activity for bromination of organic substrate was subsequently investigated. MCD was the first organic substrate being tested. As shown in **Fig. 47**, the bromination of MCD was followed by UV spectrum at loss of intensity at 258 nm, which reveals that the presence of **36** accelerated the bromination almost twice, as the slope of the curve in the presence of **36** is sharper than that at the absence of **36**. The half lifetime of MCD bromination ($t_{1/2}$) is almost doubled without **36** compared that with **36**.
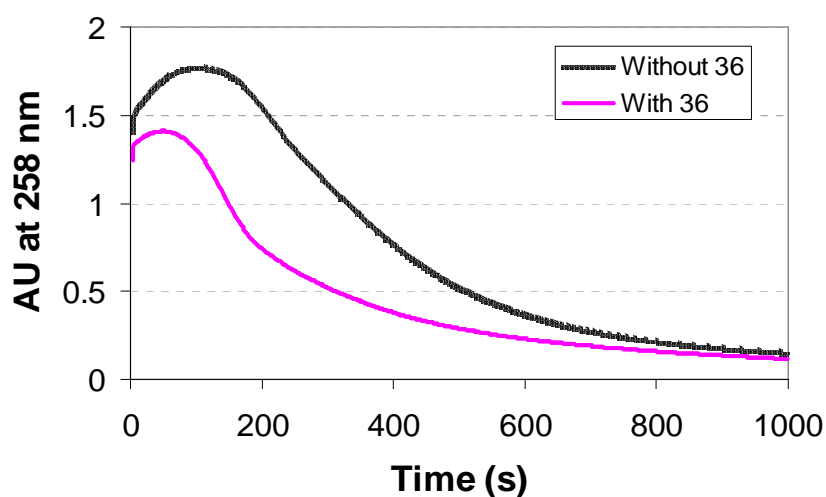
Figure 47. Comparison of catalytic bromination of MCD with or without 3 μM 36. Reaction is followed by UV-vis spectroscopy at 258 nm. Reaction conditions are 6 μM vanadate (counted as V1), 0.12 mM MCD, 0.3 mM H_2O_2, 0.12 mM HBr. The reaction is initiated by addition of HBr.

74

Whether this enhancement of catalytic activity is also applicable for the bromination of other organic substrates is of interests, particularly for electron rich aromatics. However, since little UV change is coupled with the bromination for most of the aromatics substrates, a kinetic study is difficult. To overcome this obstacle, a competitive bromination experiment was designed using both TMB and MCD as substrates in one reaction at the same time. Since TMB is much more reactive than MCD due to its electron rich characteristic, the former should be preferentially brominated over the latter. Little change of UV at 258 nm should be observed during the bromination of TMB. However, as soon as the bromination of TMB is completed, MCD will start to be brominated which will initiate the decreasing of UV intensity at 258 nm. Hence, the period of UV-insensitive time is corresponding to the total reaction time of TMB bromination. **Fig. 48** shows that in the absence of **36** the UV absorption at 258 nm is almost constant during 480 seconds, in the course of this time gap TMB is totally consumed. The following increase of UV absorption refers to a small amount of free Br_3^- being generated. After ca. 580 seconds, the absorption at 258 nm decreases steadily within about 1000 seconds due to the bromination of MCD. The overall reaction is 100% complete for both substrates and stoichiometric with the consumption of HBr. All of the individual steps discussed above were significantly accelerated when receptor **36** was added into the reaction system. The reaction time for TMB is shorten to about 150 seconds, indicating that TMB bromination is > 3 times faster than without **36**. In addition, the following steps including generation of Br_3^- and bromination of MCD also become faster, which is seen from the sharper slope of the curve.
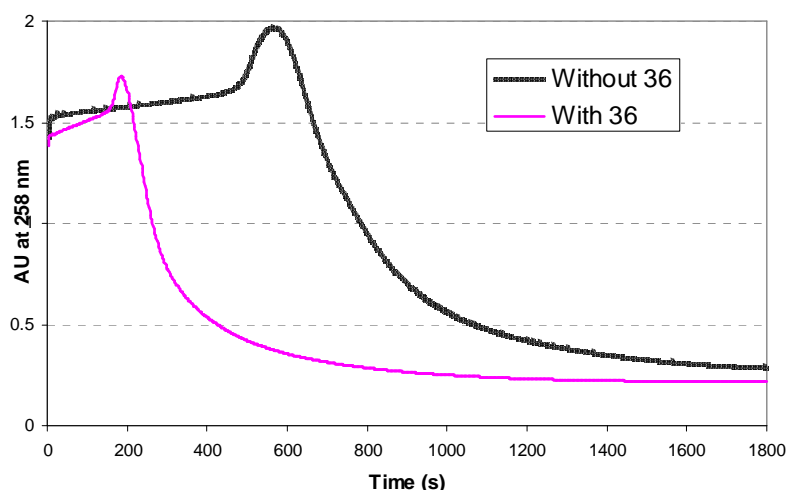
Figure 48. Comparison of competitive catalytic bromination of TMB/ MCD with or without 3 μM **36**. Reaction is followed by UV-vis spectroscopy at 258 nm. Reaction conditions are 6 μM vanadate (counted as V1), 0.12 mM MCD, 0.12 mM TMB, 0.5 mM H_2O_2, 0.24 mM HBr. The reaction is initiated by addition of HBr.

Two possible reasons are proposed here to explain the catalytic effect of **36**. Firstly, the formation of hydrogen bonds with positively charged guanidinium may increase the Lewis acidity of vanadate, as has been proposed for the enzyme of V-CPO[28]. Indeed replacement of these positively charged residues (Arg 360, and Arg 490, Lys 353) to alanine significantly decreases the activityof V-CPO[36]. Secondly, **36** may facilitate the protonation of peroxovanadate as a nearby acid base catalyst. As already described in the introduction, peroxovanadate must be protonated prior to halide oxidation both for V-HPO enzyme and the reported functional models. For V-CPO, the amino acid residue Lys 353 is proposed to play such a role. The X-ray structure of the peroxide-form of V-CPO reveals that Lys 353 is the only residue that forms direct hydrogen bond with the peroxo-oxygen atom via the ammonium group[30]. Additionally and more importantly, site directed mutagenesis of replacement of Lys 353 by alanine leads to more drastic loss of activity as compared to the replacement of Arg 360, and Arg 490. For the model systems, the pK_a value of the conjugated acid of ligand bounded peroxovanadate was estimated in the range of 5.5-6.0 (**Eq. 12**) by studying the rate dependence on acid.[128]

(12)
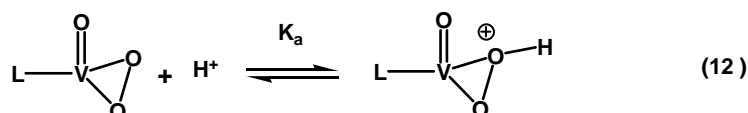
The guanidinium groups of **36** are not adequate to have efficient proton exchange with peroxovanadate due to the too higher pK_a in acetonitrile (pK_a of tetramethyl-guanidinium is 23.3 in acetonitrile and 13.2 in water[241]), however the central nitrogen atom is a reasonable candidate as one can expect based on the uncommonly low pK_{BH} value of central nitrogen of its structural analogy **1** in water ($pK_a = 2.58$).

3. 4. 3. Summary of Part 3. 4.

Using n-Bu$_4$N$^+$ as counter cation makes vanadate soluble in organic solvents. Preliminary studies reveals that simple vanadate in acetonitrile is a more efficient functional model than in water. The rate acceleration of acetonitrile can be compared to an enzyme-like hydrophobic environment in vanadate catalytic center of V-CPO. In addition, solvents also influence the pK_{BH} value for peroxovanadate, facilitating the proton transfer from the acid to it. UV and fluorescent titration shows that supramolecular receptor **36** exhibits a high affinity to the peroxovanadate. A competitive catalytic bromination experiment was designed and successfully demonstrated the kinetic process for the catalytic bromination of TMB/MCD mixtures. The addition of **36** to the reaction system significantly enhances the catalytic efficiency. The rate enhancement by **36** was discussed and reasoned to the increasing of Lewis acidity of vanadate by forming hydrogen bonds with positively charged guanidiniums of **36**. In addition, the central nitrogen atom of **36** may play as an acid base catalyst, facilitating the protonation of peroxovanadate. All together, **36** is an effective functional model for V-HPO due to the structural fidelity to the supramolecular binding fashion of the enzyme.

4. Summary and Conclusions

V-HPOs are enzymes catalyzing the halogenation of a variety of organic substrates using hydrogen peroxide and halide ions at slightly acidic condition[17, 21, 50]. The X-ray structure of V-HPO from *Curvularia inaequalis*[29, 30] reveals that the positively charged residues at the active site bind orthovanadate (HVO_4^{2-}) through electrostatic interaction and hydrogen bonds, together with one coordinating bond from the nitrogen (Nε2) of His496 to vanadium, which is the only direct bond from protein to metal center. Accordingly the coordination sphere at vanadium is trigonal-bipyramidal, resembling the transition state of **S$_N$2**-type reactions involving phosphates[65]. Apart from that, vanadate and phosphate are also very similar in the tetrahedral ground state. Thus, it is no surprise that vanadate is an inhibitor of various phosphate metabolizing enzymes[73]. Since the structural assignment and reaction mechanism of V-HPOs are still under debate, and no structural model reported so far shows high fidelity concerning the non-covalent binding fashion, we decided to prepare supramolecular models structurally related to the binding mode of HVO_4^{2-} in the enzyme, and study the influence of the binding sphere of vanadate to its catalytic activity.

The vanadate receptor tris-(2-guanidinium-ethyl)amine **1** was rationally designed and conveniently synthesized from tris-(2-aminoethyl)amine via single step. Its three guanidinium-arms can provide not only positive charges but also several hydrogen bond donor sites. The central nitrogen with pK_a=2.48 for its conjugated acid, allows the V-N coordination to occur within a broad pH window. The X-ray structure of **1** reveals that it is already preorganized in a basket shape before binding vanadate, which verifies our design.
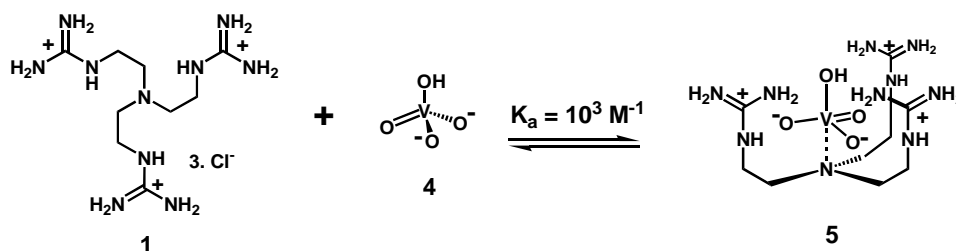
Scheme 19. Binding of vanadate to supramolecular receptor **1** and the proposed structure of complex **5**.

NMR titration data from ^{51}V of vanadate and ^{1}H of the ligand give complementary results. The ligand **1** binds vanadate as 1/1 complex **5** (**Scheme 19**) at pH 10.21 in water solution, with $K_a = 10^3$ Mol^{-1}. The complex **5** was also detected by ESI-MS.

The absorption at 306 nm observed in UV difference spectrum is an indication of a V-N bond formation in agreement with coordination in V-HPO. The time dependent DFT calculation both for enzyme and model system **5** provided in-depth evidence that V-N coordination is responsible for this UV band.

5 is the first supramolecular structural model V-HPO. These model studies provided for the first time evidence that the V-N bond of V-HPO is coordinative and not covalent as original proposed[242].

A series of more rigid novel guanidinium-cryptands containing the key scaffold of **1** were synthesized (**Scheme 20**), the preorganization was expected to provide higher affinity to vanadate. A general flexible synthetic strategy was developed which allows the preparation of the guanidinium cryptands with different size and geometry. However, spectroscopic studies failed to demonstrate any enhancement of binding constant for encapsulating vanadate. The association of vanadate most likely occurres not interior but outside of the cavity even for the largest cage receptor **35**.

32: m = 2, n = 1, R =Me
33: m = 2, n = 2, R = Bn

35
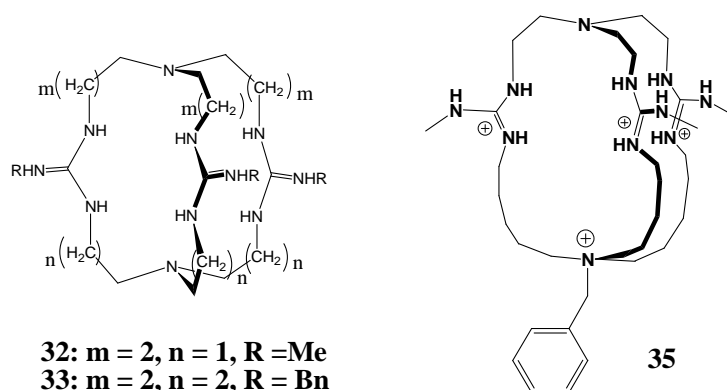
Scheme 20. Guanidinium cryptands: cage shaped receptors for vanadate.

Three pyrene moieties introduced to the terminal-N atoms of **1** not only improved the solubility of the receptor in unpolar solvent, but also served as UV and fluorescence sensor for vanadate recognition (see **Scheme 21**). In addition, the π-π stacking interaction within pyrenes holds three arms together to further preorganize itself

favoring the binding of vanadate. This preorganization was demonstrated by observing the pyrene excimer emission, which can be also observed for the neutral analogue **53**.
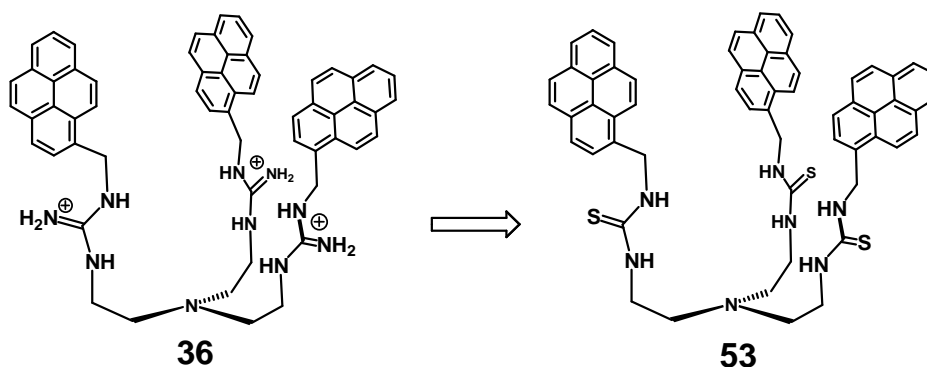
Scheme 21. More preorganized receptor and fluorescent sensor **36** and its structure analogy and synthetic precursor **53**.

The binding of vanadate to **36** and **53** is coupled with the significant UV and fluorescence response in acetonitrile. Upon the addition of vanadate, the UV bands of **36** became broader and red shifted, together with a PET-type fluorescence quenching. Therefore, deduced from the UV, fluorescence titration and additional ^{51}V-NMR data, **36** exhibits an association constant $\gg 3 \times 10^7$ mol^{-1} with pyrovanadate ($V_2O_7{}^{4-}$, V2) (**Scheme 22**) in acetonitrile, which is at least 4 times magnitude higher than that of **1** to vanadate (HVO$_4{}^{2-}$, V1). The preference of **36** to bind V2 over V1 was also confirmed in titration studies with the pyrophosphate and phosphate, the structure analogue of V2 and V1 respectively.
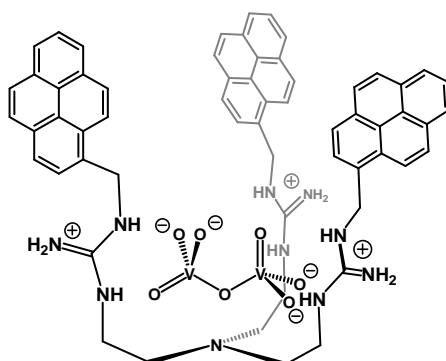
Scheme 22. The proposed complex of **36** and pyrovanadate.

The neutral thiourea receptor **53** shows much lower binding constant and almost no preference to any vanadate or phosphate species mentioned above, revealing the importance of positive charge on the affinity and selectivity for anion binding.

Kinetic studies reveal that simple vanadate in acetonitrile is a more efficient functional model than in water. The rate acceleration in acetonitrile is thought to be originated from an enzyme-like hydrophobic environment for the catalytic species. UV and fluorescence titration shows that the supramolecular receptor **36** exhibits high affinity to the peroxovanadate as well, which verifies that vanadium core keeps being bounded in the catalytical cycle. A competitive catalytic bromination experiment was designed and successfully demonstrated the kinetic process for the catalytic bromination of 1,3,5-tri-methoxy-benzene (TMB) and monochlorodimedone (MCD) mixture substrates. The addition of **36** to the reaction system significantly enhances the catalytic efficiency. The rate enhancement by **36** may be reasoned to the increasing of Lewis acidity of vanadate by forming hydrogen bonds with positively charged guanidiniums of **36**. In addition, the central nitrogen atom of **36** may act as an acid base catalyst, facilitating the protonation of peroxovanadate. All together, **36** is an effective functional model for V-HPO based on the structural fidelity to the supramolecular binding fashion of the enzyme.

Experimental Part

5. Experimental Part

5. 1. General Remarks

5. 1. 1. Solvents and Reagents

Reagents were used as received from *Fluka AG* (Buchs, Switzerland), *Merck AG* (Darmstadt, Germany) and *Aldrich* (Buchs, Switzerland) unless otherwise stated. Chemicals of the quality *purum*, *purum p. a.* or >98% were used without further purification.

Solvents for chromatography and extractions were distilled prior to use. As solvent of reaction, dry dichloromethane (CH_2Cl_2) was distilled from CaH_2, Et_2O and THF from Na/benzophenone. All freshly dried solvents were used immediately. Further solvents used for reactions corresponded to the quality *puriss p. a., abs., over Molecular Sieves* from *Fluka AG*. Degassed solvents for reactions under oxygen-free condition (*e.g.* in the glove box) were obtained by at least four freeze-pump-thaw cycles. Nano-pure water was used if necessary.

For an inert atmosphere *Argon 56* (< 4 ppm other gases) from *Carbagas AG* (Lenzburg, Switzerland) was used.

5. 1. 2. Materials & Instruments

Solvents were removed with a *Büchi* (Switzerland) rotary evaporator (Waterbath B-480, Rotavapor R 114 and Vacuum Controller 168) and a MZ 2C membrane pump (*Vacuubrand*). For cooling a mixture of EtOH and water was kept at 4° with a UKW 300 thermostat (*Vacuubrand*).

For weighing compounds and reagents *Mettler* (Switzerland) balances P1200 (> 1 g), AE163 (< 1 g), and AX205 (< 100 mg) were used.

A high-vacuum pump D5E from *Trivac* (Köln, Germany) or Edwards from *Edwards High Vacuum International* (west Sussex, England) was used for drying compounds and reagents.

Lyophilization was performed with Lyolab B from *LSL Secfroid* (Aclens, Switzerland).

Magnetic stirrers were MR3001K with thermo-controller EKT 3001 from *Heidolph* (Schwabach, Germany) and IKA-Combimag RCT from *Janke & Kunkel Gmbh & Co. KG* (Staufen, Germany).

For all non-aqueous reactions glassware were flame dried either under vacuum or argon overpressure, and the atmosphere was exchanged by three cycles of evacuating and flushing with argon.

5. 1. 3. Chromatographic Methods

Analytical thin layer chromatography (TLC) was performed on 0.25 mm precoated glass plates (5×10 cm, silica gel 60 F_{254}, *Merck AG*, Darmstadt, Germany) or on 0.2 mm precoated plastic plates (5×10 cm, ALUGRAM® aluminum oxide N/UV$_{254}$, *Macherey-Nagel*, Germany). Reverse phase TLC was performed on precoated glass plates (5×10 cm, RP-18 F_{254s}, *Merck AG*, Darmstadt, Germany). Compounds were detected at 254 nm (UV) or at 366 nm (fluorescence), or visualized by iodine vapor or spray reagents, i.e. Ninhydrin spray reagent. <u>Description</u>: TLC (solvent): R_f.

Preparative thin layer chromatography was conducted on 0.25 mm precoated glass plates (20×20 cm, silica gel 60 F_{254}, *Merck AG*, Darmstadt, Germany).

For normal phase **column chromatography** silica gel 60 from *Merck* (0.043-0.06 mm, 230-400 mesh) or aluminum oxide 90 from *Merck* (standardized (activity II-III), 0.063-0.2 mm, 70-230 mesh) were used and for eluting the compounds pressure (0.3–0.5 bar N_2) was applied (flash chromatography).

5. 1. 4. Spectroscopic and Characterization Methods

Ultra violet – visible absorption spectra (UV/Vis) were recorded on a *Hewlett-Packard* 8452A Diode Array spectrophotometer and a *Agilent* 8453 Diode Array spectrophotometer using optical 110-OS *Hellma* cuvettes (10 mm light path). For kinetic UV measurement, internal software was used to fit the reaction rate. <u>Description</u>: UV/Vis (solvent): wavelength of maxima (λ_{max}) in nm.

Fluorescence spectra were recorded on an *ISA Jobin Yvon-Spex* FluoroMax-2[®] spectrometer which was fitted with a magnetic stirrer and thermostatic cell housing controlled by external water bath, and using 10 mm path length quartz cuvettes (*Hellma*) which were fitted with an appropriate magnetic stir bar. If not otherwise stated all spectra were recorded at 23 °C. For kinetic measurement, the software OriginPro was used to fit the reaction rate.

Infrared spectra (IR) were measured on a *Perkin-Elmer* 1600 series FTIR spectrometer in KBr (1% w/w) or neat between NaCl-plates. <u>Description</u>: IR (medium): wavenumbers of transmission maxima in cm^{-1}, intensity (*s* = strong, *m* = middle, *w* = weak, *br* = broad).

^{1}H-Nuclear magnetic resonance spectroscopy (^{1}H-NMR) was performed using either a *Bruker* av250 (250 MHz), *Varian* Gemini 300 (300 MHz), *Bruker* DPX-NMR (400 MHz), *Bruker* DRX-500 (500 MHz) or a *Bruker* DRX-600 (600 MHz) spectrometer. Solvents for NMR were obtained from *Dr. Glaser AG* (Basel, Switzerland) and *Cambridge Isotope Laboratories* (Andover, MA, USA). $CDCl_3$ was filtered through basic alumina prior to use. If not otherwise stated all spectra were recorded at room temperature. If necessary for the interpretation correlated spectra like COSY, TOCSY, NOESY and ROESY were recorded also. <u>Description</u>: ^{1}H-NMR (frequency, solvent): δ_H in ppm relative to residual solvent peaks or internal TMS peak (peak multiplicity: *s* = singlet, *d* = doublet, *t* = triplet, *q* = quartet, *m* = multiplet, *b* = broad; coupling constants *J* in Hertz).

^{13}C-Nuclear magnetic resonance spectra (^{13}C-NMR) were ^{1}H-decoupled and recorded on a *Bruker* DPX-NMR (100 MHz), *Bruker* DRX-500 (125 MHz) and *Varian* Gemini 300 (75 MHz) spectrometer. For the assignment of carbons APT, DEPT, HETCOR, HMQC and HMBC experiments were carried out if essential. <u>Description</u>: ^{13}C-NMR (frequency, solvent): δ_C in ppm relative to residual solvent peaks.

^{51}V-Nuclear magnetic resonance spectra (^{51}V-NMR) were recorded on a *Bruker* DPX-600 (157.8 MHz), chemical shift is given in ppm, with VOCl3 ($\delta_v = 0.0$ ppm) as external reference; line broadening = 0-100 Hz, sweep width ~ 100 000 Hz, no relaxation delay.

^{31}P-Nuclear magnetic resonance spectra (^{31}P-NMR) were recorded on a *Bruker* DPX-600 (242.94 MHz) and *Bruker* DPX-NMR (161.97 MHz); chemical shift is given in ppm relative to inorganic phosphate ($\delta_v = 0.0$ ppm).

Electron impact mass spectra (EI-MS) and **fast atom bombardment mass spectra (FAB-MS)** were measured by *Dr. H. Nadig* on a *Varian* double focusing VG-70-250 spectrometer in the mass spectrometry laboratory of the institute. As matrix for FAB-MS nitrobenzyl alcohol was used and, if necessary KCl added. **Electron spray ionization mass spectra (ESI-MS)** were recorded on a *Finnigan Mat* LCQ-700 or a *Bruker* Esquire 3000^{plus}. Description: MS (solvent): mass peaks in *m/z* (relative intensity in %). Peaks with an intensity of less than 5% were not considered.

Single crystal X-ray structures were determined by *Dr. Markus Neuburger* and *Dr. Silvia Schaffner*. Data collection was carried out on a Nonius KappaCCD diffractometer using the COLLECT software suite. The usual corrections were applied. No absorption correction was determined. The structures were solved by direct methods using the program SIR92. Anisotropic least-squares refinement was carried out on all non-hydrogen atoms using the program CRYSTALS. Hydrogen atoms are in calculated positions.

Melting points (mp) were determined on a *Büchi* 510 apparatus and are uncorrected.

Elemental analysis (EA) was carried out by Mr. *H. Kirsch* at the institute with a *Perkin-Elmer* 240 Analyzer. Description: EA calculated (calc.) for (chemical formula, molecular weight): abundance of C, H, O in %; found abundance of C, H, O in %.

5. 1. 5. Non-linear data fit

Non-linear data fit used the program proFit 5.1 (proFit$^{®}$ QuantumSoft) performed on Mac or Origin 7.0 SR0 (Origin® OriginLab Corporation) performed on PC. The following general equation was applied for NMR, UV and fluorescent titration titration of 1:1 binding mode:

$$I_{obs} = I_{H_O} + \frac{(I_{HG} - I_{H_O})}{2[H_O]} \left([H_o] + [G_o] + \sqrt{([H_o] + [G_o] + \frac{1}{K})^2 - 4[H_o][G_o]} \right)$$

"I" refers to the chemical shift or UV/fluorescent intensity of specie H.

5. 2. Syntheses

5. 2. 1. The serial of first generation Tris- openarmed-guanidiniums

Tris(2-guanidinoethyl)amine trihydochloride (**1**)
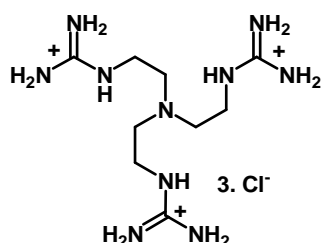
300 μl tris-(2-aminoethyl)amine (**2**, 2 mmol) and 1.03 ml N,N-di-isopropyl-ethylamine (DIEA, 6 mmol) were dissolved in 6 ml DMF to get a clear solution. White solid precipitated when the solution of 903 mg (6.16 mmol) of 1H-pyrazole-1-carboxamidine monohydrochloride (**3**) in 6 ml DMF was added in. This white solid is the hydrochloride salt of **2**. The reaction was stirred by ultrasound bath for 3 hours under argon atmospheres below 50 °C and most of the solid was dissolved. The reaction was continued at room temperature with normal magnetic stirrer over night. The reaction system was filtrated and washed with 8 ml 1:1 solution of DMF/t-butyl-methylether (TBME), and. 14 ml TBME was added to precipitate the white solid. The solution and stirred slowly at room temperature for 2 hours, then filtrated. The solid was washed with TBME to yield 762.2 mg (99.8%) crude **1** as pale yellow solid. Yield of the recrystallization (MeOH/CH$_2$Cl$_2$) was 72%.

^{1}H-NMR (400 MHz, DMSO-*d6*): 2.57 (t, 6H, *J* = 5.55 Hz, 3×CH$_2$-N); 3.25 (td, 6H, *J* = 5.31, 5.55 Hz, 3×**CH$_2$**-NH); 7.25 & 7.54 (br, 12H, 3× N**H$_2$**-C- N**H$_2$**); 7.64 (t, 3H, *J* = 5.18, 3×NH).

^{13}C-NMR (100 MHz, DMSO-*d6*): 39.07 (3C, 3×CH$_2$-NH); 52.06 (3C, 3×CH$_2$-N); 157.99 (3C, 3×C=NH).

ESI-MS (MeOH): Positive ion mode: 273.3 (M+H$^+$)

IR (KBr cm^{-1}): 3331 (*s*); 3158 (*s*); 1656 (*s*).

EA: calc. for C$_9$H$_{27}$Cl$_3$N$_{10}$: C 28.32, H 7.13, Cl 27.86, N 36.69; found: C 28.30, H 7.10, N 36.58, Cl 27.84.

X-ray structure: The single crystal for X-ray structure determination was obtained by vapor diffusion of CH$_2$Cl$_2$ into the solution of **1** in methanol. **1** was cocrystallized with one molar MeOH. The structural details see **chapter 5.5**.

Tris(2-guanidinopropyl)amine trihydochloride (6)
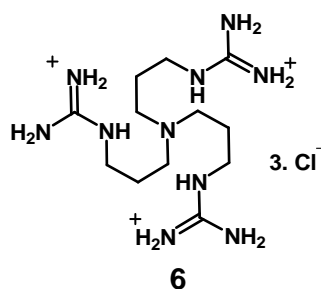
Compound **6** was synthesized via the similar manner as **1** from tris-(3-aminopropyl)amine. However, **6** can not be precipitated as solid by adding TBME to the final reaction solution. Instead, the crude product was precipitated as yellow oil under this condition. Decant the up layer solution and the oil was soaked by 1:1 mixture of DMF/TBME, then by pure TBME and diethyl ether subsequently. Accurate yield was not able to be obtained due to the high hydroscopic nature of **6**.

^{1}H-NMR (400 MHz, DMSO-*d6*): 1.63 (tt, 6H, *J* = 6.57, 6.82 Hz, 3×N-CH$_2$**CH$_2$**CH$_2$-NH); 2.44 (t, 6H, *J* = 6.82 Hz, 3×CH$_2$-N); 3.16 (t, 6H, *J* = 6.56 Hz, 3×CH$_2$-NH); 6.8-8.9 (br m, 15 H, 3×gunidinium-H).

^{13}C-NMR (100 MHz, DMSO-*d6*): 26.71 (3C, 3×N-CH$_2$**CH$_2$**CH$_2$-NH);39.79 (3C, 3×CH$_2$-NH); 50.96 (3C, 3×CH$_2$-N);157.96 (3C, 3×C=NH).

ESI-MS (MeOH): Positive ion mode: 315.2 (M+H$^+$); Negative ion mode: 349.8 (M+Cl$^-$).

Tris(2-guanidinoethyl)amine tri-tetraphenylborate (7)
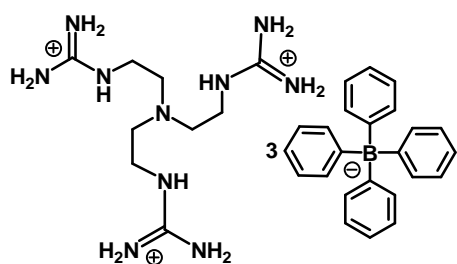
38.17 mg compound **1** (0.1 mmol) was dissolved in 2 ml water and this clear solution was heated up to 45 ˚C by oil bath. The 3 ml aqueous solution of 131.51 mg NaBPh$_4$ (0.38 mmol) was added in and white solid started to precipitate. The system continued to be stirred at 45-50 ˚C for 30 minutes and at rt for overnight. After filtration and washing with water, the solid was dried under vacuum to afford 113.09 mg **7** as white powder (91.7%).

^{1}H-NMR (400 MHz, CD$_3$CN): 2.62 (t, 6H, *J* = 6.32 Hz, 3×CH$_2$-N); 3.10 (t, 6H, *J* = 6.32 Hz, 3×CH$_2$-NH); 6.01 (br m, 15H, 3×5-gunidinium-H); 6.87 (t, 12H, *J* = 7.07 Hz, 12×Ar-CH^p); 7.02 (t, 24H, *J* = 7.33 Hz, 24×Ar-CH^m); 7.30 (m, 24H, 24×Ar-CH^o).

^{13}C-NMR (100 MHz, CD$_3$CN): 39.50 (3C, 3×CH$_2$-NH); 51.85 (3C, 3×CH$_2$-N); 122.24 (12C, 12×Ar-CH^p); <u>126.02, 126.05, 126.08, 126.11 </u>(q, coupling with B, 24C, 24×Ar-CH^o); 136.15 (24C, 24×Ar-CH^m); 157.99 (3C, 3×C=NH); <u>163.48, 163.96, 164.46, 164.96</u> (q, coupling with B, 12C, 12×Ar-C-B).

Tris(2-guanidinopropyl)amine tri-tetraphenylborate (**8**)
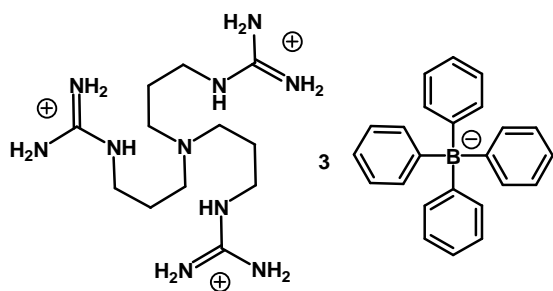
Compound 8 was prepared in a same way as for 7, albeit directly from the final reaction mixture for preparation of **6** with overall yield of 87.0% according to tris-(2-aminopropyl)amine.

^{1}H-NMR (400 MHz, CD$_3$CN): 1.62 (tt, 6H, *J* = 6.82, 7.07 Hz, 3×N-CH$_2$**CH$_2$**CH$_2$-NH); 2.42 (t, 6H, *J* = 7.07 Hz, 3×CH$_2$-N); 3.03 (t, 6H, *J* = 6.82 Hz, 3×CH$_2$-NH); 6.87 (t, 12H, *J* = 7.16 Hz, 12×Ar-CH^p); 7.02 (t, 24H, *J* = 7.41 Hz, 24×Ar-CH^m); 7.30 (m, 24H, 24×Ar-CH^o).

^{13}C-NMR (100 MHz, CD$_3$CN): 25.09 (3C, 3×N-CH$_2$CH$_2$CH$_2$-NH); 40.28 (3C, 3×CH$_2$-NH); 49.76 (3C, 3×CH$_2$-N); 122.25 (12C, 12×Ar-CH^p); <u>126.03, 126.06, 126.09, 126.11</u> (q, coupling with B, 24C, 24×Ar-CH^o), 136.15 ((24C, 12×Ar-CH^m); 157.14 (3C, 3×C=NH); <u>163.47, 163.96, 164.45, 164.94</u> (q, 12C, 12×Ar-C-B).

5. 2. 2. Guanidinium cryptands

N,N-bis(4-phthalimidobutyl)benzylamine (**11**)
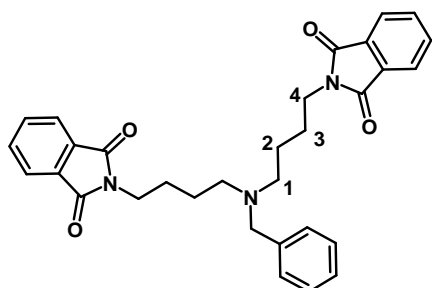
4.55 g N-(4-bromobutyl)-phthalimide (**9**) (16.1 mmol), 0.88 ml benzylamine (8.05 mmol) and 2.80 g KF-545-Celite* were mixed in 27 ml acetonitrile. The reaction was carried under argon atmosphere at rt over night. The KF-545-Celite

was removed by filtration and washed with fresh acetonitrile. The filtrate was concentrated by evaporator and subsequently purified by flash chromatography (silica gel, toluene/acetone = 20:1) to afford 1.99 g (48.0%) product **11** as white solid.

*) The catalyst KF-545-Celite was prepared by mixing 125 ml aqueous solution of 5 g potassium fluoride with 5 g of Celite 353. Water was removed and the resulting solid was washed with 25 ml acetonitrile then dried under vacuum.

TLC (toluene/acetone = 7: 1): R_f = 0.35.

mp: 105-7 ˚C.

1H-NMR (400 MHz, CDCl$_3$): 1.49 (tt, 4H, J = 7.2, 7.3 Hz, 2×CH$_2$-2); 1.66 (tt, 4H, J = 7.4, 7.5 Hz, 2×CH$_2$-3); 2.43 (t, 4H, 2×CH$_2$-1); 3.51 (s, 2H, PhCH$_2$); 3.63 (t, 4H, J = 7.2 Hz, 2×CH$_2$-4); 7.16-7.29 (m, 5H, Ph-CH); 7.70 (m, 4H, 4×Ph-CH); 7.80 (m, 4H, 4×Ph-CH).

13C-NMR (100 MHz, CDCl$_3$): 24.8 (2C, 2×CH$_2$-3); 26.8 (2C, 2×CH$_2$-2); 38.3 (2C, 2×CH$_2$-4); 53.6 (2C, 2×CH$_2$-1); 59.1 (PhCH$_2$), 123.5, 127.1, 128.5, 129.2, 132.6, 134.2, 140.3 (18C, Ph-C, CH); 168.8 (4C, 4×C=O).

MS (ESI, m/z): 510.6 (M+H$^+$), 532.4 (M+Na$^+$).

EA: calc. for C$_{31}$H$_{31}$N$_3$O$_4$: C 73.06, H 6.13, N 8.25, O 12.56; found: C 72.85, H 6.05, N 8.21, O 12.90.

IR (KBr, cm^{-1}): 3062 (*w*.), 2933 (*m*), 2788 (*m*), 1708 (*s*).

N,N-bis(5-phthalimidopentyl)benzylamine (12)
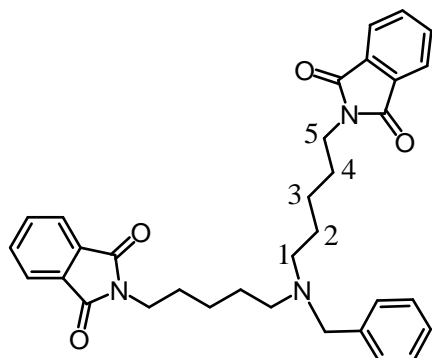
12 was prepared in similar way as **11** from N-(5-bromopentyl)-phthalimide (**10**).

TLC (CH$_2$Cl$_2$/MeOH = 20:1.5): R_f = 0.45.

1H-NMR (400 MHz, CDCl$_3$): 1.30 (m, 4H, 2×CH$_2$-3); 1.48 (t, 4H, J = 6.52 Hz, 2×CH$_2$-2); 1.63 (tt, 4H, J = 7.45, 7.54 Hz, 2×CH$_2$-4); 2.36 (t,

4H, J = 6.37 Hz, 2×CH$_2$-1); 3.50 (s, 2H, PhCH$_2$); 3.65 (t, 4H, J = 7.25 Hz, 2×CH$_2$-5); 7.16-7.26 (m, 5H, Ph-CH); 7.69 (AA' of AA'BB', 4H, J = 3.04, 5.44 Hz, 4×Ph-CH); 7.82 (BB' of AA'BB', 4H, J = 3.03, 5.46 Hz, 4×Ph-CH).

^{13}C-NMR (100 MHz, CDCl$_3$): 25.05, 26.97, 28.88 (6C, 2×C-2, 2×C-3, 2×C-4); 38.38 (2C, 2×C-5); 53.89 (2C, 2×C-1); 58.96 (PhCH$_2$); 123.55, 127.01, 128.48, 128.63, 129.15, 132.58, 134.23 (18C, 3×Ph-C, CH); 168.83 (4C, 4×C=O).

MS (ESI, m/z): 538.1 (M+H$^+$).

N,N-Bis-(4-phthalimidobutyl)amine (13)
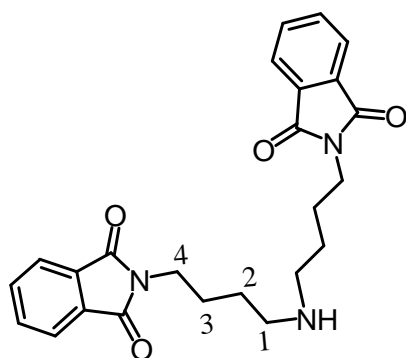
1.81 g compound **11** (3.6 mmol) was dissolved in 10 ml acetic acid and 100 mg 10% Pd/C was added in. The inner atmosphere of the reaction system was exchanged three times with argon and another three times with H$_2$. The reaction was performed at 70 °C under H$_2$ balloon overnight then cooled down to rt. The catalyst was removed by filtration over Celite. The acetic acid was removed under vacuum, and then 20 ml CHCl$_3$ and 20 ml 4N ammonia aqueous solution were added in together. The organic phase was washed with brine and dried over Na$_2$SO$_4$. Solvent was removed and dried under vacuum to get 1.66 g **13** (91.0%) which was enough pure for next step.

TLC (CH$_2$Cl$_2$/MeOH/NEt$_3$ = 20:1:0.1): R$_f$ = 0.23

^{1}H-NMR (400 MHz, CDCl$_3$): 1.55 – 1.78 (m, 8H, 2×CH$_2$-2 + 2×CH$_2$-3); 2.71 (t, 4H, J = 7.2 Hz, 2×CH$_2$-1); 3.70 (t, 4H, J = 7.2 Hz, 2×CH$_2$-4); 7.69 (AA' of AA'BB', 4H, J = 3.0, 5.5 Hz, 4×Ph-CH); 7.82 (BB' of AA'BB', 4H, J = 3.0, 5.5 Hz, 4×Ph-CH).

^{13}C-NMR (100 MHz, CDCl$_3$): 25.3, 26.8, (4C, 2×C-2, 2×C-3); 38.0 (2C, 2×C-4); 49.1 (2C, 2×C-1); 123.6, 132.5, 134.3 (12C, Ph-C and -CH); 168.8 (4C, 4×C=O).

ESI-MS (m/z): 420.5 (M+H$^+$).

Tris-(4-phthalimidobutyl)amine (15)
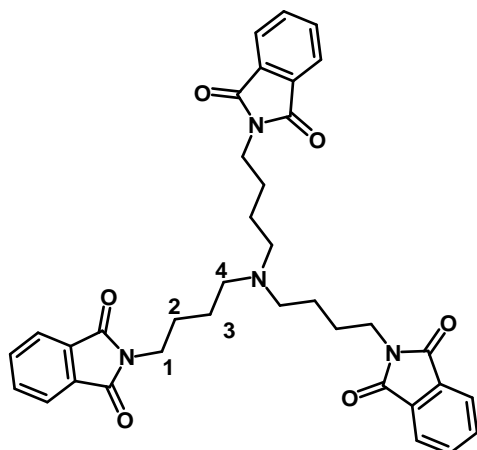
1.20 g KF-545-Celite was added into the 5.0 ml acetonitrile solution of N-(4-bromobutyl)-phthalimide (**9**, 422 mg, 1.49 mmol) and 482 mg compound **13** (1.15 mmol). The mixture was stirred under argon atmosphere over night; then the catalyst was removed by flirtation and washed with fresh acetonitrile. The filtrate was concentrated *in vacuo* and purified by flash chromatography (silica gel, toluene/acetone = 20:1) to afford 196 mg (27.0%) **15** as white solid.

TLC (toluene/acetone = 5:1): R_f = 0.12.

mp: 122.5-123.5 °C.

^{1}H-NMR (400 MHz, CD$_3$CN): 1.39 (tt, 6H, J = 7.3 Hz, J = 7.3 Hz, 3×CH$_2$-2); 1.61 (tt, 6H, J = 7.3 Hz, J = 7.3 Hz, 3×CH$_2$-3); 2.33 (t, 6H, J = 6.9 Hz, 3×CH$_2$-1); 3.56 (t, 6H, J = 7.1 Hz, 3×CH$_2$-4); 7.72 - 7.74 (m, 12×Ph-CH).

^{13}C-NMR (100 MHz, CD$_3$CN): 24.7, 26.5 (6C, 2×C-2, 2×C-3); 38.0 (3C, 2×C-4); 53.4 (3C, 2×C-1); 123.1, 132.7, 134.3 (18C, Ph-C and -CH); 168.7 (6C, 6×C=O).

ESI-MS (m/z): 621.7 (M+H$^+$);

EA: calc. for C$_{36}$H$_{36}$N$_4$O$_6$: C 69.66, H 5.85, N 9.03, O 15.47; found: C 69.42, H 5.92, N 8.42, O 15.76.

Tris-(4-aminobutyl)amine tetrahydrochloride (17)
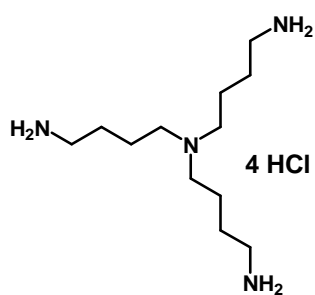
0.17 ml hydrazine monohydrate (3.56 mmol) was added to the solution of 245 mg Tris-(4-phthalimidobutyl)amine (**15**) in 4.6 ml ethanol. The reaction was stirred at room temperature for two hours and white solid precipitated during this procedure. All the volatile was removed *in vacuo* and 5.0 ml 2 M HCl aqueous solution was added in. The mixture was filtrated and the solution was dried under vacuum. The residue was dissolved in 1 ml water and loaded to ion exchange resin (Amberlite IR-120, H$^+$ form,

6.56 g, pre-wash with 3M HCl and then water to pH neutral). 3 M HCl was used as eluent and the Ninhydrin positive fragments were collected and lyophilized to afford 77.3 mg compound **17** (52.0%) as white solid.

^{1}H-NMR (400 MHz, D$_2$O): 1.60 – 1.80 (12H, 3×CH$_2$-2 + 2×CH$_2$-3); 2.96 (t, 6H, 2×CH$_2$-1); 3.15 (br, 6H, 2×CH$_2$-4).

^{13}C-NMR (100 MHz, D$_2$O): 21.1 (3C, 3×C-2); 24.4 (3C, 3×C-3); 39.3 (3C, 3×C-4); 52.8 (3C, 3×C-1).

ESI-MS (m/z): 231.3 (M+H$^+$)

N-(4-iodobutyl)-phthalimide (**19**)
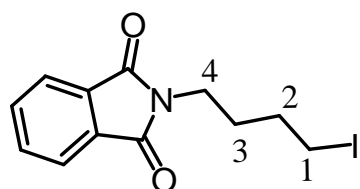
5.64 g N-(4-bromobutyl)-phthalimide (**9**) (20 mmol) and 7.20 g fine powdered sodium iodide (48 mmol) were mixed with 40 ml acetone and refluxed under argon atmosphere for 24 hours. Another 7.20 g fine powdered sodium iodide was added in and continue to reflux for 24 hours more. The volatiles were removed *in vacuo*; then 100 ml CH$_2$Cl$_2$ and 100 ml water were added to the residue and the two phases were separated. The water layer was extracted again with 2×100 ml CH$_2$Cl$_2$. All the organic layers were combined and wash with 10% NaS$_2$O$_3$ aqueous solution, water and brine, then dried over Na$_2$SO$_4$ anhydrite. After filtration, the solvent was removed and resulting solid was dried under vacuum to afford 6.22 g **19** (94.5%) which is already pure enough for next step reaction.

TLC (toluene/acetone = 20:3): R$_f$ = 0.58; (hexane/ethyl acetate = 4:1): R$_f$ = 0.35; (CH$_2$Cl$_2$): R$_f$ = 0.41.

mp: 88-89 ˚C

^{1}H-NMR (400 MHz, CDCl$_3$): 1.83 (m, 4H, CH$_2$-2 + CH$_2$-3); 3.21 (t, 2H, J = 6.53 Hz, CH$_2$-1); 3.70 (t, 2H, J = 6.59 Hz, CH$_2$-4); 7.71 (AA' of AA'BB', 2H, J = 3.06, 5.42 Hz, 2×Ph-CH); 7.83 (BB' of AA'BB', 2H, J=3.03, 5.46 Hz, 2×Ph-CH).

^{13}C-NMR (100 MHz, CDCl$_3$): 5.99 (C-3); 29.93 (C-2); 30.94 (C-1); 37.13 (C-4); 123.68, 132.43, 134.41 (6C, Ph-C, CH); 168.77 (2C, 2×C=O).

IR (CHCl$_3$, cm^{-1}): 1765, 1703

N-(5-iodopentyl)-phthalimide (20)
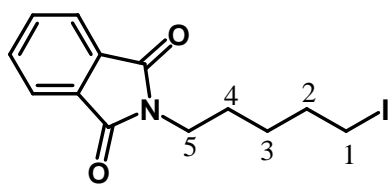
Compound **20** was prepared in a same way as **19** from N-(5-bromopentyl)-phthalimide (**10**) with a yield of 96.5%.

TLC (hexane/ethyl acetate = 4:1): R_f = 0.29, (toluene/acetone = 20:3): R_f = 0.60

mp: 73-75 ˚C

^{1}**H-NMR** (400 MHz, CDCl$_3$): 1.45 (tt, 2H, J = 7.33, 8.08 Hz, CH$_2$-3); 1.70 (tt, 2H, J = 7.33, 7.58 Hz, CH$_2$-2); 1.87 (tt, 2H, J = 7.08, 7.33 Hz, CH$_2$-4); 3.17 (t, 2H, J = 6.95 Hz, CH$_2$-1); 3.68 (t, 2H, J = 7.21 Hz, CH$_2$-5); 7.71 (AA' of AA'BB', 2H, J = 3.03, 5.56 Hz, 2×Ph-CH); 7.83 (BB' of AA'BB', 2H, J=3.03, 5.56 Hz, 2×Ph-CH).

^{13}**C-NMR** (100 MHz, CDCl$_3$): 6.82 (C-3); 27.91, 28.11 (C-2, C-4); 33.30 (C-1); 38.05 (C-5); 123.64, 132.51, 134.34 (6C, Ph-C, CH); 168.81 (2C, 2×C=O).

EI-MS (70 ev, m/z): 343 (3.8 M^{+}), 261.1 (49.2), 160 (100); **ESI-MS** (m/z): 365.9 (M+Na^{+}).

EA: calc. for C$_{13}$H$_{14}$INO$_2$: C 45.50, H 4.11, N 4.08, O 9.32; found: C 45.92, H 4.27, N 4.03;

Benzyl-tris-(4-phthalimidobutyl)-ammonium iodide (21)
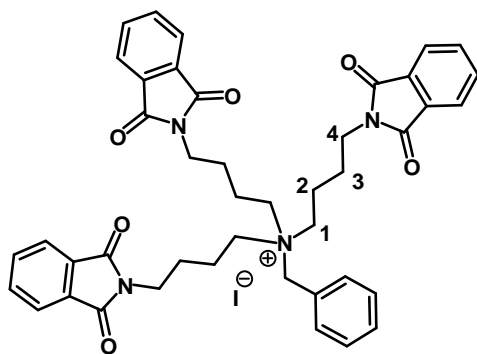
1.50 g KF-545-Celite was added into the 15.0 ml solution of 1.645 g N-(4-iodobutyl)-phthalimide (**19**) (5 mmol) and 110 μl benzylamine (1.0 mmol) in acetonitrile. The mixture was refluxed under argon atmosphere for 48 hours; then the KF-545-Celite was removed by flirtation and washed with fresh acetonitrile. The filtrate was concentrated *in vacuo* and the residue was soaked in benzene. The reaction flask stood in ultra sonic bath for 30 minutes and was cooled down in ice bath for one hour; then the benzene up-layer was decanted. The residue was repeated this washing procedure by benzene once more to remove the excess of **19** and the bis- alkylated side product. 10 ml CH$_2$Cl$_2$ was added to the residue, and the mixture was filtrated to remove small

amount of white inorganic salts. The solution was dried under vacuum to give 516 mg (60.8%) **21** as yellow solid which can be used directly for next step reaction. However, all the NMR signals of **21** shows more than two group of signals which did not improve after flash chromatography (silica gel, CH_2Cl_2/MeOH gradient from 100:1 to 10:1), and the reason is not clear yet. Only the main signal is listed bellow.

TLC (CH_2Cl_2/MeOH = 40:3): R_f = 0.26,

^{1}H-NMR (400 MHz, CDCl$_3$): 1.78 – 1.91 (m, 12H, CH$_2$-2 CH$_2$-3); 3.47 – 3.50 (m, 6H, Hz, CH$_2$-1); 3.69 – 3.71 (m, 2H, J = 6.95 Hz, CH$_2$-4); 4.87 (s, 2H, PhCH$_2$); 7.26 – 7.81 (m, 17H, Ph-H).

^{13}C-NMR (100 MHz, CDCl$_3$): 20.05, 25.70 (6C, 3×C-2, 3×C-3); 32.26 (3C, 3×C-1); 59.01 (3C, 3×C-4); 63.87 (PhCH$_2$); 123.39, 127.00, 129.56, 130.95, 131.89, 132.50, 134.19 (24C, 4×Ph-C, CH); 168.51 (6C, 6×C=O).

ESI-MS (m/z): 711.2 (M $^+$).

Benzyl-tris-(5-phthalimidopentyl)-ammonium iodide (22)
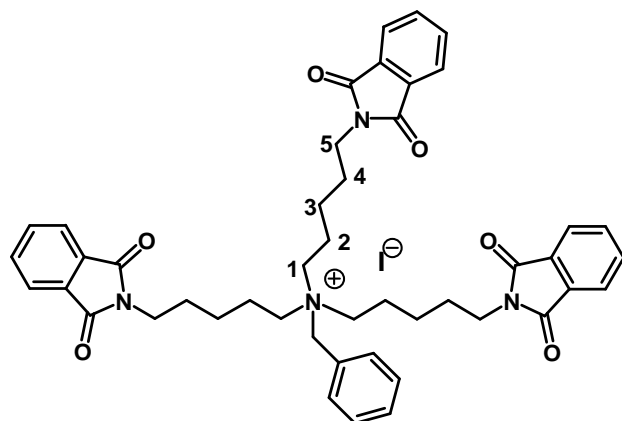
Compound **25** was obtained from N-(5-iodopentyl)-phthalimide (**20**) via the same way as **21**., Yield: 66.0%.

TLC (CH_2Cl_2/MeOH = 40:3): R_f = 0.53;

^{1}H-NMR (400 MHz, CDCl$_3$): 1.43 (tt, 6H, J = 7.43 Hz, 3×CH$_2$-3); 1.83 (tt, 6H, J = 6.87 Hz, 3×CH$_2$-2); 1.97 (m, 6H, 3×CH$_2$-4); 3.32 (t, 6H, J = 8.31 Hz, 3×CH$_2$-1); 3.73 (t, 6H, J = 6.59 Hz, 3×CH$_2$-5); 4.86 (s, 2H, PhC**H$_2$**); 7.44-7.56 (m, 5H, Ph-CH); 7.71 (AA' of AA'BB', 6H, J = 3.03, 5.47 Hz, 6×Ph-CH); 7.82 (BB' of AA'BB', 6H, J = 3.03, 5.49 Hz, 6×Ph-CH).

^{13}C-NMR (100 MHz, CDCl$_3$): 22.23, 23.65, 28.28 (9C, 3×C-2, 3×C-3, 3×C-4); 32.26 (3C, 3×C-1); 37.17 (3C, 3×C-5); 59.27 (PhCH$_2$); 123.72, 128.74, 132.39, 132.94, 134.47 (24C, 4×Ph-C, CH); 168.92 (6C, 6×C=O).

ESI-MS (m/z): 753.2 (M $^+$).

Benzyl-tris-(4-aminobutyl)-ammonium iodide (23)
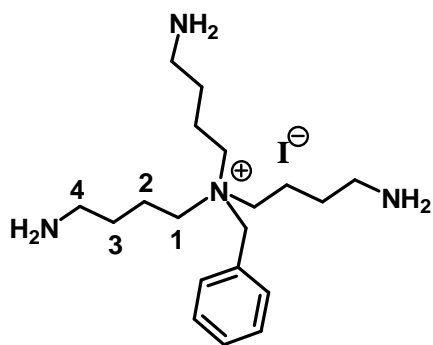
167.7 mg Benzyl-tris-(4-phthalimidobutyl)-ammonium iodide (**21**) (0.2 mmol) and 159 μl hydrazine monohydrate were added to 2 ml ethanol. The reaction mixture was refluxed under argon atmosphere for two hours and white solid precipitated. Subsequently the system was cooled down and stirred at room temperature for over night, then stored at 4 °C fridge for two hours. Keep the system cool and the white solid was removed by filtration. All the volatiles were removed under high vacuum to afford the crude product **23** as yellow gum which contain small amount of N,N'-phthaloyl hydrazine. Though it can be further purified by reverse phase chromatography (RP18, CH$_3$CN/H$_2$O), the crude product was used directly for next step.

^{1}H-NMR (400 MHz, CD$_3$OD): 1.64 (tt, 6H, J = 7.40 Hz, J = 7. 64 Hz, 3×CH$_2$-2); 1.93 (tt, 6H, J = 5.30 Hz, J = 10.59 Hz, 3×CH$_2$-2); 2.99 (t, 6H, J = 7.27 Hz, CH$_2$-4); 3.14 (t, 6H, J = 8.32 Hz, CH$_2$-1); 7.50 (m, 5×Ph-H).
ESI-MS (m/z): 321.3 (M$^+$)

Benzyl-tris-(5-aminopentyl)-ammonium iodide (24)
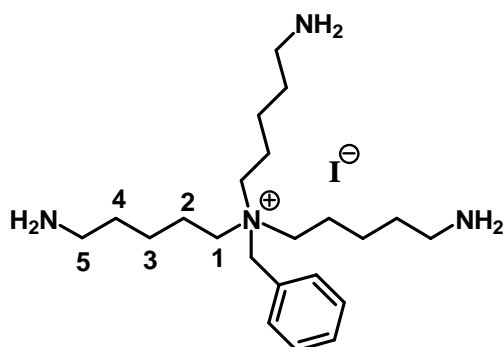
Compound **24** was prepared from **22** in a same way as **23**.

TLC (RP$_{18}$, H$_2$O/acetonitrile = 3:1): R$_f$ = 0.85;
^{1}H-NMR (400 MHz, CDCl$_3$): 1.42 (m, 6H, 3×CH$_2$-3); 1.61 (tt, 6H, J = 7.42 Hz, 3×CH$_2$-2); 1.87 (m, 6H, 3× CH$_2$-4); 2.73 (t, 6H, J = 7.16 Hz, 3×CH$_2$-5); 3.21 (t, 6H, J = 7.37 Hz, 3×CH$_2$-1); 4.59 (s, 2H, Ph-CH$_2$); 7.53 (m, 5H, Ph-CH).

^{13}C-NMR (100 MHz, CDCl$_3$): 22.20, 23.68, 31.25 (12C, 3×C-1, 3×C-2, 3×C-3, 3×C-4); 40.94 (3C, 3×C-5); 58.60 (Ph-CH$_2$); 126.05, 127.89, 129.59, 130.93, 131.85, 132.75 (6C, Ph-C, CH).

ESI-MS (m/z): 363.3 (M$^+$)

Tris-(2-isothiocyanate-ethyl)amine (26)
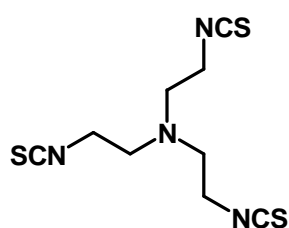
(2-Aminoethyl) amine **2** (0.29g, 2.00mmol) dissolved in 8.0 ml of THF was added dropwise to a solution of DCC (1.65g, 8mmol) and 3.2ml of CS$_2$ (large excess) in 8.0 ml of THF at -10ºC. The reaction was warm up to room temperature slowly and stirred overnight. 5ml of ether was added in to precipitate the solid of N,N'-dicyclohexyl-thiourea, then filtrate and wash with 5ml ether. The filtrate was evaporated and the resulting solid was washed with hexane. Purification by chromatography on silica gel (chloroform) gave 0.42g (76%) titled compound as yellow solid.

TLC (CH$_2$Cl$_2$) Rf = 0.68;

mp: 48-49 ˚C;

^{1}H NMR (400 MHz, CDCl$_3$): 2.97 (t, *J* = 6.2 Hz, 6H, N-CH$_2$); 3.60 (t, *J* = 6.2 Hz, 6H, CH$_2$-NCS).

^{13}C NMR (100 MHz, CDCl$_3$): 44.7 (N-CH$_2$); 54.9 (CH$_2$-NCS); 133.5 (NCS).

FAB-MS (*m/z*): 273 (M$^+$, 25.8); 200 (100).

EA. calc. for C$_9$H$_{12}$N$_4$S$_3$: C 39.68, H 4.44, N 20.57; found: C 39.88, H 4.41, N 20.66.

IR (KBr): 2201, 2120 cm^{-1}.

Tris-(3-isothiocyanate-propyl)amine (27)
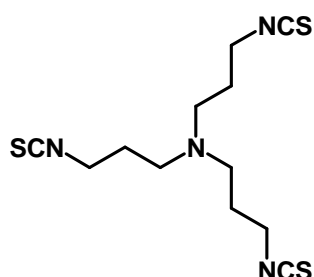
27 was prepared similarly as **26** from (3-aminopropyl) amine (**25**). Yield: 74.1%.

TLC (CH$_2$Cl$_2$) R$_f$ = 0.28;

mp: 43-44 ˚C;

^{1}H-NMR (400 MHz, CDCl$_3$): 1.84 (tt, 6H, J = 6.31, 6.57 Hz, 3×CH$_2$**CH$_2$**CH$_2$); 2.52 (t, 6H, J = 6.57 Hz, 3×CH$_2$-N); 3.61 (t, 6H, J = 6.31 Hz, 3×CH$_2$-N=C=S).

^{13}C-NMR (100 MHz, CDCl$_3$): 27.96 (3C, 3×CH$_2$**CH$_2$**CH$_2$); 43.23 (3C, 3×CH$_2$-N=C=S); 50.56 (3C, 3×CH$_2$-N); 130.90 (3C, 3×N=C=S).

ESI-MS (m/z): 315.5 (M+H$^+$)

EA: calc. for C$_{12}$H$_{18}$N$_4$S$_3$: C 45.83, H 5.77, N 17.81; found: C 46.03, H 5.78, N 17.89.

IR (KBr): 2200, 2123 cm^{-1}.

1,4,6,9,12,14,19,21 –Octaaza –bicyclo[7,7,7]tricosane-5,13,20 –trithione (**28**)
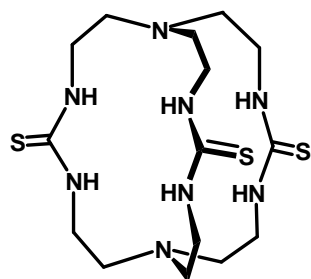
A solution of Tris-(2-isothiocyanate-ethyl)amine (**26**) (272.4 mg, 1.0mmol) in 200 ml of CHCl$_3$ and a solution of **2** (146.1 mg, 1.0 mmol) were added dropwise simultaneously to 100ml of CHCl$_3$ at 60 ºC. The mixture was refluxed for 30 min and stirred at room temperature overnight. The solvent was removed to dryness to give 422mg **3** (100%) as white solid.

mp: >300˚C (decomposed).

^{1}H NMR (400 MHz, CDCl$_3$): 2.441 (br., 6H, CH$_2$-N); 2.803 (br., 6H, CH$_2$-N); 3.019 (br., 6H, NH-CH$_2$); 4.621 (br., 6H, NH-CH$_2$); 6.685 (br., 6H, NH).

^{1}H NMR (400 MHz, DMSO-d$_6$): 7.068 (broad s, 6H, NH); 3.448 (broad s, 12H, NH-CH$_2$); 2.530 (t, 12H, J = 5.32 Hz, CH$_2$-N).

^{13}C-NMR (100 MHz, DMSO-d$_6$): 42.15 (6C, 6 × CH$_2$NH$_2$); 51.26 (6C, 6 × CH$_2$N); 182.70 (3C, 3 × C=S).

FAB-MS (*m/z*): 419 (M+1$^+$, 100), 129 (48.3); **ESI-MS** positive ion mode (*m/z*): 419.3 (M+H$^+$), negative ion mode (*m/z*): 417.1 (M-1$^-$, 100), 383.1 (70.8).

IR (KBr): 3304, 3250, 1570, 1361 cm^{-1}.

EA calc. for C$_{15}$H$_{30}$N$_8$S$_3$: C 43.03, H 7.22, N 26.77, S 22.98; Found: C 42.87, H 7.03, N 25.81.

X-ray structure: The single crystal suitable for X-ray structure determination was obtained by slow evaporation of solvent of the solution of **28** in CH_2Cl_2. The structural details **chapter 5.4**.

3-2H$^+$-bis-picrate

16.7 mg (0.04mmol) of **3** and 33.6mg (0.09mmol) of picric acid (containing 40% water) were dissolved in 40 ml acetone. The solution was opened to the air to allow the slow evaporation of solvent. Yellow crystals grew and were collected by filtration one week later. The structure was characterized by **X-ray** crystallography and one acetone molecule was observed as cocrystallized solvent. For the structural details see **chapter 5.5**.

1,4,6,10,14,16,21,23 –Octaaza –bicyclo[8,8,8]hexacosane-5,15,22 –trithione (**29**)
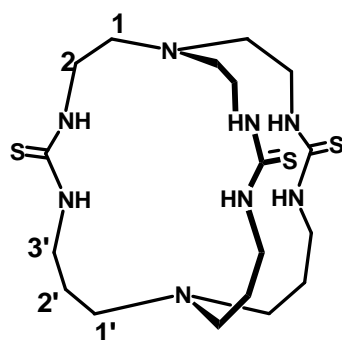
Compound **29** was prepared similarly as **28**. However **29** is almost insoluble in $CHCl_3$, therefore it can be obtained by filtration without removing solvent. This unsymmetrical thiourea cryptand was able to be obtained from different starting materials. Both the condensation of Tris-(2-isothiocyanate-ethyl)amine (**26**) with Tris-(3-aminopropyl)amine (**25**) (yield = 93%) , or Tris-(3-isothiocyanate-propyl)amine (**27**) with Tris-(2-aminoethyl)amine (**2**) (yield = 84%) gave the identical product.

mp: >300˚C (decomposed);

^{1}H-NMR (400 MHz, DMSO-d_6): 1.65 (m, 6H, 3×CH$_2$-2'); 2.28 (m, 6H, 3×CH$_2$-1'); 2.60 (m, 6H, 3×CH$_2$-1); 3.03 (bs, 6H, 3×CH$_2$-3'); 3.49 (bs, 6H, 3×CH$_2$-2); 6.35 (bs, 3H, 3×N**H**-C-2); 7.55 (bs, 3H, 3×N**H**-C-3').

^{13}C-NMR (100 MHz, DMSO): 23.60 (3C, 3×C-2'); 39.33 (3C, 3×C-3'); 42.00 (3C, 3×C-2); 48.40 (3C, 3×C-1'); 51.47 (3C, 3×C-1); 181.96 (3C, 3×C=S).

ESI-MS positive ion mode (*m/z*): 461.3 (M+H$^+$); negative ion mode (*m/z*): 459.5 (M-1$^-$, 100), 495.5 & 497.4 (M+Cl$^-$, 81.5 & 39.6).

X-ray structure: The single crystal suitable for X-ray structure determination was obtained by vapor diffusion of water into the solution of **28** in DMSO. The structural details **chapter 5.4**.

1,5,7,11,15,17,24,26 –Octaaza –bicyclo[9,9,9]nonacosane-6,16,25 –trithione (**30**)
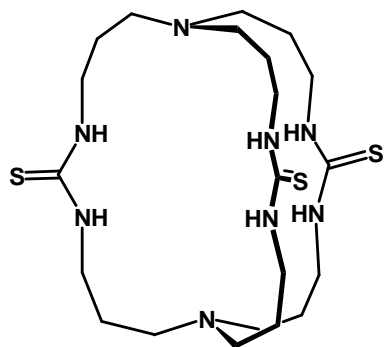
Compound **30** was prepared from **25** and **27** in a same way as for **29** (87%).

TLC (CH$_2$Cl$_2$/MeOH/NEt$_3$ = 20:2:1) R$_f$ = 0.33;

mp: >300˚C (decomposed);

^{1}H-NMR (400 MHz, DMSO-d_6): 1.61 (bs, 12H, 6×N-CH$_2$**CH$_2$**CH$_2$-NH); 2.38 (bs, 12H, 6×CH$_2$-N); 3.35 (bs, 12H, 6×CH$_2$-NH); 7.62 (bs, 6H, 6×NH).

^{13}C-NMR (100 MHz, DMSO-d_6): 26.79 (6C, 6×N-CH$_2$**CH$_2$**CH$_2$-NH); 40.41 (6C, 6×CH$_2$-NH); 52.66 (6C, 6×CH$_2$-N); 181.48 (3C, 3×C=S).

ESI-MS positive ion mode (*m/z*): 503.6 (M+H$^+$), 525.6 (M+Na$^+$); negative ion mode (*m/z*): 501.7 (M-1$^-$), 537.6 (M+Cl$^-$).

IR (KBr): 3222, 1222 cm^{-1}.

1,5,7,12,17,19,28,28 –Octaaza –bicyclo[10,10,10]dotriacontane-6,18,27 –trithione (**31**)
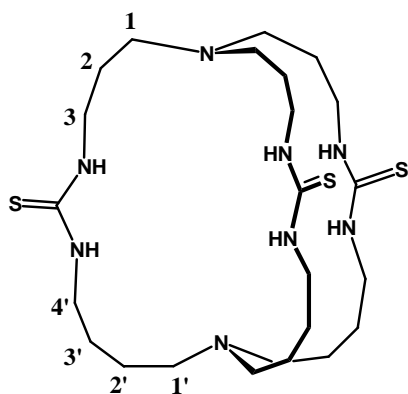
Similar as **30**, compound **31** was prepared from **17** and **27**(60.1%). Its ^{1}H-NMR spectrum was too broad to be assigned at room temperature, therefore, the ^{1}H chemical shifts and all the 2D spectra were obtained at 340 K. The ^{13}C-NMR chemical shift can not be obtained due to the broadness.

TLC (CH$_2$Cl$_2$/MeOH/NEt$_3$ = 20:4:1) Rf = 0.77.

mp: >300˚C (decomposed).

¹H-NMR (400 MHz, DMSO-d_6, 340K): 1.34 (bs, 6H, 3×CH₂-2'); 1.47 (bs, 6H, 3×CH₂-3'); 1.64 (bs, 6H, 3×CH₂-2); 2.24 (bs, 6H, 3×CH₂-1'); 2.40 (bs, 6H, 3×CH₂-1); 3.26 (bs, 6H, 3×CH₂-4'); 3.39 (bs, 6H, 3×CH₂-3); 7.44 (bs, 3H, 3×**NH**-C-4'); 7.55 (bs, 3H, 3×**NH**-C-3).

ESI-MS (MeOH+CH₃COOH) positive ion mode (m/z): 545.5 (M+H⁺), 567.5 (M+Na⁺); negative ion mode (m/z): 543.7 (M-1⁻), 603.4 (M+CH₃COO⁻).

5,15,22,-Tris-methylimino-1,4,6,10,14,16,21,23 –octaaza –bicyclo[8,8,8]hexacosane (**32**)
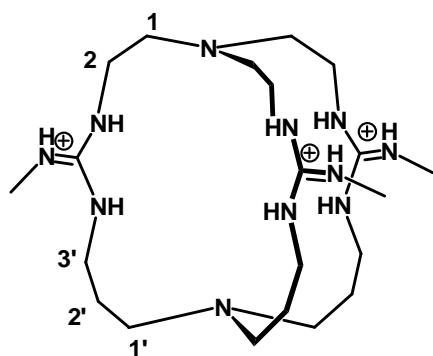
23.0 mg 1,4,6,10,14,16,21,23 –Octaaza – bicyclo[8,8,8]hexacosane-5,15,22 –trithione (**29**) (0.05 mmol) was suspended in 7.5 ml fresh distilled THF. 25 µl MeI was injected in and the system was slightly warmed up to 38 °C and stirred for 24 hours, then another 25 µl MeI was added. The reaction was continued for 24 hours more till the starting material was no more detectable by ESI-MS. All the volatiles were evaporated and the residue was dried *in vacuo* to afford 37.13 mg crude S-methyl-isothiourea derivative of **29** as dark yellow solid. Without purification, 9.80 mg of this intermediate was suspended in 2 ml 8 mol/l solution of MeNH2 in ethanol. The reaction was stirred 70 °C for 72 hours and followed by ESI-MS. The mixture was filtrated and washed with ethanol to remove the insoluble impurity. All the volatiles were removed and the remaining solid was dried under high vacuum to afford 11.07 mg product, presumably as tris-iodide salt.

¹H-NMR (500 MHz, CD₃OD): 1.90 (t, 6H, J = 4.95 Hz, 3×CH₂-2'); 2.50 (m, 6H, 3×CH₂-1'); 2.87 (t, 6H, J = 5.09 Hz, 3×CH₂-1); 2.91 (s, 9H, 3×CH₃); 3.30 (t, 6H, J = 6.25 Hz, 3×CH₂-3'); 3.37 (bs, 6H, 3×CH₂-2).

ESI-MS (CD₃OD): positive ion mode (m/z): 452.4 (M+H⁺), 226.6 (M+2H⁺)/2; negative ion mode (m/z): 450.4 (M-1⁻), 486.3 (M+ Cl⁻).

6,16,25-Tris-benzylimino-1,5,7,11,15,17,24,26 –octaaza –bicyclo[9,9,9]nonacosane-
(33)
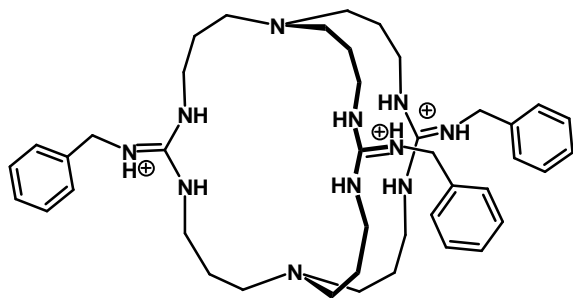
The pre-dried thiourea cryptand **30** (209.2 mg, 0.417 mmol) and 375.6 mg 2-Chloro-1-methylpyridinium iodide (Mukaiyama reagent) (1.47 mmol) were mixed with 400 μl triethylamine and 32 ml acetonitrile. The system was refluxed under argon atmosphere for 5 hours and most solid got soluble during the refluxing; the solution became more deeply colored. ESI indicated that all the thiourea groups converted to carbodiimide (Caution: this intermediate is unstable to moisture.). 157 μl benzylamine was injected in and the color quickly changed to orange. The reaction continued to reflux for 36 hours more, then cool down to room temperature and stirred for another 12 hours. The liquid part was carefully decanted and the sticky solid was washed 3 times by fresh acetonitrile. 10 ml methanol was added to this crude mixture and then the insoluble impurity was removed by filtration. The solution was concentrated *in vacuo* and the remaining 267 mg yellow solid was purified by fresh chromatography (silica gel, CH_2Cl_2/MeOH = 1:1) to give 162.6 mg yellow solid (35.3%).

^{1}H-NMR (400 MHz, MeOD): 1.68 (bs, 12H, 6×N-CH$_2$**CH$_2$**CH$_2$-NH); 2.44 (bs, 12H, 6×**CH$_2$**-N); 3.30 (bs, 12H, 6×**CH$_2$**-NH); 4.49 (s, 6H, 3×PhC**H$_2$**); 7.26-7.39 (m, 15H, 3×Ph-CH).

^{13}C-NMR (100 MHz, MeOD): 26.66 (6C, 6×N-CH$_2$**CH$_2$**CH$_2$-NH); 40.32 (6C, 6×**CH$_2$**-NH); 44.79 (3C, 3×Ph**CH$_2$**); 51.15 (6C, 6×**CH$_2$**-N); 127.57, 128.04, 128.95, 137.08 (6C, 6×Ph-C, CH); 155.31 (3C, 3×C=N).

ESI-MS (MeOH): positive ion mode (*m/z*): 722.47 (M+H$^+$), 361.81 (M+2H$^+$)/2; negative ion mode (*m/z*): 720.74 (M-1$^-$), 756.73 (M+ Cl$^-$).

12-Benzyl -1,4,6,12,18,20,25,27 –octaaza –bicyclo[10,10,10]dotriacontane -5,19,26,-trithione (34)
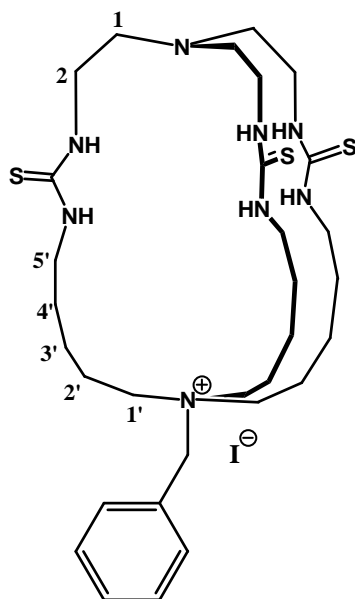
A super diluted condition is required for synthesis of **34** due to the relatively long and flexible chain of the starting material **24**. A six liter three necked flask was installed with two dropping funnels. One liter DMF and one liter chloroform were mixed in the flask and heated up to reflux. The solution of 462 mg **24** (0.846 mmol) in one liter DMF and another solution of 243.6 mg **26** (0.894 mmol) in one liter chloroform were dropped into the refluxing system from dropping funnels slowly and simultaneously at same speed. The adding was finished within 5 hours. After stirring under reflux for another 1.5 hours, the reaction was cooled down to room temperature and stirred over night. The solution was concentrated *in vacuo* then 20 ml DMF was re-added in. The first part white solid was collected by filtration and washed by methanol. 30 ml methanol was added to the filtrate and the mixture stood in fridge for overnight. The second part solid was again collected by filtration and wash with methanol, which is of almost the same purity as the first part. The two parts white solid was dried under high vacuum to give the totally 157.34 mg product (24.4%). Similar as **31**, the 1H-NMR signals of **34** are very broad and overlapped at room temperature. The ^{1}H-NMR chemical shifts and 2D spectra were collected at 325 K.

TLC (CH$_2$Cl$_2$/MeOH/NEt$_3$ = 20:2:0.5) Rf = 0.56.

mp: >300˚C (decomposed).

^{1}**H-NMR** (600 MHz, DMSO-d_6, 325 K): 1.53 (bs, 6H, 3×CH$_2$-3'); 1.58 (bs, 6H, 3×CH$_2$-4'); 1.87 (bs, 6H, 3×CH$_2$-2'); 2.51 (bs, 6H, 3×CH$_2$-1); 3.41 (bs, 6H, 3×CH$_2$-1'); 3.50 (bs, 6H, 3×CH$_2$-5'); 3.55 (bs, 6H, 3×CH$_2$-2); 4.48 (s, 2H, PhCH$_2$); 7.49-7.51 (m, 5H, Ph-CH); 7.77 (bs, 3H, 3×NH); 7.86 (bs, 3H, 3×NH');

ESI-MS (MeOH): positive ion mode (*m/z*): 635.3 (M$^+$); negative ion mode (*m/z*): 633.4 (M-2H) $^-$, 669.3 (M-H + Cl$^-$).

12-Benzyl-5,19,26-tris-methylimino-1,4,6,12,18,20,25,27–octaaza–bicyclo[10,10,10] dotriacontane (35)
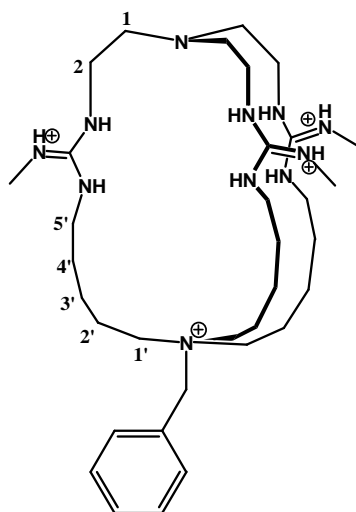
50.69 mg compound **34** (0.066 mmol) was suspended in 6 ml acetonitrile, and 600 μl MeI was added in. The reaction was heated up to reflux and the solid was dissolved. The reaction was followed by ESI-MS, and after 6 hours, all the thiourea groups were converted to S-methyl-isothiourea. The system was cooled down to room temperature. Then all the volatiles were removed and the residue was dried under high vacuum. 6.0 ml 8 mol/l $MeNH_2$ ethanol solution was added in and the mixture was stirred under reflux for 60 hours. The insoluble impurity was removed by filtration and the filtrate was concentrated then dried *in vacuo* to give 89.6 mg crude product as colorless gum which was then purified by flash chromatography (silica gel, MeOH). The iodide salt of 35 was converted to free base by passing through strong basic ion exchange resin (Dowex 1×2, OH⁻ form) to afford 39.50 mg base form of **35** (95%) as colorless gum after dried under high vacuum. After being loaded to acidic ion exchange resin (Amberlite CG-50, H⁺ form), the compound was washed down by HCl aqueous solution (gradient from 1 mM to 50 mM). The positive fragments of iodine vapor test were collected and dried *in vacuo*; the hydrochloride salt of **35** was finally obtained as white powder after lyophilization.

TLC (H_2O/MeOH/HCOOH = 16:8:1) R_f = 0.22.

^{1}H-NMR of free base form (600 MHz, D_2O): 1.28 (t, 6H, J = 6.67 Hz, 3×CH$_2$-3'); 1.49 (t, 6H, J = 6.44 Hz, 3×CH$_2$-4'); 1.62 (m, 6H, 3×CH$_2$-2'); 2.60 (s, 9H, 3×CH$_3$); 2.66 (t, 6H, J = 5.90 Hz, 3×CH$_2$-1); 3.00 (t, 6H, J = 7.50 Hz, 3×CH$_2$-1'); 3.03 (t, 6H, J = 6.55 Hz, 3×CH$_2$-5'); 3.15 (m, 6H, 3×CH$_2$-2); 4.31 (s, 2H, PhCH$_2$); 7.30-7.39 (m, 5H, Ph-CH).

^{13}C-NMR of free base form (150 MHz, D_2O): 20.87 (3C, 3×CH$_2$-2'); 22.46 (3C, 3×CH$_2$-3'); 26.79 (3C, 3×CH$_2$-4'); 27.52 (3C, 3×CH$_3$); 40.08 (3C, 3×CH$_2$-5'); 48.77 (3C, 3×CH$_2$-2); 51.72 (3C, 3×CH$_2$-1); 58.39 (3C, 3×CH$_2$-1'); 63.40 (1C, Ph**C**H$_2$); 126.63, 129.24, 130.80, 132.52 (6C, Ph-C, CH); 155.61 (3C, 3×C=NH).

¹H-NMR of HCl salt form (500 MHz, MeOD): 1.54 (bs, 6H, 3×CH$_2$-3'); 1.81 (bs, 6H, 3×CH$_2$-4'); 1.97 (bs, 6H, 3×CH$_2$-2'); 2.88 (s, 9H, 3×CH$_3$); 3.01-3.44 (m, 12H, 3×CH$_2$-5', 3×CH$_2$-1'); 3.63 (bs, 6H, 3×CH$_2$-1); 3.87 (bs, 6H, 3×CH$_2$-2); 4.52 (s, 2H, PhCH$_2$); 7.50-7.54 (m, 5H, Ph-CH).

¹³C-NMR of HCl salt form (125 MHz, MeOD): 21.45 (3C, 3×CH$_2$-2'); 22.99 (3C, 3×CH$_2$-3'); 27.49 (6C, 3×CH$_2$-4', 3×CH$_3$); 36.73 (3C, 3×CH$_2$-2); 41.14 (3C, 3×CH$_2$-5'); 54.16 (3C, 3×CH$_2$-1); 59.20 (3C, 3×CH$_2$-1'); 63.77 (1C, Ph**C**H$_2$); 127.64, 129.01, 129.19, 130.38, 132.34, 132.64 (6C, Ph-C, CH); 155.16 (3C, 3×C=NH).

ESI-MS (MeOH): positive ion mode (*m/z*): 626.5 (M$^+$), 313.8 (M$^+$+H$^+$)/2; negative ion mode (*m/z*): 624.5 (M-2H)$^-$.

5. 2. 3 The Pyrene Modified Receptors

Tris-(2- (N'-pyren-1yl-methyl-thiourea)-ethyl)- amine (**53**)
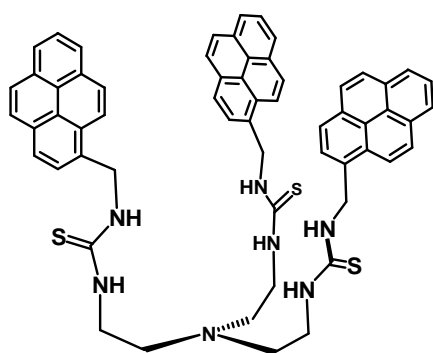
Tris-(2-isothiocyanate-ethyl)amine (**26**) (210 mg, 0.77 mmol), 1-pyrenemethylamine hydrochloride (606.3 mg 2.27 mmol) and 330 μl triethylamine were mixed in 30 ml CH$_2$Cl$_2$ and stirred under argon atmosphere for one week. All the volatiles were removed *in vacuo* then the residue was purified by flash chromatography (silica gel, CH$_2$Cl$_2$/MeOH gradient from 100:0 to 100:2) to afford 619.5 mg product (83.2%) as yellow solid.

TLC (CH$_2$Cl$_2$/MeOH = 20:0.5) R$_f$ = 0.40.

¹H-NMR (600MHz, CD$_2$Cl$_2$): 2.65 (m, 6H, 3×CH$_2$-N); 3.67 (bs, 6H, 3×CH$_2$-NH); 5.05 (bs, 6H, 3×CH$_2$-Pyrene); 7.68-8.11 (m, 27H, 27×Pyrene-CH).

ESI-MS (MeOH): positive ion mode (*m/z*): 966.2 (M+H$^+$); negative ion mode (*m/z*): 964.2 (M-H)$^-$, 1000.2 (M+Cl$^-$).

UV (3 μM in CH$_3$CN): 242 nm (0.4517), 266 nm (0.178047), 277 nm (0.244112), 315 nm (sh, 0.088458), 328 nm (0.196298), 344 nm (0.251476).

Fluorescence (3 μM in CH$_3$CN, λ$_{ex}$ = 344 nm): 377 nm (77510), 397 nm (109970), 477 nm (846610).

Tris-(2- (N'-pyren-1yl-methyl-guanidinium)-ethyl)- amine tri-chloride **(36)**
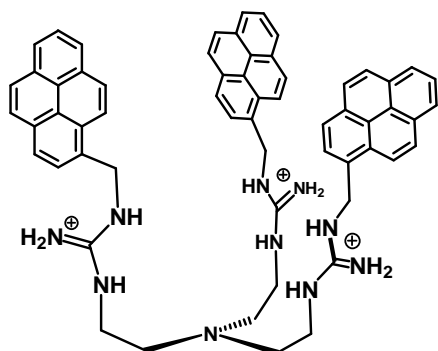
Compound **53** (477.4 mg, 0.494 mmol) was dissolved in 5 ml CH_2Cl_2 and 128 μl HI aqueous solution (56%) was added in. The mixture was stirred at room temperature for 30 minutes then 10 ml ethanol was added in. The system stood in ultrasonic bath for another 30 minutes and then was filtrated, washed with fresh Et_2O. The resulting hydroiodide salt of **53** (530.6 mg) was dried under high vacuum, and then was suspended in 20 ml CH_2Cl_2/MeOH (3:1) mixture. 850 μl MeI was added in and the reaction was stirred under sealed condition at room temperature and followed by ESI-MS. After 70 hours, all the thiourea groups were converted completely to S-methyl isothiourea. All the volatiles were removed *in vacuo* then the resulting residue was dried under high vacuum. 622 mg out of 645.44 mg of the S-methyl-isothiourea intermediate was transferred into a grass tube equipped with a J-Young valve, 10 ml ammonia solution (7N in MeOH) was added in and the tube was sealed and the reaction was stirred at 55 °C over night. Most of the solid became soluble during the reaction procedure. The system was concentrated *in vacuo* then the residue (670 mg) was purified by flash chromatography (silica gel, CH_2Cl_2/MeOH gradient from 490:10 to 300:200) to afford 290 mg pale yellow solid (47% for three steps) as triiodide salt. The counter anion was able to be exchanged to chloride by ion exchange resin (Dowex 1×2, Cl⁻ form, eluent: MeOH/CH_3CN = 4:1).

TLC (CH_2Cl_2/MeOH = 2:1) R_f = 0.29.

¹H-NMR (400MHz, $CDCl_3$): 2.69 (t, 6H, *J* = 5.33 Hz, 3×CH_2-N); 3.37 (t, 6H, *J* = 5.50 Hz, 3×CH_2-NH); 4.79 (bs, 6H, 3×CH_2-Pyrene); 7.71-7.91 (m, 27H, 27×Pyrene-CH).

¹³C-NMR (500MHz, $CDCl_3$): 39.07 (3C, 3×CH_2-N); 43.52 (3C, 3×CH_2-Pyrene); 52.39 (3C, 3×CH_2-NH); 121.87, 124.23, 124.62, 124.67, 125.35, 125.47, 126.06, 127.08, 127.54, 127.75, 128.25, 130.37, 131.00, 131.18 (48C, 48×Pyrene-C, CH); 155.88 (3C, 3×C=NH).

ESI-MS (MeOH): positive ion mode (*m/z*): 915.3 (M+H⁺), 458.2 (M+2H⁺)/2, 1043.2 (M+2H⁺+I⁻); negative ion mode (*m/z*): 913.3 (M-H)⁻, 949.3 (M+Cl⁻) 1041.2 (M+I⁻).

UV (3 μM in CH$_3$CN): 242 nm (0.416618), 265 nm (0.160328), 276 nm (0.266125), 314 nm (sh, 0.079722), 327 nm (0.17845), 343 nm (0.231993).

Fluorescence (3 μM in CH$_3$CN, λ_{ex} = 343 nm): 376 nm (335250), 396 nm (316140), 474 nm (1896021).

5. 2. 4 The Catalytic Bromination in Preparative Scale

The preparation of vanadate catalyst stock solution

The 0.2 M (n-Bu$_4$N)$_2$HVO$_4$ aqueous solution was prepared according to the following equation:

$$V_2O_5 + 4 \times n\text{-Bu}_4\text{N·OH} \rightarrow 2 \times (n\text{-Bu}_4\text{N})_2 \text{·HVO}_4 + H_2O$$
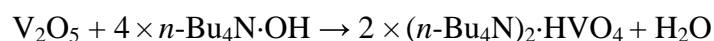
A 5 ml volumetric flask was added with 90.94 mg V$_2$O$_5$ (0.5 mmol) and 1.5999 g n-Bu$_4$N·OH.30H$_2$O (2 mmol), then 1 ml nano-pure water was added in. The flask stood in ultra sonic bath for 30 minutes till the solid was soluble and the solution became clear and colorless. The whole volume was adjusted to 5 ml by adding water. The solution is ready to use and can be diluted to the concentration wanted in acetonitrile or water for binding titration or catalytic reaction. This solution can be store in dark at room temperature under argon for one month. ***Caution:*** *since this solution is readily frozen (≤ 4 °C), proper flask is needed if the sample would like to be stored in fridge, in order to avoid the grass container being destroyed due to swell of volume.*

The general procedure for preparative catalytic bromination:

The reaction flask equipped with two dropping funnels was added with organic substrate (2 mmol), 80 ml acetonitrile and 100 μl 0.2 M vanadate stock solution (0.02 mmol). The solution of 225 μl 48% HBr$_{aq}$* (2 mmol) ** in 30 ml acetonitrile and the solution of 217 μl 30% H$_2$O$_2$ (2 mmol)** in 30 ml acetonitrile were dropped in separately and simultaneously within one hour. The reaction was continued to stir at room temperature and followed by TLC till all the starting material disappeared. 20 ml sodium hydrogen sulfite solution (38-40%) was added in and stirred for 30 minutes. The most of organic solvent was removed *in vacuo* then CH$_2$Cl$_2$ was used to extract the product. The organic layer was washed with water and brine, dried over Na$_2$SO$_4$ then purified with flash chromatography.

*) Equal amount of *n*-Bu$_4$N·Br and HClO$_4$ combination can be used instead. In case of chlorination, HCl aqueous solution was used.

**) Excess amount of HBr (or HCl) and H$_2$O$_2$ were needed for bis- halogenations.

Physical properties of the brominated products

The flowing data were compared with literature value or authentic samples.

2,4,6-(Trimethoxy)bromobenzene (66)
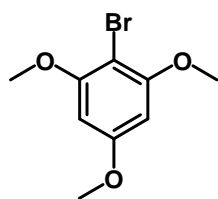
TLC (hexane/EtOAc = 20:7) R$_f$ = 0.39.

^{1}H-NMR (400 MHz, CDCl$_3$): 3.77 (s, 3H, OCH$_3$-C-4); 3.86 (s, 6H, OCH$_3$-C-2, OCH$_3$-C-6); 6.13 (s, 2H, CH-3, CH-5).

^{13}C-NMR (100 MHz, CDCl$_3$): 55.97 (O$\underline{C}$H$_3$-C-4); 56.78 (2C, O$\underline{C}$H$_3$-C-2, O$\underline{C}$H$_3$-C-6); 92.06 (2C, C-3, C-5); 92.26 (C-1); 157.83, 160.91 (3C, C-2, C-4, C-6).

4-bromoanisole (68)
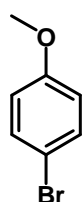
TLC (hexane/EtOAc = 20:1) R$_f$ = 0.41.

^{1}H-NMR (400 MHz, CDCl$_3$): 3.77 (s, 3H, OCH$_3$); 6.78 (d, 2H, *J* = 9.10 Hz, CH-3, CH-5); 7.37 (d, 2H, *J* = 9.10 Hz, CH-2, CH-6).

^{13}C-NMR (100 MHz, CDCl$_3$): 55.83 (OCH$_3$); 113.20 (C-1); 116.15 (2C, C-2, C-6); 132.64 (2C, C-3, C-5); 159.11 (C-4).

4-bromo-N,N-dimethylaniline (70)
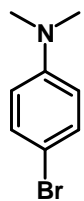
TLC (hexane/EtOAc = 20:4) R$_f$ = 0.46.

^{1}H-NMR (400 MHz, CDCl$_3$); 2.92 (s, 6H, 2×CH$_3$); 6.69 (d, 2H, *J* = 9.09 Hz, CH-2, CH-6); 7.30 (d, 2H, *J* = 8.84 Hz, CH-3, CH-5).

^{13}C-NMR (100 MHz, CDCl$_3$): 40.98 (2C, 2×$\underline{C}$H$_3$); 108.91 (C-4); 114.50 (2C, C-2, C-6); 132.08 (2C, C-3, C-5); 149.92 (C-1).

ESI-MS (MeOH): (*m/z*): 199.9 & 201.9 (relative intensity ≈ 1:1 M+H$^+$).

2,4-Dibromo-N,N-dimethylaniline (71)
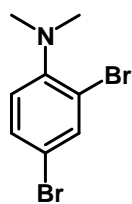
TLC (hexane/EtOAc = 20:1) R_f = 0.53.

^{1}H-NMR (400 MHz, CDCl$_3$): 2.78 (s, 6H, 2×CH$_3$); 6.94 (d, 1H, J = 8.6 Hz, CH-6); 7.36 (dd, 1H, J = 2.0, 8.6 Hz, CH-5); 7.68 (d, 1H, J = 2.0 Hz, CH-3).

^{13}C-NMR (100 MHz, CDCl$_3$): 44.49 (2C, 2×$\underline{C}$H$_3$); 115.75 (C-2); 120.08 (C-4); 122.03, 131.40, 136.44 (C-3, C-5, C-6); 151.55 (C-1).

ESI-MS (MeOH): m/z): 277.8, 279.8 & 281.8 (relative intensity ≈ 1:2:1 M+H$^+$).

2-Chloro-1,3,5-trimethoxybenzene (72)
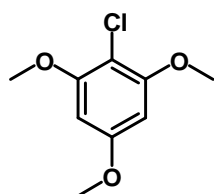
TLC (hexane/EtOAc = 20:7) R_f = 0.36.

^{1}H-NMR (400 MHz, CDCl$_3$): 3.80 (s, 3H, OCH$_3$-C-5); 3.87 (s, 6H, OCH$_3$-C-1, OCH$_3$-C-3); 6.17 (s, 2H, CH-4, CH-6).

^{13}C-NMR (100 MHz, CDCl$_3$): 55.93 (OCH$_3$-C-5); 56.69 (2C, O$\underline{C}$H$_3$-C-1, O$\underline{C}$H$_3$-C-3); 91.95 (2C, C-4, C-6); 103.00 (C-2); 156.93 (C-5); 159.82 (2C, C-1, C-3).

EI-MS (70 ev, m/z): 202.0 (100 M$^+$), 204.0 (32.28 ^{37}Cl-M$^+$), 159.0 (26.85), 161.0 (8.23).

2,4-Dichloro-1,3,5-trimethoxybenzene (73)
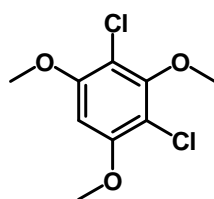
TLC (hexane/EtOAc = 20:7) R_f = 0.31.

^{1}H-NMR (400 MHz, CDCl$_3$): 3.88 (s, 3H, OCH$_3$-C-3); 3.90 (s, 6H, OCH$_3$-C-1, OCH$_3$-C-5); 6.35 (s, 1H, CH-6).

^{13}C-NMR (100 MHz, CDCl$_3$): 56.93 (OCH$_3$-C-3); 61.01 (2C, O$\underline{C}$H$_3$-C-1, O$\underline{C}$H$_3$-C-5); 93.63 (C-6); 110.19 (2C, C-2, C-4); 154.30 (2C, C-1, C-5); 155.22 (C-3).

EI-MS (70 ev, m/z): 236.0 (100 M$^+$), 238.0 (63.56 ^{37}Cl$_{bis}$-M$^+$), 240.0 (10.37 ^{37}Cl$_{mono}$-M$^+$).

(1S, 2RS, 4R, 4R, 8R)-4,7,7-Trimethyl-3-oxo-2-oxa-bicyclo-[2.2.1]heptane-1-carboxylate 8-bromo-2,5,7,8-tetramethyl-2-(4,8,12-trimethyl-tridecyl)-chroman-6-yl-ester (75)
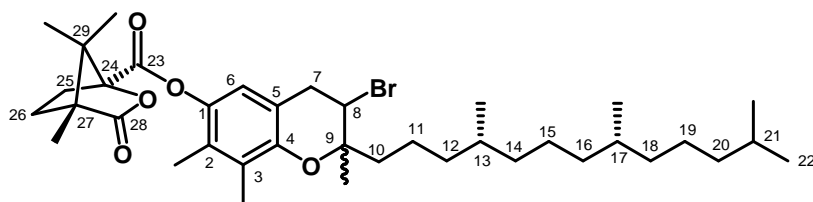
18.5 µl vanadate stock solution (5.4 mM in acetonitrile) (0.1 µmol) was added into the solution of 5 mg compound **74** (8.38 µmol) in 5 ml acetonitrile. Then 200µl 54 mM HBr and 100 µl 108 mM H2O2 were added in. The solution became yellow colored and the reaction was followed by TLC. After stirring at room temperature overnight and the starting material disappeared completely in TLC, 2 ml NaHSO$_3$ (38-40%) was added in and stirred for 30 minutes. The most of organic solvent was removed *in vacuo* then CH$_2$Cl$_2$ was used to extract the product. The organic layer was washed with water and brine, dried over Na$_2$SO$_4$ then purified with preparative TLC. It's important to note that the final product containing two diastereomers (see ^{13}C signal of CH$_3$ at position 9) which is very well separate by HPLC.

TLC (hexane/EtOAc = 20:8) R$_f$ = 0.38; (toluene/acetone = 20:0.7) R$_f$ = 0.46.

^{1}H-NMR (400 MHz, CDCl$_3$): 0.836, 0.854, 0.871 (3s, 12H, CH$_3$-13, 17, 22, 22), 1.00-1.55 (m, 19H, alky-H), 1.12, 1,16, 1.17 (3s, 9H, 3×CH$_3$-Cam$_{27,29,29}$), 1.346/1.350 (s, 3H, CH$_3$-9), 1.71-1.87 (m, 3H, 1H26 and CH$_2$-10), 1.95-2.01 (m, 1H, H26), 2.05 (s, 3H, CH$_3$-3), 2.11 (s, 3H, CH$_3$-2), 2.15-2.24 (m, 1H, H25), 2.52-2.59 (ddd, 1H, = 14.15 Hz, 10.10 Hz, 4.22 Hz, H25), 3.20-3.36 (m, 2H-7), 4.29 (dd, 1H, *J* = 8.97 Hz, 5.93 Hz 1H-8), 6.55 (s, 1H, Ar-H).

ESI-MS (MeOH): 697.1/699.1 (1:1, M+Na$^+$).

UV (detected during HPLC run): 206 nm (λ$_{max}$), 225 nm (sh), 287 nm (w).

5. 3. Determination of Binding Mode and Binding Constants

5. 3. 1. NMR Titration

General procedure

The stock solution of 2 mM $(n\text{-}Bu_4N)_2HVO_4$ in D_2O was prepared according to the procedure previously described in **chapter 5.2.4.** and the pD was adjusted to 10.21 by $n\text{-}Bu_4N.OH$. The stock solution shows a single peak at – 536.5 ppm in ^{51}V-NMR spectrum. The *first point solution* was obtained by adding 38.17 mg of receptor **1** (10 eq.) to 5 ml of vanadate *stock solution* and the pD was carefully adjusted to about 10.2 by $n\text{-}Bu_4N.OH/HCl$. The ratio of ligand **1** and vanadate (V1) was 10:1 in this *first point solution*. Different ratio of **1**/vanadate from 0 to 10 were systemically obtained by mixing the different volumes of *stock solution* and *first point solution*. Importantly, the total concentration of vanadate was kept constantly at 2 mM for all these points and pD was controlled within 10.2±0.1. Both ^{51}V and ^1H-NMR were measured at different **1**/vanadate ratio.

For binding study with phosphate and pyrophosphate, the commercial available $n\text{-}Bu_4N.H_2PO_4$ and $(n\text{-}Bu_4N)_3HP_2O_7$ were used.

Determination of the Binding Mode

The stoichiometry of complex formed between of host and guest molecules was determined by Job plot, which was made by plotting molecular fraction χ ($[host]_{total}$/ ($[host]_{total}+[guest]_{total}$)) against the relative chemical shift change ($\chi \times (\delta_{obs}-\delta_{host})$). The position of maximum value of relative chemical shift change is corresponding for the stoichiometry of the complex formation. For example, maximum at $\chi = 0.5$ means 1:1 complex, since at that point, $[host]_{total} = [guest]_{total}$; on contrast, for 2:1 mode, the maximum should appear at 1/3 when $2\times [host]_{total} = [guest]_{total}$. For sharp binding curve, the stoichiometry can also be judged from the position of break point.

Binding Constants

The chemical shift values were plotted against the value of **1**/vanadate ratio and the data were fitted to the appropriate function using proFit 5.1 (proFit® QuantumSoft) or

Origin 7.0 SR0 (Origin® OriginLab Corporation). The binding constant was obtained from the fitting if the systemic error was acceptable.

5. 3. 2. UV-vis and Fluorescent Titration

General procedure

The titration experiments were performed on a 3.6 ml scale in 1-cm path quartz fluorescence cuvettes. The stock solution of 1.08 mM (A) and 5.4 mM (B) vanadate were prepared by dilution of 0.2 M $(n\text{-}Bu_4N)_2 \cdot HVO_4$ water solution in acetonitrile. The proportional addition of the stock solution by syringe to 3.6 ml 3 μM solution of receptor **36** or **53** in a fluorescent cuvette gave rise to different ratio of vanadate to receptor at 0:1, 0.25:1, 0.5:1, 1:1, 1.5:1, 2:1, 3:1, 5:1, 8:1, 13:1, 23:1, and 43:1. The solution stirred for 5 minutes to be equilibrated for every step. Before reached the ratio of 3:1, solution (A) was used, and solution (B) was used after this point in order to minimize the total volume of vanadate solution added. Therefore, the concentration of receptor can be approximately treated as constant by this manner. Both UV-vis and fluorescence spectra were recorded for every single step. 2 nm slid was adopted for both excitation and emission for fluorescence spectra.

For binding study with phosphate and pyrophosphate were performed in a similar way, and the commercial available $n\text{-}Bu_4N.H_2PO_4$ and $(n\text{-}Bu_4N)_3HP_2O_7$ were used for making stock solution.

The *stoichiometry* and *binding constants* were determined similarly as for NMR titration.

5. 4. Kinetic Study of Catalytic Bromination

The kinetic of catalytic experiments were performed on a 3.6 ml scale in 1-cm path quartz cuvettes. Spectra were collected primarily on an *Agilent* 8453 Diode Array spectrophotometer under "kinetic mode" and cycle time was 2 seconds for all measurements. Tribromide (Br_3^-) formation was measured at 268 nm; the bromination of phenol red was followed at 391, 395 and 415 nm and the bromination of MCD was monitored at decreasing of intensity at 258 nm ($\Delta\varepsilon = 11.8 \text{ mM}^{-1} \text{ cm}^{-1}$). The stock solution of the reagents in acetonitrile were 54 mM HBr (or *n*-Bu$_4$N.Br and HClO$_4$), H_2O_2, MCD, TMB, 5.4 mM Phenol red and 5.4 mM vanadate.

General procedure

A typical procedure for bromination of MCD is given bellow:

The blank UV spectrum of 3.6 ml acetonitrile in a 1-cm path quartz cuvette was measured prior to the addition of reagents. The stock solutions of vanadate (4 μl), MCD (8 μl), H_2O_2 (20 μl) were added in subsequently by syringe. The kinetic UV measurement monitoring the intensity at 258 and 268 nm started as soon as 8 μl HBr stock solution was injected in. The measurement lasted for 10 minutes and UV intensity of the targeted wavelength was plotted against time. The rate was determined by the internal software of instrument.

5. 5. Detailed Parameters of X-ray Structures

Crystallographic data for compounds 1, 28, 28-bis picrate and 29.

Compound	**1**	**28**	**28.2H⁺-2Picrate**	**29**
Molecular formula	$C_{10}H_{31}Cl_3N_{10}O_1$	$C_{15}H_{30}N_8S_3$	$C_{30}H_{42}N_{14}O_{15}S_3$	$C_{20}H_{42}N_8O_1S_4$
Formula weight	413.78	418.66	934.95	538.87
Color	colorless	colorless	paleyellow	colourless
Temperature (K)	173	173	173	173
Crystal size (mm³)	0.16×0.20×0.26	0.10×0.16×0.34	0.30×0.36×0.37	0.10×0.20×0.30
Crystal system	Monoclinic	Orthorhombic	Monoclinic	Monoclinic
Space group	P 21/c	P c 21 n	P 21/n	P 21/n
a (Å)	8.82200(10)	7.5935(2)	10.6325(2)	11.5701(3)
b (Å)	20.7240(4)	10.8892(3)	23.0332(3)	13.6077(4)
c (Å)	11.77740(10)	24.1172(5)	16.7530(5)	17.5134(5)
α (°)	90	90	90	90
β (°)	105.1454(9)	90	108.0013(18)	91.961(2)
γ (°)	90	90	90	90
Volume (Å³)	2078.44(5)	1994.2	3902.0	2755.7
Z	4	4	4	4
Density (calc.) (g cm⁻³)	1.322	1.394	1.591	1.299
μ (Mo Kα) (mm⁻¹)	0.461	0.390	0.280	0.374
Scan type	φ and ω scans	ω scans	φ and ω scans	φ and ω scans
$F(000)$	880	897.661	1954.425	1162.247
θ range for data collection (°)	1.965-27.486	4.11-32.49	4.08 - 29.20	4.14 - 30.81
Completeness to max θ	1.000	1.00	0.999	1.000
Reflection measured	16065	37873	79708	69442
Independent reflections	4772	7214	10558	8647
Reflection used	2952	3959	6110	4867
Number of parameters	281	259	560	323
R	0.0337 ($I > 3\sigma(I)$)	0.0386 ($I > 2\sigma(I)$)	0.0384 ($I > 2\sigma(I)$)	0.0652 ($I > 4\sigma(I)$)
wR	0.0380	0.0423	0.0243	0.0530
Goodness of fit on F	1.0760	1.0462	1.0585	0.9633
Recidual density (e⁻ Å⁻³)	-0.23 0.74	-0.94 0.83	-0.44 0.35	-0.55 0.93

Structure(ORTEP view) and atoms coordination for compound 1
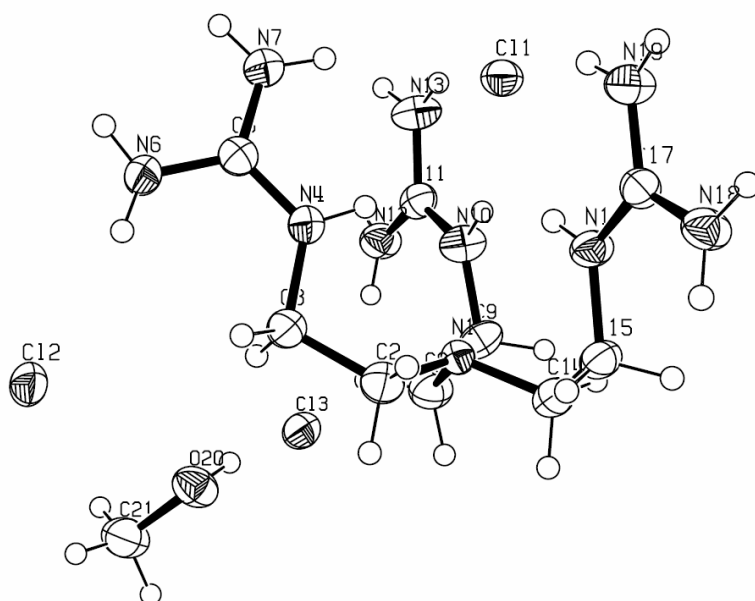
Atom	X	Y	Z	Uiso
N1	0.48181(19)	0.15815(8)	0.91931(14)	0.0242
N4	0.2400(2)	0.20862(9)	1.00742(17)	0.0321
N6	0.0985(2)	0.28904(9)	1.06926(17)	0.0329
N7	0.0954(3)	0.18575(10)	1.13805(19)	0.0393
N10	0.5809(2)	0.11133(10)	1.16422(16)	0.0368
N12	0.7038(3)	0.15811(10)	1.34363(17)	0.0392
N13	0.4857(3)	0.09465(12)	1.32478(19)	0.0430
N16	0.2788(2)	0.05661(9)	0.80558(15)	0.0316
N18	0.1381(2)	0.00263(10)	0.64022(16)	0.0354
N19	0.0646(2)	-0.00473(10)	0.81261(17)	0.0367
C2	0.3858(3)	0.21199(11)	0.8587(2)	0.0379
C3	0.3111(3)	0.25118(11)	0.9371(2)	0.0340
C5	0.1437(2)	0.22793(10)	1.07004(18)	0.0291
C8	0.6227(3)	0.18154(12)	1.0078(2)	0.0377
C9	0.6914(3)	0.13166(12)	1.09900(19)	0.0365
C11	0.5917(3)	0.12246(11)	1.27690(19)	0.0317
C14	0.5283(3)	0.11512(12)	0.8359(2)	0.0376
C15	0.3929(3)	0.08318(11)	0.74817(19)	0.0330
C17	0.1603(2)	0.01887(10)	0.75254(18)	0.0288
C21	0.7300(4)	0.42188(13)	1.1072(2)	0.0486
O20	0.6652(2)	0.35947(8)	1.07648(14)	0.0409
Cl1	0.23919(6)	0.04583(3)	1.07739(5)	0.0333
Cl2	0.16744(7)	0.41232(3)	0.91486(5)	0.0364
Cl3	0.88935(7)	0.27660(3)	1.26261(5)	0.0395
H41	0.265(3)	0.1683(6)	1.013(2)	0.037(7)
H61	0.118(3)	0.3170(10)	1.0206(19)	0.039(7)
H62	0.036(2)	0.2971(12)	1.1130(19)	0.037(7)
H71	0.127(3)	0.1465(6)	1.137(2)	0.043(7)
H72	0.035(3)	0.1991(13)	1.179(2)	0.042(7)
H101	0.497(2)	0.0915(12)	1.125(2)	0.044(7)
H121	0.706(3)	0.1590(13)	1.4173(10)	0.037(7)
H122	0.762(3)	0.1832(12)	1.315(2)	0.050(8)
H131	0.485(3)	0.1060(14)	1.3953(13)	0.049(8)
H132	0.407(2)	0.0737(13)	1.281(2)	0.053(9)
H161	0.288(3)	0.0667(12)	0.8775(11)	0.036(7)
H181	0.180(3)	0.0253(12)	0.594(2)	0.045(7)

H182	0.067(3)	-0.0259(11)	0.610(2)	0.048(8)
H191	-0.019(2)	-0.0256(11)	0.776(2)	0.037(7)
H192	0.078(3)	0.0072(12)	0.8844(11)	0.038(7)
H201	0.715(3)	0.3315(12)	1.127(2)	0.056(9)
H211	0.7514	0.4319	1.1901	0.0603
H212	0.8299	0.4257	1.0853	0.0609
H213	0.6602	0.4546	1.0644	0.0610
H21	0.4515	0.2399	0.8273	0.0469
H22	0.3039	0.1948	0.7955	0.0469
H31	0.3899	0.2773	0.9885	0.0423
H32	0.2316	0.2785	0.8896	0.0423
H81	0.5941	0.2186	1.0464	0.0457
H82	0.7007	0.1936	0.9681	0.0457
H91	0.7826	0.1494	1.1531	0.0440
H92	0.7212	0.0947	1.0606	0.0440
H141	0.5940	0.0819	0.8798	0.0472
H142	0.5871	0.1398	0.7930	0.0472
H151	0.4329	0.0489	0.7093	0.0411
H152	0.3417	0.1146	0.6911	0.0411

Structure (ORTEP view) and atoms coordination for compound 28
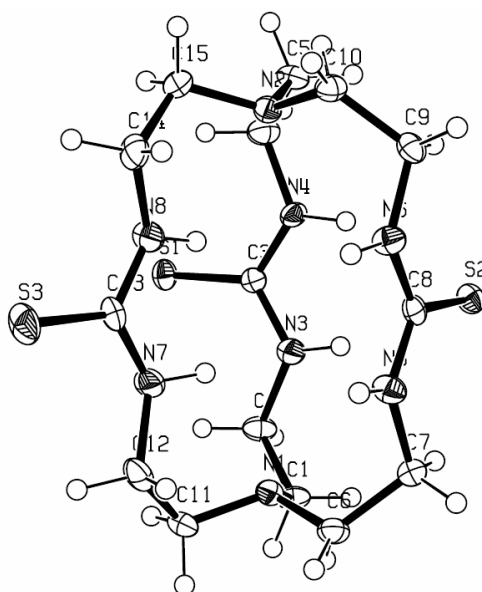
Atom	X	Y	Z	Uiso
S1	0.81134(7)	-0.27261(9)	0.08290(2)	0.0224
S2	0.30610(8)	-0.25049(8)	0.25523(2)	0.0216
S3	0.13781(9)	-0.28450(9)	-0.04675(3)	0.0309
N1	0.3239(3)	-0.54274(19)	0.12832(9)	0.0197
N2	0.3450(3)	0.0090(2)	0.11356(9)	0.0185
N3	0.5954(4)	-0.3657(2)	0.16002(11)	0.0238
N4	0.6091(4)	-0.1579(2)	0.1571(1)	0.0208
N6	0.1000(3)	-0.1536(2)	0.1766(1)	0.0220
N5	0.0914(4)	-0.3599(2)	0.1824(1)	0.0229
N7	0.2925(4)	-0.3807(2)	0.0424(1)	0.0248
N8	0.2998(4)	-0.1740(2)	0.0372(1)	0.0257
C1	0.4845(4)	-0.5755(2)	0.15825(12)	0.0222
C2	0.6362(4)	-0.4910(2)	0.14424(12)	0.0230

C3	0.6654(3)	-0.2643(3)	0.13605(8)	0.0170
C4	0.6562(4)	-0.0368(3)	0.13627(14)	0.0250
C5	0.5027(4)	0.0516(2)	0.14211(12)	0.0222
C10	0.1819(4)	0.0485(2)	0.14035(11)	0.0209
C9	0.1395(4)	-0.0272(2)	0.19107(11)	0.0209
C8	0.1580(3)	-0.2545(3)	0.20216(9)	0.0178
C7	0.1229(4)	-0.4817(2)	0.20416(11)	0.0219
C6	0.1633(4)	-0.5725(2)	0.15849(12)	0.0223
C11	0.3216(4)	-0.5894(2)	0.07124(11)	0.0237
C12	0.2202(4)	-0.5018(3)	0.03380(11)	0.0258
C13	0.2467(3)	-0.2791(3)	0.01404(8)	0.0205
C14	0.2392(4)	-0.0534(3)	0.02181(11)	0.0260
C15	0.3471(4)	0.0388(2)	0.05413(11)	0.0247
H3	0.513(4)	-0.347(3)	0.1874(12)	0.028(7)
H4	0.538(4)	-0.160(3)	0.1880(11)	0.029(7)
H6	0.029(4)	-0.168(3)	0.146(1)	0.017(6)
H5	0.007(4)	-0.355(3)	0.1548(11)	0.023(7)
H7	0.317(5)	-0.368(3)	0.0801(8)	0.029(7)
H8	0.354(4)	-0.183(3)	0.0720(9)	0.018(6)
H11	0.5166(4)	-0.6581(2)	0.14872(12)	0.0270
H12	0.4620(4)	-0.5705(2)	0.19735(12)	0.0270
H21	0.7395(4)	-0.5177(2)	0.16378(12)	0.0276
H22	0.6577(4)	-0.4943(2)	0.10504(12)	0.0276
H41	0.7547(4)	-0.0060(3)	0.15699(14)	0.0300
H42	0.6878(4)	-0.0431(3)	0.09783(14)	0.0300
H51	0.4762(4)	0.0609(2)	0.18080(12)	0.0270
H52	0.5364(4)	0.1297(2)	0.12692(12)	0.0270
H61	0.2575(4)	-0.6304(2)	0.16310(12)	0.0269
H62	0.0682(4)	-0.6108(2)	0.13873(12)	0.0269
H71	0.2210(4)	-0.4788(2)	0.22922(11)	0.0262
H72	0.0197(4)	-0.5085(2)	0.22376(11)	0.0262
H91	0.2388(4)	-0.0257(2)	0.21572(11)	0.0250
H92	0.0391(4)	0.0079(2)	0.20934(11)	0.0250
H101	0.2799(4)	0.1041(2)	0.14114(11)	0.0251
H102	0.0880(4)	0.0839(2)	0.11902(11)	0.0251
H111	0.2663(4)	-0.6687(2)	0.07063(11)	0.0284
H112	0.4404(4)	-0.5966(2)	0.05797(11)	0.0284
H121	0.2336(4)	-0.5257(3)	-0.00428(11)	0.0310
H122	0.0976(4)	-0.5026(3)	0.04348(11)	0.0310
H141	0.2551(4)	-0.0408(3)	-0.01727(11)	0.0312
H142	0.1168(4)	-0.0447(3)	0.03097(11)	0.0312
H151	0.4664(4)	0.0371(2)	0.04097(11)	0.0299
H152	0.2988(4)	0.1194(2)	0.04870(11)	0.0299

Structure (ORTEP) and atoms coordination for compound 28-bis picrates

(a) The view from the top of cryptand
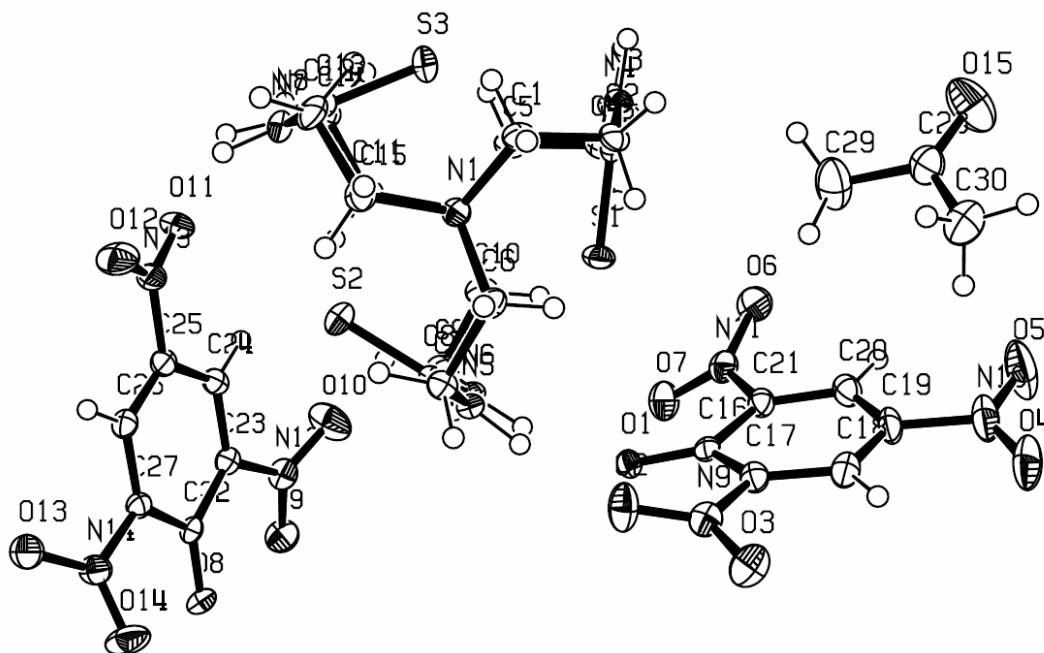
(b) The side view for cryptand. Picrate and acetone molecules are omitted for clarity.
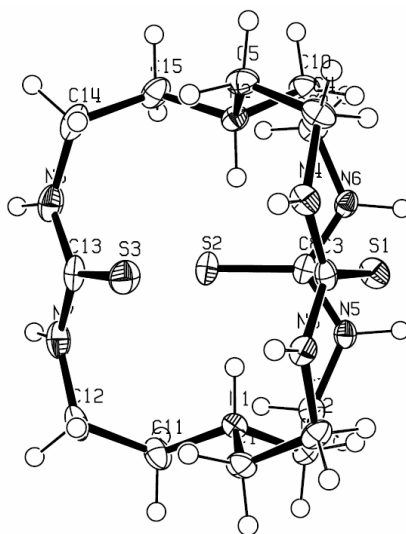
Atom	X	Y	Z	Uiso
N1	0.95841(16)	0.17649(7)	0.9156(1)	0.0178
N2	1.28070(16)	0.20045(7)	0.7534(1)	0.0186
N3	1.13482(16)	0.05983(7)	0.9059(1)	0.0179
N4	1.27864(17)	0.06991(7)	0.8314(1)	0.0199
N5	0.82455(16)	0.21203(7)	0.7187(1)	0.0191
N6	0.97232(16)	0.22062(7)	0.6466(1)	0.0195
N7	1.18277(18)	0.27623(8)	0.98766(11)	0.0258
N8	1.33979(18)	0.28644(8)	0.92258(11)	0.0261
C1	0.9948(2)	0.12200(9)	0.96810(12)	0.0214
C2	1.0101(2)	0.06650(9)	0.92247(13)	0.0202
C3	1.1553(2)	0.07674(8)	0.83471(12)	0.0171
C4	1.3221(2)	0.08985(9)	0.76222(13)	0.0228

C5	1.3788(2)	0.15106(9)	0.77286(13)	0.0227
C6	0.81955(19)	0.17064(9)	0.85597(13)	0.0208
C7	0.7758(2)	0.21814(9)	0.78974(13)	0.0221
C8	0.93576(19)	0.23678(8)	0.71334(12)	0.0181
C9	1.0896(2)	0.24130(9)	0.62981(13)	0.0245
C10	1.2090(2)	0.2017(1)	0.65991(13)	0.0241
C11	0.9651(2)	0.22807(9)	0.97263(13)	0.0252
C12	1.1018(2)	0.2455(1)	1.02906(13)	0.0276
C13	1.2705(2)	0.25102(9)	0.95630(13)	0.0223
C14	1.4226(2)	0.26694(9)	0.87385(13)	0.0270
C15	1.3514(2)	0.25760(9)	0.78025(13)	0.0251
S1	1.03346(5)	0.10583(2)	0.75513(3)	0.0218
S2	1.02408(6)	0.28434(2)	0.78576(4)	0.0275
S3	1.29277(6)	0.17864(2)	0.95876(4)	0.0255
C16	0.7617(2)	0.07346(9)	0.58809(11)	0.0181
C17	0.6468(2)	0.04637(9)	0.60090(12)	0.0204
C18	0.6191(2)	-0.01204(9)	0.58969(12)	0.0243
C19	0.7110(2)	-0.04819(9)	0.57365(13)	0.0265
C20	0.8306(2)	-0.02739(9)	0.56789(13)	0.0256
C21	0.8529(2)	0.03104(9)	0.57430(12)	0.0205
N9	0.55221(18)	0.08187(8)	0.62482(11)	0.0238
N10	0.6815(2)	-0.10949(9)	0.56139(13)	0.0370
N11	0.97916(18)	0.05074(8)	0.56732(11)	0.0244
O1	0.78006(14)	0.12697(6)	0.58903(9)	0.0200
O2	0.58581(17)	0.12981(7)	0.65650(11)	0.0348
O3	0.44120(16)	0.06184(8)	0.6149(1)	0.0332
O4	0.5683(2)	-0.12578(7)	0.55359(12)	0.0458
O5	0.7705(2)	-0.14272(8)	0.55885(16)	0.0629
O6	1.07368(16)	0.01772(7)	0.59188(11)	0.0341
O7	0.98629(16)	0.09889(7)	0.5376(1)	0.0307
C22	0.97193(19)	0.44681(8)	0.56856(12)	0.0170
C23	1.0938(2)	0.41448(9)	0.58538(12)	0.0187
C24	1.17907(19)	0.40367(8)	0.66434(12)	0.0191
C25	1.1479(2)	0.42494(9)	0.73330(12)	0.0204
C26	1.0334(2)	0.45550(8)	0.72475(12)	0.0194
C27	0.94898(19)	0.46587(9)	0.64560(12)	0.0181
N12	1.12897(17)	0.38842(8)	0.51626(11)	0.0238
N13	1.23364(18)	0.41218(8)	0.81659(11)	0.0245
N14	0.83021(17)	0.49813(8)	0.64072(11)	0.0250
O8	0.89551(14)	0.45761(6)	0.49793(8)	0.0217
O9	1.08064(16)	0.40703(7)	0.44497(9)	0.0312
O10	1.20559(19)	0.34679(8)	0.53192(11)	0.0449
O11	1.34320(16)	0.39147(7)	0.8237(1)	0.0309
O12	1.19286(17)	0.42057(8)	0.8764(1)	0.0372
O13	0.83245(16)	0.53163(7)	0.6982(1)	0.0341
O14	0.73148(16)	0.49003(9)	0.5809(1)	0.0412
C28	0.9263(3)	-0.1198(1)	0.80196(14)	0.0317
C29	0.9680(3)	-0.05902(11)	0.7925(2)	0.0472
C30	0.7836(3)	-0.12989(12)	0.78951(19)	0.0477
O15	1.0056(2)	-0.15903(9)	0.82147(15)	0.0576
H1	1.01903(16)	0.18201(7)	0.8840(1)	0.0217
H2	1.21821(16)	0.19479(7)	0.7836(1)	0.0223
H3	1.20693(16)	0.04226(7)	0.9485(1)	0.0204
H4	1.34183(17)	0.05070(7)	0.8774(1)	0.0233
H5	0.77406(16)	0.18873(7)	0.6724(1)	0.0216
H6	0.91683(16)	0.19363(7)	0.6077(1)	0.0223
H7	1.17279(18)	0.31760(8)	0.98235(11)	0.0289
H8	1.33421(18)	0.32744(8)	0.93128(11)	0.0292
H11	1.0774(2)	0.12913(9)	1.01080(12)	0.0258
H12	0.9270(2)	0.11530(9)	0.99386(12)	0.0258

H21	0.9999(2)	0.03416(9)	0.95606(13)	0.0238
H22	0.9410(2)	0.06575(9)	0.86963(13)	0.0238
H41	1.3891(2)	0.06374(9)	0.75637(13)	0.0283
H42	1.2477(2)	0.08892(9)	0.71206(13)	0.0283
H51	1.4330(2)	0.15519(9)	0.83018(13)	0.0275
H52	1.4327(2)	0.15486(9)	0.73654(13)	0.0275
H61	0.75967(19)	0.17069(9)	0.88869(13)	0.0250
H62	0.81366(19)	0.13414(9)	0.82739(13)	0.0250
H71	0.8062(2)	0.25471(9)	0.81618(13)	0.0259
H72	0.6809(2)	0.21808(9)	0.76922(13)	0.0259
H91	1.1128(2)	0.27823(9)	0.65693(13)	0.0286
H92	1.0693(2)	0.24605(9)	0.57024(13)	0.0286
H101	1.2715(2)	0.2136(1)	0.63230(13)	0.0294
H102	1.1797(2)	0.1629(1)	0.64303(13)	0.0294
H111	0.9120(2)	0.21925(9)	1.00810(13)	0.0300
H112	0.9282(2)	0.26082(9)	0.93784(13)	0.0300
H121	1.0906(2)	0.2700(1)	1.07271(13)	0.0319
H122	1.1479(2)	0.2108(1)	1.05342(13)	0.0319
H141	1.4905(2)	0.29545(9)	0.87904(13)	0.0298
H142	1.4622(2)	0.23077(9)	0.89704(13)	0.0298
H151	1.4163(2)	0.26137(9)	0.75146(13)	0.0295
H152	1.2868(2)	0.28790(9)	0.76235(13)	0.0295
H181	0.5368(2)	-0.02723(9)	0.59306(12)	0.0295
H201	0.8959(2)	-0.05347(9)	0.55961(13)	0.0306
H241	1.25867(19)	0.38179(8)	0.67155(12)	0.0229
H261	1.0128(2)	0.46936(8)	0.77331(12)	0.0235
H291	0.8917(3)	-0.03421(11)	0.7768(2)	0.0587
H292	1.0284(3)	-0.04599(11)	0.8447(2)	0.0587
H293	1.0108(3)	-0.05775(11)	0.7497(2)	0.0587
H301	0.7690(3)	-0.17035(12)	0.79719(19)	0.0542
H302	0.7564(3)	-0.10743(12)	0.82957(19)	0.0542
H303	0.7331(3)	-0.11839(12)	0.73372(19)	0.0542

Structure (ORTEP view) and atoms coordination for compound 29

(a) The view from side of cryptand
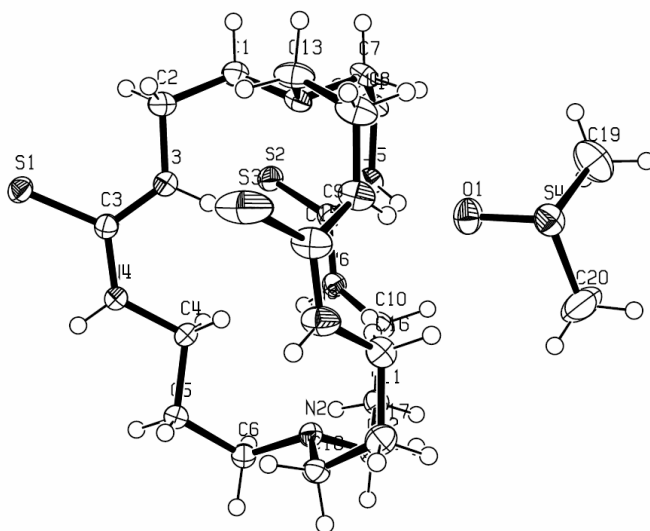
(b) The view from top of cryptand, hydrogen atoms were omitted for clarity
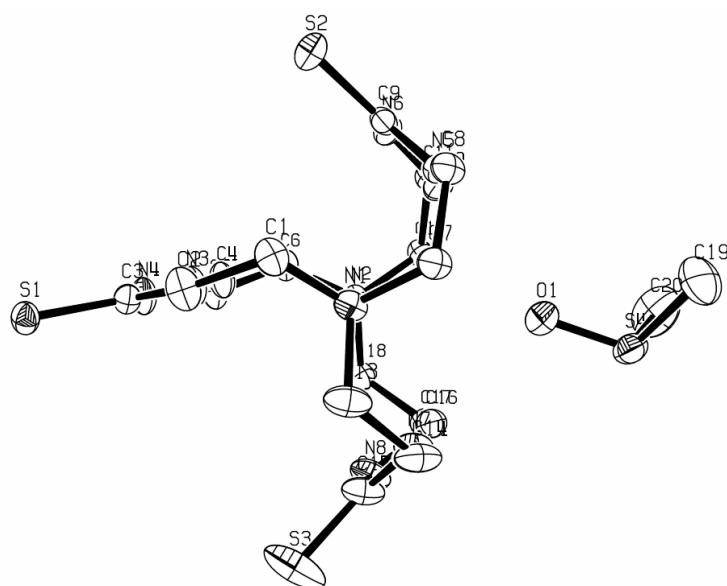
Atom	X	Y	Z	Uiso
S1	1.16867(5)	0.10687(4)	0.64481(3)	0.0240
S2	0.69811(5)	-0.07548(5)	0.57669(3)	0.0287
S3	0.94006(9)	0.47959(8)	0.61644(4)	0.0593
N1	0.73271(16)	0.20452(14)	0.6801(1)	0.0221
N2	0.80883(16)	0.23366(14)	0.3381(1)	0.0215
N3	0.94515(17)	0.13451(17)	0.61949(11)	0.0282
N4	1.05493(16)	0.13340(16)	0.5139(1)	0.0254
N5	0.58781(17)	0.09710(14)	0.56790(11)	0.0230
N6	0.65685(17)	0.03874(14)	0.45656(11)	0.0237
N7	0.7369(2)	0.39222(15)	0.59186(12)	0.0301
N8	0.8357(2)	0.42910(17)	0.48551(12)	0.0337
C1	0.7996(2)	0.12455(19)	0.71527(13)	0.0267
C2	0.9275(2)	0.1284(2)	0.70105(13)	0.0308
C3	1.04863(18)	0.12613(16)	0.58916(12)	0.0213
C4	0.95694(19)	0.14816(19)	0.46038(12)	0.0253
C5	1.0000(2)	0.16500(19)	0.38083(12)	0.0264
C6	0.9012(2)	0.16493(18)	0.32100(12)	0.0248
C7	0.61019(19)	0.18797(17)	0.68937(12)	0.0240
C8	0.56194(19)	0.09728(17)	0.64825(13)	0.0244
C9	0.64366(18)	0.02640(16)	0.53166(12)	0.0215
C10	0.6206(2)	0.12412(17)	0.41396(14)	0.0272
C11	0.64523(19)	0.11506(17)	0.32917(13)	0.0245
C12	0.70125(19)	0.20715(17)	0.29718(12)	0.0229
C13	0.7683(2)	0.29901(19)	0.71291(13)	0.0328
C14	0.7159(3)	0.38882(18)	0.67303(15)	0.0338
C15	0.8316(2)	0.42997(19)	0.56186(15)	0.0331
C16	0.7396(2)	0.40095(18)	0.43511(14)	0.0278
C17	0.7658(2)	0.41297(18)	0.35178(14)	0.0295
C18	0.84524(19)	0.33402(17)	0.32132(12)	0.0236
S4	0.42338(6)	0.37060(4)	0.51817(4)	0.0307
O1	0.52371(16)	0.30288(14)	0.53266(11)	0.0346
C19	0.3037(3)	0.3129(3)	0.5587(2)	0.0570
C20	0.3802(4)	0.3540(3)	0.42099(19)	0.0600
H1	0.8862(16)	0.150(2)	0.5913(14)	0.024(6)
H2	1.1185(17)	0.118(2)	0.4936(18)	0.036(6)
H3	0.570(2)	0.1499(13)	0.5438(14)	0.020(6)
H4	0.7003(18)	-0.0036(14)	0.4360(13)	0.012(5)
H5	0.684(2)	0.368(2)	0.5623(16)	0.036(6)

H6	0.8947(19)	0.457(2)	0.4671(18)	0.039(7)
H11	0.7894	0.1264	0.7693	0.0321
H12	0.7698	0.0635	0.6950	0.0321
H21	0.9607	0.1853	0.7259	0.0373
H22	0.9643	0.0703	0.7213	0.0373
H41	0.9133	0.2043	0.4760	0.0306
H42	0.9083	0.0909	0.4603	0.0306
H51	1.0386	0.2276	0.3795	0.0328
H52	1.0537	0.1140	0.3689	0.0328
H61	0.9318	0.1822	0.2726	0.0298
H62	0.8693	0.0999	0.3183	0.0298
H71	0.5969	0.1811	0.7429	0.0290
H72	0.5689	0.2446	0.6699	0.0290
H81	0.5961	0.0399	0.6717	0.0296
H82	0.4799	0.0957	0.6532	0.0296
H101	0.6605	0.1804	0.4343	0.0325
H102	0.5386	0.1325	0.4192	0.0325
H111	0.6963	0.0602	0.3224	0.0295
H112	0.5736	0.1033	0.3013	0.0295
H121	0.6482	0.2609	0.3011	0.0275
H122	0.7176	0.1959	0.2447	0.0275
H131	0.7468	0.3000	0.7654	0.0398
H132	0.8511	0.3038	0.7107	0.0398
H141	0.7480	0.4470	0.6965	0.0412
H142	0.6334	0.3881	0.6798	0.0412
H161	0.6743	0.4417	0.4463	0.0334
H162	0.7211	0.3336	0.4445	0.0334
H171	0.8023	0.4757	0.3452	0.0354
H172	0.6942	0.4113	0.3225	0.0354
H181	0.9212	0.3436	0.3435	0.0283
H182	0.8474	0.3410	0.2668	0.0283
H191	0.2362	0.3539	0.5512	0.0684
H192	0.3187	0.3040	0.6126	0.0684
H193	0.2901	0.2506	0.5349	0.0684
H120	0.3155	0.3959	0.4086	0.0715
H121	0.4432	0.3699	0.3892	0.0715
H122	0.3580	0.2866	0.4128	0.0715

6. References

[1] G. W. Gribble, in *Handbook of Environmental Chemistry, Vol. 3*, **2003**, pp. 1.

[2] G. W. Gribble, *Chemical Society Reviews* **1999**, *28*, 335.

[3] G. W. Gribble, *Progress in the Chemistry of Organic Natural Products* **1996**, *68*, 1.

[4] G. W. Gribble, *Speciality Chemicals Magazine* **2003**, *23*, 22.

[5] M. C. R. Franssen, *Biocatalysis* **1994**, *10*, 87.

[6] M. C. R. Franssen, *Catalysis Today* **1994**, *22*, 441.

[7] M. C. R. Franssen, H. C. Van der Plas, *Advances in Applied Microbiology* **1992**, *37*, 41.

[8] P. D. Shaw, L. P. Hager, *Journal of Biological Chemistry* **1961**, *236*, 1626.

[9] C. Dong, F. Huang, H. Deng, C. Schaffrath, J. B. Spencer, D. O'Hagan, J. H. Naismith, *Nature (London, United Kingdom)* **2004**, *427*, 561.

[10] D. O'Hagan, C. Schaffrath, L. Cobb Steven, T. G. Hamilton John, D. Murphy Cormac, *Nature* **2002**, *416*, 279.

[11] A. Butler, J. V. Walker, *Chemical Reviews (Washington, DC, United States)* **1993**, *93*, 1937.

[12] O. Kirk, L. S. Conrad, *Angewandte Chemie, International Edition* **1999**, *38*, 977.

[13] A. Butler, J. N. Carter-Franklin, *Natural Product Reports* **2004**, *21*, 180.

[14] M. Weyand, H. J. Hecht, M. Kiesz, M. F. Liaud, H. Vilter, D. Schomburg, *Journal of Molecular Biology* **1999**, *293*, 595.

[15] D. J. Sheffield, A. J. Smith, T. R. Harry, L. J. Rogers, *Biochemical Society Transactions* **1993**, *21*, 445S.

[16] E. De Boer, H. Plat, M. G. M. Tromp, R. Wever, M. C. R. Franssen, H. C. Van der Plas, E. M. Meijer, H. E. Schoemaker, *Biotechnology and Bioengineering* **1987**, *30*, 607.

[17] H. Vilter, *Metal Ions in Biological Systems* **1995**, *31*, 325.

[18] H. Vilter, *Phytochemistry (Elsevier)* **1984**, *23*, 1387.

[19] H. Plat, B. E. Krenn, R. Wever, *Biochemical Journal* **1987**, *248*, 277.

[20] J. W. P. M. van Schijndel, E. G. M. Vollenbroek, R. Wever, *Biochimica et Biophysica Acta* **1993**, *1161*, 249.

[21] R. Wever, B. E. Krenn, **1990**, pp. 81.

[22] E. G. M. Vollenbroek, L. H. Simons, W. P. M. van Schijndel, P. Barnett, M. Balzar, H. Dekker, C. van der Linden, R. Wever, *Biochemical Society Transactions* **1995**, *23*, 267.

[23] M. Almeida, S. Filipe, M. Humanes, M. F. Maia, R. Melo, N. Severino, J. A. L. da Silva, J. J. R. Frausto da Silva, R. Wever, *Phytochemistry* **2001**, *57*, 633.

[24] H. Vilter, D. Rehder, *Inorganica Chimica Acta* **1987**, *136*, L7.

[25] C. J. Carrano, M. Mohan, S. M. Holmes, R. de la Rosa, A. Butler, J. M. Charnock, C. D. Garner, *Inorganic Chemistry* **1994**, *33*, 646.

[26] J. M. Arber, E. De Boer, C. D. Garner, S. S. Hasnain, R. Wever, *Physica B: Condensed Matter (Amsterdam, Netherlands)* **1989**, *158*, 126.

[27] E. De Boer, C. P. Keijzers, A. A. K. Klaassen, E. J. Reijerse, D. Collison, C. D. Garner, R. Wever, *FEBS Letters* **1988**, *235*, 93.

[28] E. De Boer, K. Boon, R. Wever, *Biochemistry* **1988**, *27*, 1629.

[29] A. Messerschmidt, R. Wever, *Proceedings of the National Academy of Sciences of the United States of America* **1996**, *93*, 392.

[30] A. Messerschmidt, L. Prade, R. Wever, *Biological Chemistry* **1997**, *378*, 309.

[31] A. Messerschmidt, R. Wever, *Inorganica Chimica Acta* **1998**, *273*, 160.

[32] S. Macedo-Ribeiro, W. Hemrika, R. Renirie, R. Wever, A. Messerschmidt, *JBIC, Journal of Biological Inorganic Chemistry* **1999**, *4*, 209.

[33] A. Messerschmidt, *Structure and Bonding (Berlin)* **1998**, *90*, 37.

[34] B. H. Simons, P. Barnett, E. G. M. Vollenbroek, H. L. Dekker, A. O. Muijsers, A. Messerschmidt, R. Wever, *European Journal of Biochemistry* **1995**, *229*, 566.

[35] J. W. P. M. van Schijndel, L. H. Simons, E. G. M. Vollenbroek, R. Wever, *FEBS Letters* **1993**, *336*, 239.

[36] R. Renirie, W. Hemrika, R. Wever, *Journal of Biological Chemistry* **2000**, *275*, 11650.

[37] M. N. Isupov, A. R. Dalby, A. A. Brindley, Y. Izumi, T. Tanabe, G. N. Murshudov, J. A. Littlechild, *Journal of Molecular Biology* **2000**, *299*, 1035.

[38] J. Littlechild, E. Garcia-Rodriguez, *Coordination Chemistry Reviews* **2003**, *237*, 65.

[39] A. G. J. Ligtenbarg, R. Hage, B. L. Feringa, *Coordination Chemistry Reviews* **2003**, *237*, 89.

[40] M. Casny, D. Rehder, H. Schmidt, H. Vilter, V. Conte, *Journal of Inorganic Biochemistry* **2000**, *80*, 157.

[41]   D. Rehder, C. Schulzke, H. Dau, C. Meinke, J. Hanss, M. Epple, *Journal of Inorganic Biochemistry* **2000**, *80*, 115.

[42]   W. Hemrika, R. Renirie, S. Macedo-Ribeiro, A. Messerschmidt, R. Wever, *Journal of Biological Chemistry* **1999**, *274*, 23820.

[43]   L. P. Hager, D. R. Morris, F. S. Brown, H. Eberwein, *Journal of biological chemistry* **1966**, *241*, 1769.

[44]   A. Butler, R. A. Tschirret-Guth, *Verhandelingen - Koninklijke Nederlandse Akademie van Wetenschappen, Afdeling Natuurkunde, Tweede Reeks* **1997**, *98*, 55.

[45]   N. Itoh, A. K. M. Q. Hasan, Y. Izumi, H. Yamada, *European Journal of Biochemistry* **1988**, *172*, 477.

[46]   B. E. Krenn, Y. Izumi, H. Yamada, R. Wever, *Biochimica et Biophysica Acta* **1989**, *998*, 63.

[47]   E. De Boer, R. Wever, *Journal of Biological Chemistry* **1988**, *263*, 12326.

[48]   R. A. Tschirret-Guth, **1996**.

[49]   R. A. Tschirret-Guth, A. Butler, *Journal of the American Chemical Society* **1994**, *116*, 411.

[50]   A. Butler, *Current Opinion in Chemical Biology* **1998**, *2*, 279.

[51]   J. S. Martinez, G. L. Carroll, R. A. Tschirret-Guth, G. Altenhoff, R. D. Little, A. Butler, *Journal of the American Chemical Society* **2001**, *123*, 3289.

[52]   J. N. Carter-Franklin, J. D. Parrish, R. A. Tschirret-Guth, R. D. Little, A. Butler, *Journal of the American Chemical Society* **2003**, *125*, 3688.

[53]   M. Andersson, A. Willetts, S. Allenmark, *Journal of Organic Chemistry* **1997**, *62*, 8455.

[54]   H. B. ten Brink, A. Tuynman, H. L. Dekker, W. Hemrika, Y. Izumi, T. Oshiro, H. E. Schoemaker, R. Wever, *Inorganic Chemistry* **1998**, *37*, 6780.

[55]   M. A. Andersson, S. G. Allenmark, *Tetrahedron* **1998**, *54*, 15293.

[56]   H. B. ten Brink, H. L. Holland, H. E. Schoemaker, H. Van Lingen, R. Wever, *Tetrahedron: Asymmetry* **1999**, *10*, 4563.

[57]   W. Hemrika, R. Renirie, H. L. Dekker, P. Barnett, R. Wever, *Proceedings of the National Academy of Sciences of the United States of America* **1997**, *94*, 2145.

[58]   A. F. Neuwald, *Protein Science* **1997**, *6*, 1764.

[59]   J. Stukey, G. M. Carman, *Protein Science* **1997**, *6*, 469.

[60]   N. Tanaka, R. Wever, *Journal of Inorganic Biochemistry* **2004**, *98*, 625.

[61]   J. Littlechild, E. Garcia-Rodriguez, A. Dalby, M. Isupov, *Journal of Molecular Recognition* **2002**, *15*, 291.

[62]   P. J. Stankiewicz, A. S. Tracey, D. C. Crans, *Metal Ions in Biological Systems* **1995**, *31*, 287.

[63]   K. Ishikawa, Y. Mihara, K. Gondoh, E.-I. Suzuki, Y. Asano, *EMBO Journal* **2000**, *19*, 2412.

[64]   Y. Lindqvist, G. Schneider, P. Vihko, *European Journal of Biochemistry* **1994**, *221*, 139.

[65]   W. Plass, *Angewandte Chemie, International Edition* **1999**, *38*, 909.

[66]   N. Tanaka, V. Dumay, Q. Liao, A. J. Lange, R. Wever, *European Journal of Biochemistry* **2002**, *269*, 2162.

[67]   R. Renirie, W. Hemrika, S. R. Piersma, R. Wever, *Biochemistry* **2000**, *39*, 1133.

[68]   F. van de Velde, I. W. C. E. Arends, R. A. Sheldon, *Journal of Inorganic Biochemistry* **2000**, *80*, 81.

[69]   F. Van de Velde, I. W. C. E. Arends, R. A. Sheldon, *Topics in Catalysis* **2000**, *13*, 259.

[70]   F. Van de Velde, L. Konemann, F. Van Rantwijk, R. A. Sheldon, *Biotechnology and Bioengineering* **2000**, *67*, 87.

[71]   F. van de Velde, L. Konemann, F. van Rantwijk, R. A. Sheldon, *Chemical Communications (Cambridge)* **1998**, 1891.

[72]   N. Tanaka, V. Dumay, Q. Liao, J. Lange Alex, R. Wever, *European journal of biochemistry / FEBS* **2002**, *269*, 2162.

[73]   C. Crans Debbie, J. Smee Jason, E. Gaidamauskas, L. Yang, *Chemical reviews* **2004**, *104*, 849.

[74]   F. H. Westheimer, *Science* **1987**, *235*, 1173.

[75]   D. C. Crans, A. S. Tracey, *ACS Symposium Series* **1998**, *711*, 2.

[76]   D. C. Crans, *Comments on Inorganic Chemistry* **1994**, *16*, 1.

[77]   J. J. Cruywagen, *Advances in Inorganic Chemistry* **2000**, *49*, 127.

[78]   L. Pettersson, B. Hedman, A. M. Nenner, I. Andersson, *Acta Chemica Scandinavica, Series A: Physical and Inorganic Chemistry* **1985**, *A39*, 499.

[79]   L. Pettersson, I. Andersson, B. Hedman, *Chemica Scripta* **1985**, *25*, 309.

[80]   L. Pettersson, B. Hedman, I. Andersson, N. Ingri, *Chemica Scripta* **1983**, *22*, 254.

[81]   D. C. Crans, C. D. Rithner, L. A. Theisen, *Journal of the American Chemical Society* **1990**, *112*, 2901.

[82]   D. C. Crans, S. M. Schelble, L. A. Theisen, *Journal of Organic Chemistry* **1991**, *56*, 1266.

[83]   E. Heath, O. W. Howarth, *Journal of the Chemical Society, Dalton Transactions* **1981**, 1105.

[84]   D. J. Rigden, J. E. Littlejohn, K. Henderson, M. J. Jedrzejas, *Journal of Molecular Biology* **2003**, *325*, 411.

[85]   P. Y. Zavalu, F. Zhang, M. S. Whittingham, *Acta Crystallographica, Section C: Crystal Structure Communications* **1997**, *C53*, 1738.

[86]   C. F. G. C. Geraldes, M. M. C.A. Castro, *Journal of Inorganic Biochemistry* **1989**, *37*, 213.

[87]   A. S. Tracey, M. J. Gresser, S. Liu, *Journal of the American Chemical Society* **1988**, *110*, 5869.

[88]   R. Nitta, M. Kikkawa, Y. Okada, N. Hirokawa, *Science (Washington, DC, United States)* **2004**, *305*, 678.

[89]   D. G. Drueckhammer, J. R. Durrwachter, R. L. Pederson, D. C. Crans, L. Daniels, C. H. Wong, *Journal of Organic Chemistry* **1989**, *54*, 70.

[90]   A. F. Nour-Eldeen, M. M. Craig, M. J. Gresser, *Journal of Biological Chemistry* **1985**, *260*, 6836.

[91]   J. J. Cruywagen, J. B. B. Heyns, A. N. Westra, *Inorganic Chemistry* **1996**, *35*, 1556.

[92]   A. Butler, *Chemical & Engineering News* **2003**, *81*, 72.

[93]   K. Kustin, *ACS Symposium Series* **1998**, *711*, 170.

[94]   D. R. Davies, W. G. J. Hol, *FEBS Letters* **2004**, *577*, 315.

[95]   P. J. Stankiewicz, A. S. Tracey, D. C. Crans, *Metal ions in biological systems* **1995**, *31*, 287.

[96]   R. N. Lindquist, J. L. Lynn, Jr, G. E. Lienhard, *Journal Of The American Chemical Society* **1973**, *95*, 8762.

[97]   M. F. Perutz, M. G. Rossmann, A. F. Cullis, H. Muirhead, G. Will, A. C. T. North, *Nature (London, United Kingdom)* **1960**, *185*, 416.

[98]   S. J. Lippard, J. M. Berg, Editors, *Bioinorganic Chemistry*, **1995**.

[99]   W. R. Rypniewski, S. Mangani, B. Bruni, P. L. Orioli, M. Casati, K. S. Wilson, *Journal of Molecular Biology* **1995**, *251*, 282.

[100]   H. E. Parge, R. A. Hallewell, J. A. Tainer, *Proceedings of the National Academy of Sciences of the United States of America* **1992**, *89*, 6109.

[101]   K. Djinovic, G. Gatti, A. Coda, L. Antolini, G. Pelosi, A. Desideri, M. Falconi, F. Marmocchi, G. Rotilio, M. Bolognesi, *Journal of Molecular Biology* **1992**, *225*, 791.

[102]   Y. Kitagawa, N. Tanaka, Y. Hata, M. Kusunoki, G. P. Lee, Y. Katsube, K. Asada, S. Aibara, Y. Morita, *Journal of Biochemistry (Tokyo, Japan)* **1991**, *109*, 477.

[103]   K. M. Holtz, B. Stec, E. R. Kantrowitz, *Journal of Biological Chemistry* **1999**, *274*, 8351.

[104]   Y. Kakuta, E. V. Petrotchenko, L. C. Pedersen, M. Negishi, *Journal of Biological Chemistry* **1998**, *273*, 27325.

[105]   W. J. Ray, Jr., J. M. Puvathingal, Y. Liu, *Biochemistry* **1991**, *30*, 6875.

[106]   J. M. Denu, D. L. Lohse, J. Vijayalakshmi, M. A. Saper, J. E. Dixon, *Proceedings of the National Academy of Sciences of the United States of America* **1996**, *93*, 2493.

[107]   M. Zhang, M. Zhou, R. L. Van Etten, C. V. Stauffacher, *Biochemistry* **1997**, *36*, 15.

[108]   D. Rehder, *Coordination Chemistry Reviews* **1999**, *182*, 297.

[109]   C. Slebodnick, B. J. Hamstra, V. L. Pecoraro, *Structure and Bonding (Berlin)* **1997**, *89*, 51.

[110]   M. J. Clague, A. Butler, *Advances in Inorganic Biochemistry* **1994**, *9*, 219.

[111]   A. Butler, A. H. Baldwin, *Structure and Bonding (Berlin)* **1997**, *89*, 109.

[112]   R. H. Holm, E. I. Solomon, *Chemical Reviews (Washington, DC, United States)* **2004**, *104*, 347.

[113]   R. H. Holm, P. Kennepohl, E. I. Solomon, *Chemical Reviews (Washington, D. C.)* **1996**, *96*, 2239.

[114]   W. Plass, *Coordination Chemistry Reviews* **2003**, *237*, 205.

[115]   D. Rehder, *Inorganic Chemistry Communications* **2003**, *6*, 604.

[116]   A. Butler, M. J. Clague, G. E. Meister, *Chemical Reviews (Washington, DC, United States)* **1994**, *94*, 625.

[117]   V. Conte, O. Bortolini, M. Carraro, S. Moro, *Journal of Inorganic Biochemistry* **2000**, *80*, 41.

[118]   L. Pettersson, K. Elvingson, *ACS Symposium Series* **1998**, *711*, 30.

[119]   O. W. Howarth, L. Pettersson, I. Andersson, **2001**, pp. 145.

[120]   A. Gorzsas, K. Getty, I. Andersson, L. Pettersson, *Dalton Transactions* **2004**, 2873.

[121]   V. Conte, F. Di Furia, S. Moro, *ACS Symposium Series* **1998**, *711*, 136.

[122]   L. Pettersson, I. Andersson, A. Gorzsas, *Coordination Chemistry Reviews* **2003**, *237*, 77.

[123]   C. Kimblin, X. Bu, A. Butler, *Inorganic Chemistry* **2002**, *41*, 161.

[124]   R. I. De la Rosa, M. J. Clague, A. Butler, *Journal of the American Chemical Society* **1992**, *114*, 760.

[125]   M. J. Clague, A. Butler, *Journal of the American Chemical Society* **1995**, *117*, 3475.
[126]   F. Secco, *Inorganic Chemistry* **1980**, *19*, 2722.
[127]   A. Butler, *Coordination Chemistry Reviews* **1999**, *187*, 17.
[128]   C. Slebodnick, N. A. Law, V. L. Pecoraro, **2000**, pp. 215.
[129]   C. Slebodnick, V. L. Pecoraro, *Inorganica Chimica Acta* **1998**, *283*, 37.
[130]   V. Sucha, M. Sivak, J. Tyrselova, J. Marek, *Polyhedron* **1997**, *16*, 2837.
[131]   M. Andersson, V. Conte, F. Di Furia, S. Moro, *Tetrahedron Letters* **1995**, *36*, 2675.
[132]   V. Conte, F. Di Furia, S. Moro, S. Rabbolini, *Journal of Molecular Catalysis A: Chemical* **1996**, *113*, 175.
[133]   O. Bortolini, M. Carraro, V. Conte, S. Moro, *European Journal of Inorganic Chemistry* **2003**, 42.
[134]   V. L. Pecoraro, C. Slebodnick, B. Hamstra, *ACS Symposium Series* **1998**, *711*, 157.
[135]   M. J. Clague, N. L. Keder, A. Butler, *Inorganic Chemistry* **1993**, *32*, 4754.
[136]   B. J. Hamstra, G. J. Colpas, V. L. Pecoraro, *Inorganic Chemistry* **1998**, *37*, 949.
[137]   G. J. Colpas, B. J. Hamstra, J. W. Kampf, V. L. Pecoraro, *Journal of the American Chemical Society* **1996**, *118*, 3469.
[138]   G. J. Colpas, B. J. Hamstra, J. W. Kampf, V. L. Pecoraro, *Journal of the American Chemical Society* **1994**, *116*, 3627.
[139]   A. Bianchi, K. Bowman-James, E. Garcia-Espana, Editors, *Supramolecular Chemistry of Anions*, **1997**.
[140]   A. J. Evans, S. E. Matthews, A. R. Cowley, P. D. Beer, *Dalton Transactions* **2003**, 4644.
[141]   S. L. Tobey, E. V. Anslyn, *Journal of the American Chemical Society* **2003**, *125*, 14807.
[142]   S. L. Tobey, B. D. Jones, E. V. Anslyn, *Journal of the American Chemical Society* **2003**, *125*, 4026.
[143]   S. O. Kang, S. Jeon, K. C. Nam, *Supramolecular Chemistry* **2002**, *14*, 405.
[144]   Z.-H. Xie, X.-C. Lin, G.-N. Chen, C. Xi, X.-R. Wang, *Analytical Sciences* **2001**, *17*, a57.
[145]   H. H. Zepik, S. A. Benner, *Journal of Organic Chemistry* **1999**, *64*, 8080.
[146]   B. Dietrich, D. L. Fyles, T. M. Fyles, J. M. Lehn, *Helvetica Chimica Acta* **1979**, *62*, 2763.
[147]   T. H. Wirth, N. Davidson, *Journal of the American Chemical Society* **1964**, 4325.
[148]   J. F. Riordan, *Molecular and Cellular Biochemistry* **1979**, *26*, 71.
[149]   C. L. Hannon, E. V. Anslyn, *Bioorganic Chemistry Frontiers* **1993**, *3*, 193.
[150]   M. D. Best, S. L. Tobey, E. V. Anslyn, *Coordination Chemistry Reviews* **2003**, *240*, 3.
[151]   P. D. Beer, G. B. Drew. Michael, D. K. Smith, *Journal of Organometallic Chemistry* **1997**, *543*, 259.
[152]   M. Berger, F. P. Schmidtchen, *Journal of the American Chemical Society* **1996**, *118*, 8947.
[153]   M. Berger, F. P. Schmidtchen, *Angewandte Chemie, International Edition* **1998**, *37*, 2694.
[154]   M. Berger, F. P. Schmidtchen, *Journal of the American Chemical Society* **1999**, *121*, 9986.
[155]   B. Dietrich, T. M. Fyles, J. M. Lehn, L. G. Pease, D. L. Fyles, *Journal of the Chemical Society, Chemical Communications* **1978**, 934.
[156]   R. P. Dixon, S. J. Geib, A. D. Hamilton, *Journal of the American Chemical Society* **1992**, *114*, 365.
[157]   A. Echavarren, A. Galan, J. De Mendoza, A. Salmeron, J. M. Lehn, *Helvetica Chimica Acta* **1988**, *71*, 685.
[158]   A. Echavarren, A. Galan, J. M. Lehn, J. De Mendoza, *Journal of the American Chemical Society* **1989**, *111*, 4994.
[159]   P. A. Gale, *Coordination Chemistry Reviews* **2000**, *199*, 181.
[160]   A. Gleich, F. P. Schmidtchen, *Chemische Berichte* **1990**, *123*, 907.
[161]   A. Gleich, F. P. Schmidtchen, P. Mikulcik, G. Mueller, *Journal of the Chemical Society, Chemical Communications* **1990**, 55.
[162]   H. Kurzmeier, F. P. Schmidtchen, *Journal of Organic Chemistry* **1990**, *55*, 3749.
[163]   F. Liu, G.-Y. Lu, W.-J. He, J. Hu, Y.-H. Mei, L.-G. Zhu, *Synthesis* **2001**, 607.
[164]   G.-Y. Lu, W. Song, F. Tang, C.-M. Jin, F. Liu, X.-B. Wan, *Chinese Journal of Chemistry* **2000**, *18*, 924.
[165]   J. A. Martinez-Perez, M. A. Pickel, E. Caroff, W.-D. Waggon, *Synlett* **1999**, 1875.
[166]   S. Nishizawa, Y. Kato, N. Teramae, *Journal of the American Chemical Society* **1999**, *121*, 9463.
[167]   W. Peschke, P. Schiessl, F. P. Schmidtchen, P. Bissinger, A. Schier, *Journal of Organic Chemistry* **1995**, *60*, 1039.
[168]   J. Rebek, Jr., *Chemtracts: Organic Chemistry* **1990**, *3*, 240.
[169]   B. Springs, P. Haake, *Bioorganic Chemistry* **1977**, *6*, 181.

[170] O. W. Howarth, *Progress in Nuclear Magnetic Resonance Spectroscopy* **1990**, *22*, 453.
[171] N. Pooransingh, E. Pomerantseva, M. Ebel, S. Jantzen, D. Rehder, T. Polenova, *Inorganic Chemistry* **2003**, *42*, 1256.
[172] D. C. Crans, R. L. Bunch, L. A. Theisen, *Journal of the American Chemical Society* **1989**, *111*, 7597.
[173] A. S. Tracey, M. J. Gresser, *Inorganic Chemistry* **1988**, *27*, 1269.
[174] J. E. D. Davies, J. A. Ripmeester, Editors, *Comprehensive Supramolecular Chemistry, Volume 8: Physical Methods in Supramolecular Chemistry*, **1996**.
[175] L. Fielding, *Tetrahedron* **2000**, *56*, 6151.
[176] J. Frisch, G.W. Trucks, H.B. Schlegel, P. M W. Gill, B.G. Johnson, M.A. Robb, J.R. Cheeseman, T. Keith, G.A. Petersson, J.A. Montgomery, K. Raghavachari, M.A. Al-Laham, V.G. Zakrzewski, J. B. J.V. Ortiz, Foresman, J. Cioslowski, B.B. Stefanov, A. Nanayakkara, M. Challocombe, C.Y. Peng, P.Y. Ayala, W. Chen, M.W. Wong, J.L. Andres, E.S. Replogle, R. Gomperts, R.L. Martin, D.J. Fox, J.S. Bnikley, D.H. Defrees, J. Baker, J.P. Stewart, M. Head-Gordon, C. Gonzalez, J. A. Pople., Revision A.2. ed., Gaussian, Inc.,, Pittsburgh, PA., **1998**.
[177] I. Andersson, S. Angus-Dunne, O. Howarth, L. Pettersson, *Journal of Inorganic Biochemistry* **2000**, *80*, 51.
[178] J. M. Lehn, *Pure and Applied Chemistry* **1978**, *50*, 871.
[179] J. M. Lehn, *Pure and Applied Chemistry* **1977**, *49*, 857.
[180] J. M. Lehn, *Accounts of Chemical Research* **1978**, *11*, 49.
[181] B. Dietrich, J. M. Lehn, J. P. Sauvage, *Chemie in Unserer Zeit* **1973**, *7*, 120.
[182] J. M. Lehn, *Recherche* **1971**, *2*, 276.
[183] V. McKee, J. Nelson, R. M. Town, *Chemical Society Reviews* **2003**, *32*, 309.
[184] N. G. Lukyanenko, T. I. Kirichenko, V. V. Limich, *Synthesis* **1986**, 928.
[185] J. C. Manimala, E. V. Anslyn, *European Journal of Organic Chemistry* **2002**, 3909.
[186] L. Nie, Z. Li, J. Han, X. Zhang, R. Yang, W.-X. Liu, F.-Y. Wu, J.-W. Xie, Y.-F. Zhao, Y.-B. Jiang, *Journal of Organic Chemistry* **2004**, *69*, wx6449.
[187] Z.-Y. Zeng, Y.-B. He, J.-L. Wu, L.-H. Wei, X. Liu, L.-Z. Meng, X. Yang, *European Journal of Organic Chemistry* **2004**, 2888.
[188] T. Gunnlaugsson, A. P. Davis, G. M. Hussey, J. Tierney, M. Glynn, *Organic & Biomolecular Chemistry* **2004**, *2*, 1856.
[189] S.-Y. Liu, Y.-B. He, J.-L. Wu, L.-H. Wei, H.-J. Qin, L.-Z. Meng, L. Hu, *Organic & Biomolecular Chemistry* **2004**, *2*, 1582.
[190] K. Choi, A. D. Hamilton, *Coordination Chemistry Reviews* **2003**, *240*, 101.
[191] D. H. Lee, J. H. Im, J.-H. Lee, J.-I. Hong, *Tetrahedron Letters* **2002**, *43*, 9637.
[192] F.-Y. Wu, Z. Li, Z.-C. Wen, N. Zhou, Y.-F. Zhao, Y.-B. Jiang, *Organic Letters* **2002**, *4*, 3203.
[193] T. Gunnlaugsson, A. P. Davis, J. E. O'Brien, M. Glynn, *Organic Letters* **2002**, *4*, 2449.
[194] S.-i. Sasaki, D. Citterio, S. Ozawa, K. Suzuki, *Journal of the Chemical Society, Perkin Transactions 2* **2001**, 2309.
[195] S. Nishizawa, T. Yokobori, T. Shioya, N. Teramae, *Chemistry Letters* **2001**, 1058.
[196] K. H. Lee, J. I. Hong, *Tetrahedron Letters* **2000**, *41*, 6083.
[197] T. Hayashita, T. Onodera, R. Kato, S. Nishizawa, N. Teramae, *Chemical Communications (Cambridge)* **2000**, 755.
[198] S.-i. Sasaki, M. Mizuno, K. Naemura, Y. Tobe, *Journal of Organic Chemistry* **2000**, *65*, 275.
[199] S. Nishizawa, K. Shigemori, N. Teramae, *Chemistry Letters* **1999**, 1185.
[200] Y. Tobe, S.-I. Sasaki, M. Mizuno, K. Naemura, *Chemistry Letters* **1998**, 835.
[201] S. Nishizawa, R. Kato, T. Hayashita, N. Teramae, *Analytical Sciences* **1998**, *14*, 595.
[202] P. Buhlmann, S. Nishizawa, K. P. Xiao, Y. Umezawa, *Tetrahedron* **1997**, *53*, 1647.
[203] J. Scheerder, J. F. J. Engbersen, A. Casnati, R. Ungaro, D. N. Reinhoudt, *Journal of Organic Chemistry* **1995**, *60*, 6448.
[204] S. Nishizawa, P. Buehlmann, M. Iwao, Y. Umezawa, *Tetrahedron Letters* **1995**, *36*, 6483.
[205] M. Niitsu, K. Samejima, S. Matsuzaki, K. Hamana, *Journal of Chromatography* **1993**, *641*, 115.
[206] M. Niitsu, H. Sano, K. Samejima, *Chemical & Pharmaceutical Bulletin* **1992**, *40*, 2958.
[207] T. Shibanuma, M. Shiono, T. Mukaiyama, *Chemistry Letters* **1977**, 575.
[208] Y. F. Yong, J. A. Kowalski, M. A. Lipton, *Journal of Organic Chemistry* **1997**, *62*, 1540.
[209] A. Bencini, A. Bianchi, E. Garcia-Espana, M. Micheloni, J. A. Ramirez, *Coordination Chemistry Reviews* **1999**, *188*, 97.

[210]   D. M. Kneeland, K. Ariga, V. M. Lynch, C. Y. Huang, E. V. Anslyn, *Journal of the American Chemical Society* **1993**, *115*, 10042.
[211]   R. A. Bissell, A. Prasanna de Silva, H. Q. N. Gunaratne, P. L. M. Lynch, G. E. M. Maguire, C. P. McCoy, K. R. A. S. Sandanayake, *Topics in Current Chemistry* **1993**, *168*, 223.
[212]   M. Bertinaria, A. Di Stilo, P. Tosco, G. Sorba, E. Poli, C. Pozzoli, G. Coruzzi, R. Fruttero, A. Gasco, *Bioorganic & Medicinal Chemistry* **2003**, *11*, 1197.
[213]   A. Buschauer, A. Friese-Kimmel, G. Baumann, W. Schunack, *European Journal of Medicinal Chemistry* **1992**, *27*, 321.
[214]   W. Meindl, A. Friese-Kimmel, F. Lachenmayr, A. Buschauer, W. Schunack, *Archiv der Pharmazie (Weinheim, Germany)* **1990**, *323*, 267.
[215]   A. J. Villani, L. Petka, D. W. Blackburn, D. Saunders, G. R. White, J. Winster, *Journal of Labelled Compounds and Radiopharmaceuticals* **1989**, *27*, 1395.
[216]   A. Buschauer, *Journal of Medicinal Chemistry* **1989**, *32*, 1963.
[217]   A. Buschauer, *Archiv der Pharmazie (Weinheim, Germany)* **1988**, *321*, 415.
[218]   A. Buschauer, *Archiv der Pharmazie (Weinheim, Germany)* **1988**, *321*, 281.
[219]   A. Buschauer, *Scientia Pharmaceutica* **1988**, *56*, 81.
[220]   A. Buschauer, *European Journal of Medicinal Chemistry* **1988**, *23*, 1.
[221]   A. Buschauer, H. Schickaneder, S. Elz, W. Schunack, I. Szelenyi, K. Henning, in *Ger. Offen.*, (Heumann, Ludwig, und Co. G.m.b.H., Fed. Rep. Ger.). DE, **1986**, p. 60 pp.
[222]   G. J. Durant, C. R. Ganellin, D. W. Hills, P. D. Miles, M. E. Parsons, E. S. Pepper, G. R. White, *Journal of Medicinal Chemistry* **1985**, *28*, 1414.
[223]   D. W. Hills, G. R. White, in *Eur. Pat. Appl.*, (Smith Kline and French Laboratories Ltd., UK). EP, **1981**, p. 23 pp.
[224]   S.-p. Pang, Y.-z. Yu, *Hecheng Huaxue* **2001**, *9*, 407.
[225]   J. C. Manimala, E. V. Anslyn, *Tetrahedron Letters* **2002**, *43*, 565.
[226]   F. M. Winnik, *Chemical Reviews (Washington, DC, United States)* **1993**, *93*, 587.
[227]   R. Martinez-Manez, F. Sancenon, *Chemical Reviews (Washington, DC, United States)* **2003**, *103*, 4419.
[228]   B. Valeur, I. Leray, *Coordination Chemistry Reviews* **2000**, *205*, 3.
[229]   A. P. de Silva, H. Q. N. Gunaratne, T. Gunnlaugsson, A. J. M. Huxley, C. P. McCoy, J. T. Rademacher, T. E. Rice, *Chemical Reviews (Washington, D. C.)* **1997**, *97*, 1515.
[230]   A. Warshel, E. Huler, *Chemical Physics* **1974**, *6*, 463.
[231]   F. Huang, J. W. Jones, C. Slebodnick, H. W. Gibson, *Journal of the American Chemical Society* **2003**, *125*, 14458.
[232]   J. W. Jones, H. W. Gibson, *Journal of the American Chemical Society* **2003**, *125*, 7001.
[233]   A. V. S. Rao, H. N. Ravishankar, T. Ramasarma, *Archives of Biochemistry and Biophysics* **1996**, *334*, 121.
[234]   M. Hojo, T. Ueda, K. Kawamura, M. Yamasaki, *Bulletin of the Chemical Society of Japan* **2000**, *73*, 347.
[235]   B. F. Sels, D. E. De Vos, M. Buntinx, P. A. Jacobs, *Journal of Catalysis* **2003**, *216*, 288.
[236]   S. Sarmah, D. Kalita, P. Hazarika, R. Borah, N. S. Islam, *Polyhedron* **2004**, *23*, 1097.
[237]   N. O. McHedlov-Petrossyan, V. I. Kukhtik, V. D. Bezugliy, *Journal of Physical Organic Chemistry* **2003**, *16*, 380.
[238]   A. McKillop, D. Bromley, E. C. Taylor, *Journal of Organic Chemistry* **1972**, *37*, 88.
[239]   A. Stocker, T. Netscher, A. Ruettimann, R. K. Mueller, H. Schneider, L. J. Todaro, G. Derungs, W.-D. Woggon, *Helvetica Chimica Acta* **1994**, *77*, 1721.
[240]   A. Stocker, A. Ruettimann, W. D. Woggon, *Helvetica Chimica Acta* **1993**, *76*, 1729.
[241]   I. M. Kolthoff, M. K. Chantooni, Jr., S. Bhowmik, *Journal of the American Chemical Society* **1968**, *90*, 23.
[242]   X.-a. Zhang, M. Meuwly, W.-D. Woggon, *Journal of Inorganic Biochemistry* **2004**, *98*, 1967.

Appendix

7.

Slow Down the Proton Exchange Rate: A New Approach To Measure Absolute Acidity.

The main difficulty for directly measuring proton concentration in solution is due to the high speed of proton exchange between different species. A rigid hydrophobic microenvironment and formation of hydrogen bond (HB) can slow down this procedure, in certain cases dramatically, such as the situation of interior part of a folded protein. We found such a phenomenon can also be achieved in a very small synthetic molecule and the proton exchange rate can reach the level below NMR timescale. Therefore, it can be utilized to determine the absolute proton concentration, and further the pK_a of acid by NMR spectrum.

A novel thiourea-cryptand **1** has been synthesized. The protonation behavior was studied by solution NMR (**Figure 1**) and X-ray crystallography (**Figure 2**), both indicate a rigid conformation of the cavity and the involvement of intramolecular HB for the central-ammonium-protons and S-atoms. The proton exchange is thus slowed down to the NMR time scale, even within short distance of intramolecular exchange between two central nitrogen atoms in **MP-1**. Intramolecular HB also leads an unusual negatively cooperative protonation effect, namely, $pK_{a2} > pK_{a1}$, in contrast most of other polyamine compounds for which the second protonation is usually more difficult than the first[1].
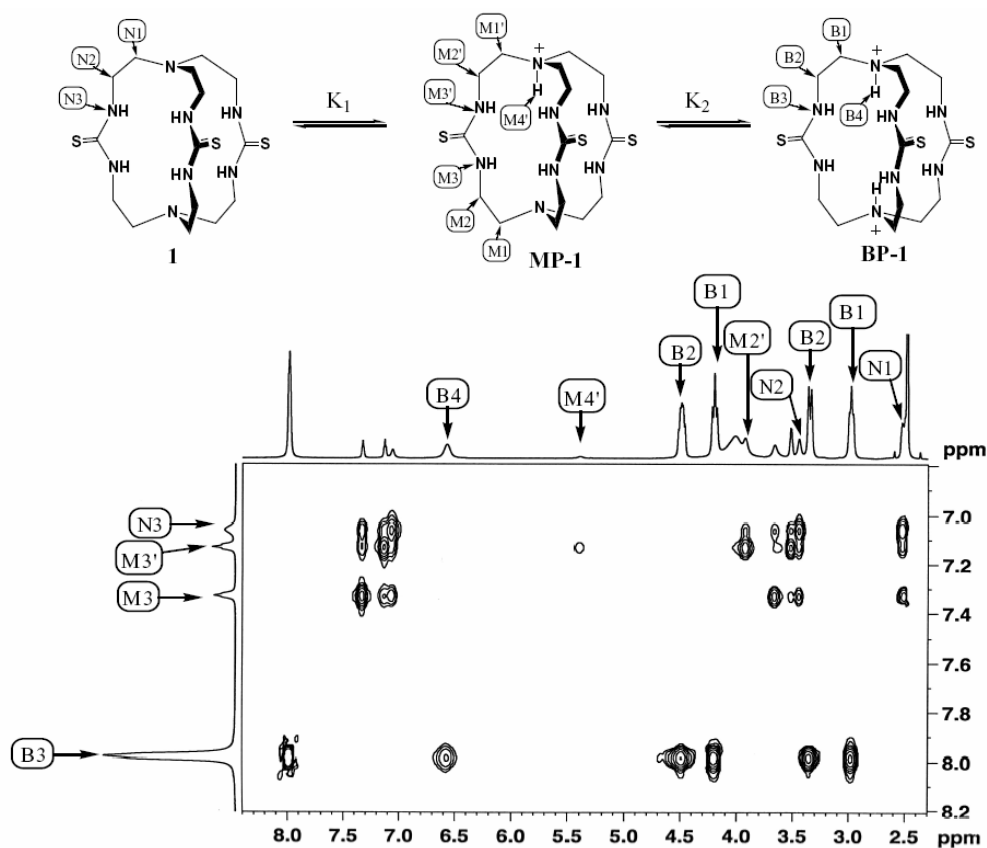
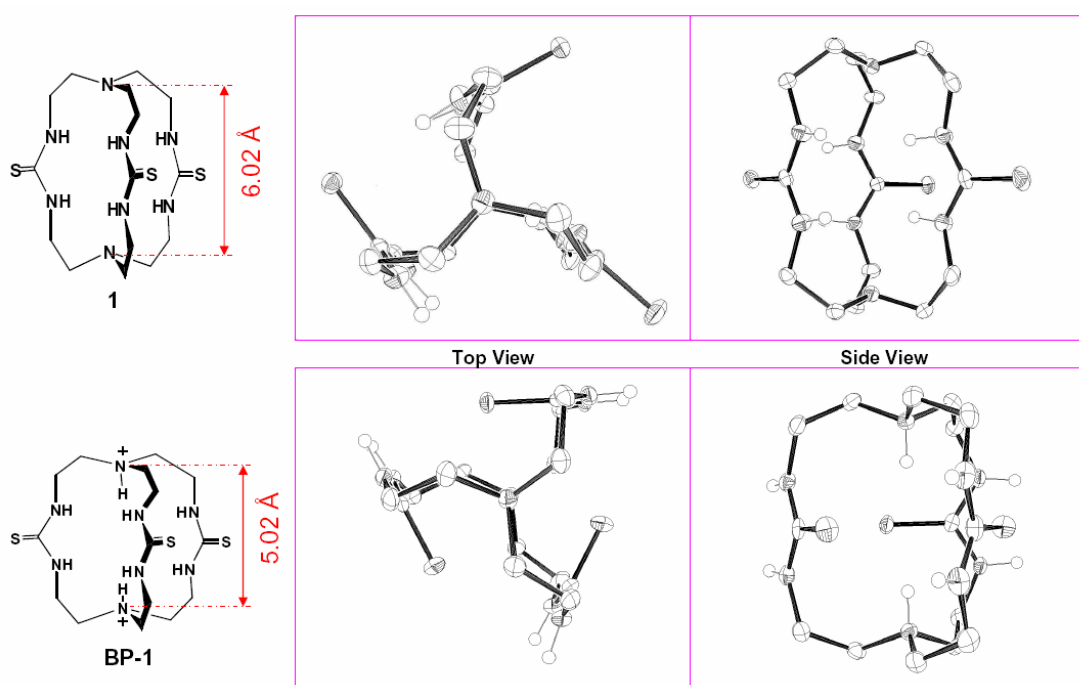**Figure 1.** TOCSY ^{1}H-NMR of **BP-1** bis-picrate and assignment of peaks of **1**, **MP-1** and **BP-1.**

Figure 2. ORTEP drawing of the X-ray structure of neutral **1** (top) and **BP-1** (bottom); left: side view; right: top view. -CH$_2$- hydrogen atoms were omitted for clarity.

131

Since the low proton exchange rate allows to distinguish all the different protonated states of **1** in the ^{1}H-NMR spectrum (**Figure 1**), the absolute concentration of the individual species can be obtained from the integral. Therefore, [H$^+$] and pK_a of the acid used can then be deduced from the population of each species by following equations (**eq.1-5**), although certain error exists due to the ion pair formation (Samples of pK_a measurement see **Table 1**).

$$K_a = \frac{[H^+][A^-]}{[HA]} \qquad \dots\dots\dots\dots\dots\dots\dots\dots\dots\dots 1$$

$$K_1 = \frac{[MP-1]}{[H^+][1]} \qquad \dots\dots\dots\dots\dots\dots\dots\dots\dots\dots 2$$

$$K_2 = \frac{[BP-1]}{[H^+][MP-1]} \qquad \dots\dots\dots\dots\dots\dots\dots\dots\dots\dots 3$$

$$[HA] + [A^-] = C_a \qquad \dots\dots\dots\dots\dots\dots\dots\dots\dots\dots 4$$

$$[A^-] = [MP-1] + [H^+] + 2[BP-1] \qquad \dots\dots\dots\dots\dots\dots\dots 5$$

* C_a is total concentration of acid used.

Table 1: The pK_a of selected acids determined by our new method and the literature values.

Acid	MeSO$_3$H	CF$_3$SO$_3$H	TsOH	MeSO$_3$H	CF$_3$COOH	HCl
Solvent (all-*d*)	DMSO	DMSO	DMSO	5%H$_2$O/ DMSO	5%H$_2$O/ DMSO	5%H$_2$O/ DMSO
K_a	0.0885	2.7118	0.0332	0.3130	0.0467	0.4296
pK_a-Exp	1.053	-0.433	1.479	0.504	1.331	0.367
lit$_{DMSO}$	1.6	0.3		1.6	3.45	1.8
lit$_{H2O}$	-2.6	-14		-2.6	0.23(-0.26)	-8.0

Accordingly it is possible to measure the acidity using the phenomenon of slow proton exchange. The modification of structure **3** should decrease the error and broaden the scope of pK_a measurement, which sheds light on its potential role as bio-sensor.

Reference

1. Andera Bencini, Antonio Bianchi, Enrique Garcia-Espana, Mauro Micheoni and Jose Antonio Ramirez, *Coord. Chem. Rev.* **1999**, 188, 97.

8. Curriculum Vitae

Xiao-an Zhang

Department of Chemistry, University of Basel
St. Johanns-Ring 19, CH-4056 Basel, Switzerland
Tel: 0041-61-2671128 (O); 0041-61-2613242 (H).
Fax: 0041-61-2671103
E-mail: Xiao-an.Zhang@unibas.ch

Personal

Date of Birth:	Aug. 2, 1973	Place of Birth:	Zhejiang Province,China
Sex:	Male	Marital Status:	Married to Ganpan Gao

Education

2000-present:	University of Basel, Basel, Switzerland. Ph.D. student. Research advisor: Prof. Wolf-D. Woggon. Research Project: Supramolecular models of vanadium haloperoxidase
1997-2000:	Shanghai Institute of Pharmaceutical Industry (SIPI), Shanghai, China. Degree awarded: Master degree. Research advisor: Prof. Houyuan Zhou. Research Projects: 1. Synthesis of chiral drug and building blocks in large scale; 2. Synthesis of new β_3-adrenergic receptor agonists.
1991-1995	Shanghai Medical University, Shanghai, China. Degree awarded: B.S. Research advisor (1995): Professor Gouqiang Lin (Shanghai Institute of Organic Chemistry, Chinese Academy of Sciences). Practical Project: Kinetic resolution of C2-symmetrical divinyl methanols using modified Sharpless reagents: Total synthesis phytosphingosine.
1988-1991	Yueqing Middle School, Zhejiang, China

Presentations

Xiao-an Zhang, Gerd Scherer, Wolf-D Woggon, **Intramolecular Hydrogen Bonds Control the Conformation, Protonation Behavior and Reactivity of a Novel Thiourea-Cryptand**, *poster presentation*, 22nd Regio Symposium of Organic and Bioorganic Chemistry, September 25-27, 2002, Falkau, Germany.

Xiao-an Zhang, Gerd Scherer, Wolf-D Woggon, **Binding of Ortho-Vanadate Anion: towards Mimics of Vanadium Haloperoxidase (VHPO),** *oral presentation*, Fall Meeting of the Swiss Chemical Society, October 12, 2002, Switzerland.

Xiao-an Zhang, Gerd Scherer, Wolf-D Woggon, **Binding of Ortho-Vanadate Anion: the First Supramolecular Model of of Vanadium Haloperoxidase (VHPO),** *oral and poster presentation*, International Symposium on Organic Synthesis and Catalysis, 23rd Regio Symposium, September 21-24, 2003, Falkau, Germany.

Publications:

(1) Fu-Li Zhang; Xiao-an Zhang; Gen-Jin Yang; Hou-Yuan Zhou. **Application of ^{1}H-NMR in the synthesis of Pyritinol**, *Zhongguo Yiyao Gongye Zazhi* (1999), 30(5), 193-196
(2) Xiao-an Zhang, Markus Meuley, Wolf-D. Woggon. **The First Supramolecular Receptor of Orthovanadate- Structural Mimics of Vanadium Haloperoxidase**, *Journal of Inorganic Biochemistry* (2004), 98(11), 1967-1970.
(3) Xiao-an Zhang, Gerd Scherer, Wolf-D. Woggon. **Determination of Absolute Acidity Values in Organic Solvents Through NMR Analysis of Cage Compounds Displaying Unusually Slow Proton Exchange,** *in preparation.*
(4) Xiao-an Zhang, Wolf-D. Woggon. **From Supramolecular Vanadate Sensor to Enzyme Model of Vanadium Haloperoxidase**, *in preparation.*

Honors:

Qimingxing Award, 1999

Experimental Skills:

Extensive experience in NMR, ESI-MS, MALDI-TOF-MS, GC/MS, HPLC, Ion Exchange Chromatography, UV-VIS, FTIR, Molecular Modeling, and Working in Glove Box, Industrial-Scale Synthesis.

Language Proficiency:

Chinese: Mother tongue
English: Fluent
German: Fair in reading

Referees:

Prof. Dr. Wolf-D. Woggon
Department of Chemistry, University of Basel
St. Johanns-Ring 19
4056 Basel, Switzerland
Tel. & Fax +41 61 267 11 02
wolf-d.woggon@unibas.ch

Prof. Dr. Andreas Pfaltz
Department of Chemistry, Universtiy of Basel
St. Johanns-Ring 19
4056 Basel, Switzerland
Tel. + 41 61 267 11 08
Fax + 41 61 267 11 03
andreas.pfaltz@unibas.ch

Jan. 24, 2005

9. Eidesstattliche Erklärung

Hiermit erkläre ich an Eides statt, dass ich meine Dissertation selbständig und nur mit den angegebenen Hilfsmitteln angefertigt habe. Ich erkläre ausserdem, dass ich diese Dissertation an keiner anderen Fakultät eingereicht habe.

Basel, den 24. Januar 2005

Xiao-an Zhang